Upcycling to Sustainable Conversion of Polypropylene Waste to Graphene Grown Talc Hybrids as Additive for Efficient Thermoplastic Processing and its Systematic Life Cycle Assessment

by

Atakan KOÇANALI

Submitted to the Graduate School of Engineering and Natural Sciences
in partial fulfillment of
the requirements for the degree of
Master of Science

Sabancı University

December 2021

Upcycling to Sustainable Conversion of Polypropylene Waste to Graphene Grown Talc Hybrids as Additive for Efficient Thermoplastic Processing and its Systematic Life Cycle Assessment

Approved by:

Assoc. Prof. Dr. Burcu SANER OKAN
(Thesis Supervisor)

Prof. Dr. Yusuf Ziya Menceloğlu

Prof. Dr. Mehmet Atilla TAŞDELEN

Approval Date: December 15, 2021

ABSTRACT

Upcycling to Sustainable Conversion of Polypropylene Waste to Graphene Grown Talc Hybrids as Additive for Efficient Thermoplastic Processing and its Systematic Life Cycle Assessment

Atakan KOÇANALI

MATERIAL SCIENCE AND NANOENGINEERING, MASTER THESIS
DECEMBER 2021

Thesis Supervisor: Assoc. Prof. Dr. Burcu SANER OKAN

Keywords: Upcycling, plastic wastes, graphene/talc hybrid additive, automotive thermoplastic composites, life cycle assessment

Plastic waste is a significant environmental and climate concern that threatens the ecosystem and leads to soil and water contamination. Although plastic recycling provides several benefits, the recycled plastics do not have the same performance as virgin plastic composites. Instead of traditional recycling processes, it is possible to produce high value-added carbon nanomaterials by using a rich hydrocarbon source in plastics. This thesis aims to grow graphene structures on talc substrate by using polypropylene sources and applying an environmentally friendly, sustainable, and cost-effective upcycling technology, and develop lightweight thermoplastic composites with this newly designed hybrid additive by reducing the main reinforcement amount in the target automotive plastics. In addition, comprehensive life cycle assessment was carried out to demonstrate the environmental gains from the proposed innovative upcycling solutions with the benchmarking study by evaluating CO_2 emission reductions. Initially, carbon source in polypropylene (PP) wastes were converted into vapor phase and bind to talc surface in

the presence of metal catalyst by initiating graphene growth in mild conditions by upcycling technology. Herein, a selective method to obtain 2D and 3D graphene structures was developed by selecting a suitable talc size, activating talc surface, producing different PP blends with talc by using two main polymer processing techniques: high shear mixing with thermokinetic mixer and twin-screw extrusion, and defining suitable pyrolysis and carbonization techniques. The results indicated that talc with a D_{50} particle size of up to 10 μm enhanced the growth of 2D graphene sheets whereas talc size less than 2 μm increased the formation of 3D graphene spheres. In other words, the developed upcycling method enables an easy and low-cost obtainment of graphene based two-dimensional and/or three-dimensional nano- or submicron-sized structures on talc surfaces. In addition, flash pyrolysis by rotating furnace provided to produce graphene/hybrid additives in a short time by decreasing the defects compared to the hybrid obtained by gradual heating in chamber furnace. There was a significant effect of blending technique on the crystal structure of hybrid additive. Thermokinetic mixer used to prepare talc/PP samples for carbonization process caused complete exfoliation of talc and changed the crystalline planes and decreased the particle size due to the occurrence of blending process at around 4000 rpm. However, twin-screw extrusion preserved the layered structure of talc and did not change its crystal structure since blending was occurred at very low mixing rates of 350 rpm. After the selection of an ideal graphene/talc hybrid additive production, the produced hybrid additives were used as a reinforcement in homopolymer PP and copolymer PP at different loading ratios to reach the automotive standards and decrease the talc content and maintain the mechanical performance of the composites. The most remarkable improvement was achieved by the addition of 5 wt% hybrid additive in CopoPP matrix, flexural modulus and tensile modulus were increased by 88% and 57%, respectively, compared to neat CopoPP. Furthermore, %10 talc reduction was provided with this new graphene/talc hybrid additive and even 6% improvement in flexural modulus was accomplished at 5 wt% hybrid loading compared to the performance of compound having 15% talc used in serial part production. In conclusion, the conversion of polypropylene waste into high value-added graphene/talc hybrid additive by circular economy targeted upcycling process brings a new insight in graphene manufacturing and the production of lightweight thermoplastic plastic. Also, life cycle assessment approach was adopted to assess the environmental sustainability performances of the new automotive thermoplastic composites in comparison to their conventional equivalents.

ÖZET

İleri Dönüşüm Tekniği ile Polipropilen Atıkların Sürdürülebilir Şekilde Katkı Malzemesi Olarak Verimli Termoplastik İşlemede Kullanmak İçin Talk Üzerinde Büyütülen Grafen Hibritlerine Dönüşümü ve Sistematik Yaşam Döngüsünün Değerlendirmesi

Atakan KOÇANALI

MALZEME BİLİMİ VE NANOMÜHENDİSLİĞİ , YÜKSEK LİSANS TEZİ, ARALIK 2021

Tez Danışmanı: Doç. Dr. Burcu SANER OKAN

Anahtar kelimeler: İleri dönüşüm tekniği, plastik atıklar, grafen/talk hibrit katkı, otomotiv termoplastik kompozitleri, yaşam döngüsü analizi

Plastik atık, ekosistemi tehdit eden, toprak ve su kirliliğine yol açan önemli bir çevre ve iklim sorunudur. Plastik geri dönüşümü çeşitli faydalar sağlamasına rağmen geri dönüştürülmüş plastikler, ham plastik kompozitlerle aynı performansa sahip değildir. Geleneksel geri dönüşüm süreçleri yerine plastiklerdeki zengin hidrokarbon kaynağı kullanarak katma değeri yüksek karbon nanomalzemeler üretmek mümkündür. Bu tez, polipropilen kaynakları kullanarak çevre dostu, sürdürülebilir ve uygun maliyetli bir ileri dönüşüm teknolojisi uygulayarak talk tabakası üzerinde grafen yapıları büyütmeyi ve hedeflenen otomotiv parçasındaki ana takviye miktarını azaltarak bu yeni tasarlanmış hibrit katkı ile hafif termoplastik kompozitleri geliştirmeyi amaçlamaktadır. Buna ek olarak, CO_2 emisyonu azaltımlarını göz önünde bulundurarak yapılan kıyaslama çalışması ile önerilen yenilikçi ileri dönüşüm çözümlerinden elde edilen çevresel kazanımları göstermek için kapsamlı olarak yaşam döngüsü değerlendirmesi yapılmıştır. İlk olarak, polipropilen (PP) atıklarındaki karbon kaynağı buhar fazına dönüştürülerek,

ileri dönüşüm teknolojisi ile ılımlı koşullarda grafen büyümesi başlatılmış ve metal katalizör varlığında talk yüzeyine bağlanmıştır. Burada, uygun bir talk boyutu seçilerek, talk yüzeyi aktive edilmiş ve iki ana polimer işleme tekniklerinden olan termokinetik karıştırma ve çift vidalı esktrüzyon kullanılarak talk ile PP karışımları üretilmiştir. Bu teknik ile 2B ve 3B grafen yapıları elde etmek için seçici bir yöntem geliştirilmiştir ve uygun piroliz ve karbonizasyon teknikleri belirlenmiştir. Sonuçlar göstermektedir ki 10 μm'ye kadar D_{50} partikül boyutuna sahip talk, 2 boyutlu grafen tabakalarının büyümesini arttırırken, 2 μm'den daha küçük talk boyutu, 3 boyutlu grafen kürelerinin oluşumunu arttırmaktadır. Başka bir deyişle, geliştirilen ileri dönüşüm yöntemi, talk yüzeyler üzerinde grafen bazlı iki boyutlu ve/veya üç boyutlu nano veya mikron altı boyutlu yapıların kolay ve düşük maliyetli bir şekilde elde edilmesini sağlamıştır. Ayrıca döner fırın ile yapılan flaş piroliz, kamara tipi fırında kademeli ısıtma ile elde edilen hibrite göre kusurları azaltarak kısa sürede grafen/hibrit katkı maddelerinin üretilmesini sağlamıştır. Karıştırma tekniğinin hibrit katkı maddesinin kristal yapısı üzerinde önemli bir etkisi olmuştur. Talk/PP numunelerinin karbonizasyon işlemine hazırlanmasında kullanılan termokinetik karıştırıcı, talk tabakalarının birbirinden ayrılmasına neden olmuş, karıştırma işleminin 4000 rpm civarında gerçekleşmesi nedeniyle kristal düzlemlerini değiştirmiş ve partikül boyutunu küçültmüştür. Öte yandan, çift vidalı ekstrüzyon, talkın katmanlı yapısını korumuştur ve karıştırma 350 rpm gibi çok düşük karıştırma hızlarında gerçekleştiği için talkın kristal yapısını değiştirmemiştir. İdeal bir grafen/talk hibrit katkı maddesi üretimi seçiminin ardından üretilen hibrit katkı maddeleri, otomotiv standartlarına ulaşmak, talk içeriğini azaltmak ve kompozitlerin mekanik performansını korumak için homopolimer PP ve kopolimer PP'ye farklı yükleme oranlarında takviye olarak eklenmiştir. En dikkat çekici gelişme, kopoPP matrisine ağırlıkça %5 hibrit katkı maddesinin eklenmesiyle elde edilmiş, eğme modülü ve çekme modülü, saf copoPP'ye kıyasla sırasıyla %88 ve %57 artış gözlemlenmiştir. Ayrıca, bu yeni grafen/talk hibrit katkı maddesi ile talk miktarında %10 azalma sağlanmış ve seri parça üretiminde kullanılan %15 talk içeren bileşiğin performansına kıyasla ağırlıkça %5 hibrit yüklemede bile eğme modülünde %6 iyileşme sağlanmıştır. Sonuç olarak, döngüsel ekonomi hedefli ileri dönüşüm süreci ile polipropilen atığı yüksek katma değerli grafen/talk hibrit katkı maddesine dönüştürmesi, grafen üretimine ve hafif termoplastik plastik üretimine yeni bir bakış açısı getirmektedir. Ayrıca, bu üretilen yeni otomotiv termoplastik kompozitlerinin, geleneksel eşdeğerlerine kıyasla çevresel sürdürülebilirlik performanslarının analizi için yaşam döngüsü değerlendirme yaklaşımı benimsenmiştir.

ACKNOWLEDGEMENTS

I would like to express my gratitude to all the people who gave me the possibility to complete this thesis.

First and foremost, I would like to extend my special thanks to my supervisor, Assoc. Prof. Dr. Burcu Saner Okan for her admirable advice throughout the research, for her dedicated support and guidance.

I would like to express my gratitude and appreciation to Prof. Dr. Yusuf Menceloğlu for his encouragement, valuable comments, and suggestions.

Furthermore, I would like to thank all SU-IMC members for their collaborative support during this journey.

I would like to thank my research teammates Dr. Havva Başkan Bayrak for her guidance and encouragement throughout the research, and Esra Yalçınkaya for her continuous support, motivation, and hard work.

I would like to thank also the Sezer Özdemir, Feyyaz Perem, Dr. Semih Doğan for their continuous support and patience and Dr. Serra Topal and Qasım Ali for their guidance.

Very special thanks go out to Gizem Arıtürk, Kuray Dericiler, Nargiz Aliyeva, Yeşim Yeniyurt, Sina Khalilvandi Behrouzyar, Sinem Elmas, Nihan Birgün, Dr. Isa Emami Tabrizi, Dr. Marjan Hezarkhani, Samet Özyiğit, Büşra Çetiner, Gülayse Şahin, Selin Öykü Gündoğdu, and Mostafa Mehdipour Aghbolagh for their support, encouragement, motivation, and their friendships. Also, I would like to thank specially to İlayda Terzi for her continuous support and motivation.

I am genuinely grateful to my parents for their immeasurable support and encouragement. Finally, I would like to express my sincere gratitude to the Scientific and Technical Research Council of Turkey (TUBITAK) 1003 programme for financial support with the project number of 218M658.

To my beloved family…

TABLE OF CONTENTS

LIST OF TABLES

LIST OF FIGURES

LIST OF ABBREVIATIONS

CVD	Chemical Vapor Deposition
CNMs	Carbon-Nano Materials
CNT	Carbon Nanotubes
CO_2	Carbon dioxide
CFC	Chlorofluorocarbon
DSC	Differential Scanning Calorimetry
EDX	Energy-dispersive X-ray
FTIR	Fourier Transform Infrared Spectroscopy
GNP	Graphene Nanoplatelet
GWP	Global Warming Potential
GO	Graphene Oxide
LCA	Life Cycle Analysis
LCI	Life Cycle Inventory
LCIA	Life Cycle Impact Assessment
LLDPE	Linear Low-density polyethylene
OMMT	Organically modified montmorillonite
PA	Polyamide
PE	Polyethylene
PP	Polypropylene
PS	Polystyrene
PET	Polyethylene Terephthalate
rGO	Reduced Graphene Oxide
MWNT	Multi-walled Carbon Nanotubes
RAMAN	Renishaw inVia Reflex Raman Microscopy System
SEM	Scanning Electron Microscope
TEM	High Resolution Transmission Electron Microscope
TGA	Thermogravimetric Analysis
Tc	Crystallization Temperature
Tm	Melting Temperature
XPS	X-ray Photoelectron Spectroscopy
XRD	X-ray Diffraction

CHAPTER 1. STATE-OF-ART

Waste plastic production is an important environmental, economic, and energy issue since 80% of manufactured plastics cannot be used again and plastic materials lose 95% of their value after usage, leading to a hundred billion euros loss in the global economy every year. Recycling has become one alternative approach to solve this problem; however, the high cost of recycling and decrease in the quality of the final product makes recycling inconvenient [1]. Another approach, upcycling, is an effective way of converting waste plastic materials into value-added products. A wide range of materials has been used for upcycling, such as waste plastics (polypropylene (PP), polyethylene (PE), polystyrene (PS), polyethylene terephthalate (PET), and polyamide (PA) [2]. Among these plastics, PP is a semi-crystalline thermoplastic polymer that has been used for many applications such as packaging, car parts, and electronics industries [3] and it has attracted great interest among researchers due to its wide usage, simple and cheap production route, low density, high mechanical and chemical properties, and recyclability [4]. In particular, graphene and various carbon nanomaterials additives can be produced from waste PP by thermal treatment such as pyrolysis and carbonization.

Graphene is a formation of a single layer of carbon atoms arranged as a hexagonal lattice [5]. Due to its superior mechanical properties and large surface area, graphene has been used as a nucleating and reinforcement agent in compound production. Although graphene provides unique properties for engineering plastics, conventional production routines such as bottom-up and top-down methods are complex, provide lower yield, and have a high cost, making them unsuitable for large-scale production. Among bottom-up routines of graphene production, thermal treatment offers potential as a convenient method for large-scale graphene production, resulting in less usage of toxic chemicals and a relatively less complex production routine [6, 7]. These advantages of thermal treatment, including less hazardous graphene production techniques, can play a crucial role in sustainable production and preserving the globe from pollutant emissions.

Life cycle assessment (LCA) is a convenient way of measuring hazardous emissions and their effects on the earth. It is a method to indicate the emissions and hotspots of production methods by using a cradle-to-grave approach [8]. Identifying hotspots enables a determination of hazardous emissions for each step of the production process, potentially decreasing CO_2 emissions for future applications.

Chapter Two reviews relevant literature that indicates the conventional methods of graphene production from waste sources by upcycling and describes state of art approaches.

In chapter Three, facile and low-cost graphene synthesis was performed on a talc surface by upcycling waste PP. It was hypothesized that degradation to hydrocarbons at elevated temperatures would result in the formation of graphene on the talc surface since talc can withstand higher temperatures and its size is bigger than the graphene itself. To increase the graphene formation, Fe was used to functionalize the talc surface due to its low cost and high catalytic activity [9]. In order to observe the effect of the talc size on graphene growth, two different talc materials with different particle sizes were used for the enhancement of the graphene growth on the talc surface, and the talc surface was functionalized with iron (III) chloride chemically. Catalytic carbonization at elevated temperatures was then performed for the degradation of PP to form graphene flakes on the surface of the talc substrate. After this, the graphene grown on the talc surface was separated from the talc surface by hydrofluoric (HF) acid treatment to scrutinize the prominent characteristics of graphene.

Chapter Four compares graphene production by catalytic carbonization in a chamber furnace and by flash pyrolysis in a custom-made three zone heated rotary furnace to investigate the quality of the graphene and determine a more suitable thermal treatment technique for large scale production applications.

Chapter Five describes the performance of graphene reinforcement with two different types of PP, copolymer polypropylene (CopoPP) and homopolymer polypropylene (HomoPP), for compound production by using a custom-built thermokinetic mixer. First, non-treated micron talc and fine talc were blended to the CopoPP and HomoPP separately. Then, graphene/Fe-micron talc hybrid after catalytic carbonization and graphene/Fe-fine talc hybrid after catalytic carbonization were each reinforced to both

CopoPP and HomoPP. The effect of hybrid reinforcement on the mechanical performance of PP based composites were investigated by changing the loading ratios and comparing with neat talc reinforced composites.

Chapter Six examines and explains in detail a consequential process-oriented LCA analysis of the different production methods of the graphene production, thermal treatment and reduced graphene oxide synthesis by Hummer's method, to understand the best production method to elucidate CO_2 emissions. In addition, comparison of the of production processes by chamber furnace and rotary furnace was investigated by LCA.

Based on this work, upcycled graphene is targeted for use for lightweight car part production as a nucleating agent and reinforcer. The lightweight, low-cost production routine and superior mechanical properties of upcycled graphene not only provide a facile production for large scale applications but also will likely result in lower emission of CO_2 to the environment.

CHAPTER 2. GRAPHENE SYNTHESIS FROM WASTE SOURCES

Graphene has received great interest in the scientific research and in the industrial applications in recent years [10]. Various ways of bulk graphene production routines such as chemical synthesis of graphene oxide (GO) from graphite flakes [11], thermal treatment of reduced graphene oxide (rGO) [12], and mechanical exfoliation of graphite [13] were proposed by researchers. In addition to these production methods, top-down methods of graphene synthesis are mechanical exfoliation, graphite intercalation, nanotube slicing, reduction of GO, and electrochemical sonication, whereas, bottom-up methods are the GO synthesis by modified Hummers' method, epitaxial growth on silicon carbide (SiC), pyrolysis and chemical vapor deposition (CVD) method [14]. Among bottom-up methods, CVD allows a controlled and scalable graphene formation on substrates [15]. In the other method, modified Hummers' method, strong oxidants are used to break the weak Van der Walls bonds between the graphene layers in the graphite structure and separates the graphene from other layers. On the other hand, utilization of inorganic minerals such as clay, talc and organically modified montmorillonite (OMMT) as a substrate results in the formation of graphene flakes [16].

The most common graphene production techniques are combustion, CVD and chemical exfoliation [17]. Among them, CVD is an appropriate way to produce graphene with high surface area, defect-free structure and low cost. CVD graphene is widely used in electronic and photonic applications [18]. On the other hand, chemical exfoliation technique, enables the production of graphene as bulk in large quantities. Considering the production capacity, the chemical exfoliation technique brings advantages, however long production time and purification time increase the production cost [19]. Therefore, a new trend towards alternative methods in the production of graphene has begun. While searching for alternative methods, it has been stated that graphene can be produced from a wide range of waste materials such vegetables, animals, and plastics [20–22]. In a study, Sun *et al.* achieved porous graphene-like nanosheet synthesis with a large surface area from renewable biomass waste coconut shell by using iron (III) chloride ($FeCl_3$) as a catalysis and zinc chloride ($ZnCl_2$) as an activating agent [23]. In another study, Gong *et al.* synthesized graphene flakes by using catalytic carbonization method at 700°C on OMMT regarding PP as a carbon source [16]. Another study conducted by Jankovic *et al.* for achieving carbon nanotube growth on OMMT by loading metal oxides such as

nickel [24]. Sharma *et al.* produced deposition of graphene onto copper foil from upcycled waste PE and PS by using atmospheric pressure CVD method under quartz tube reactor at 1020°C [25]. Moreover, Lian *et al.* synthesized highly yield graphene/mesoporous carbon composites from upcycled waste PE by performing carbonization at low temperatures where magnesium carbonate and GO presented as an additive [26], while Okan *et al.* synthesized GNPs by upcycling of waste tires [27]. In another study, Huang *et al.* produced graphene and graphene quantum dots (GQDs) from pyrolyzed polyimide carbon waste by using a single step electrochemical method [28]. Mohamed *et al.* synthesized carbon dot formatted rGO and GO by upcycling waste plastics by performing catalytic pyrolysis where titatinium dioxide (TiO_2) presented as a catalysts [29]. Choi *et al.* synthesized carbon nanosheets (CNSs) from upcycled waste PP by carbonization under low temperature [30]. Zhang *et al*. synthesized iron (II,III) oxide (Fe_3O_4)/carbon nanomaterials from upcycled waste PE by thermal treatment under the presence of ferrocene as a catalysts [31].

In addition to the graphene formation, a vast amount of carbon nanotubes (CNTs) and multi-walled carbon nanotubes (MWCNTs) synthesis were stated by these methods, as well. For example, Tripathi *et al.* synthesized carbon nanofibers (CNFs) and MWCNTs from upcycled waste PE by using CVD method where the iron, nickel and chromium composed non-oxidized stainless steel CVD furnace act as a metal catalyst [32]. Hedayati *et al.* synthesized MWCNTs from upcycled waste PS by using catalytic CVD method [33]. In addition, Wu *et al.* achieved to produce high quality-CNTs from waste plastics by catalytic gasification [34]. In one of the study, Zhang *et al.* performed the production of Fe/Carbon nanotube composites from upcycled waste PP by performing catalytical pyrolysis, and in another study a high yield production of MWCNTs were produced along with hydrogen (H_2) from upcycled waste tires by performing pyrolysis-catalytic reforming and gasification where nickel/aluminum oxide (Ni/Al_2O_3) used as a catalyst [35, 36]. Another study indicates that, Yao *et al.* synthesized high yielded CNTs from upcycled waste plastics by performing two stage method consisting of pyrolysis and catalytic activity where bi-metallic Ni-Fe/γ-Al_2O_3 are used as catalysts [37]. In addition, Wang *et al.* produced MWCNTs from upcycled PP by using two-stage pyrolysis reactor with impregnated nickel catalyst and it was revealed that nickel catalyst allowed the formation of CNTs more than iron and magnesium catalysts do [38]. Bazargan *et al.* elucidated the fact that the reactor type, reaction time, type of catalysts, operating temperature and

pressure affects the size of diameter and length of the synthesized CNTs from upcycled waste plastics (PE, PP, PS, PVC) [39]. Kong *et al.* synthesized CNTs with straight and helical arrangement from upcycled PE and maleated polypropylene (MA-PP) by using catalytic pyrolysis where ferrocene act as a catalyst [40].

Based on this literature search, various production routes for graphene and CNT production from upcycling of waste plastics were stated. Utilization of waste plastics gives promising sights on facile, economical, and environmentally friendly approach of bulk graphene production and finds a solution to the global waste management problem of a gross amount of waste plastic. In conclusion, majority of engineering thermoplastics can be used as a carbon source for the graphene growth by using thermal treatment. Among these thermal treatment, pyrolysis, and CVD methods are the most preferred methods to produce graphene due to less toxic and more economical synthesis routine.

CHAPTER 3. DEVELOPMENT OF GRAPHENE/HYBRID ADDITIVE FROM WASTE PLASTICS BY UPCYCLING PROCESS

Herein, upcycled graphene production from waste polypropylene on talc surface was reported. Two different types of talc, micron talc and fine talc, were utilized as substrates for graphene growth where waste polypropylene was regarded as carbon source. In order to improve the graphene growth on talc surfaces, micron and fine talc were activated by $FeCl_3$, chemically. Both Fe-activated and non-activated talcs were used for graphene formation and the effect of activation process and talc size on graphene formation was assessed. Upcycled graphene/talc hybrids were fabricated by thermal treatment at 1000°C for 5 min. For the verification of graphene formation, upcycled graphene/talc hybrids were subjected to hydrofluoric acid (HF) treatment. Several spectroscopic, morphological and mechanical characterization of the produced graphene/talc hybrids were conducted and graphene formation on talc surfaces was proved by the help of these characterizations.

3.1. INTRODUCTION

Plastic consumption in the world has increased dramatically because plastics are widely used in packaging, construction, transportation, electrical components, etc. Disposal of plastics is of great interest since plastics are not biodegradable and the utilization of them have been boosted [16, 41]. Landfilling or incineration is used to eliminate waste plastics but unfortunately they are harmful to environment. Therefore, recycling has come into prominence to decrease the waste excess. Due to the drawbacks of recycling which are deterioration of the polymers and resulting in low molecular weight products, a new method has been developed to achieve more valuable and economically feasible products from plastic wastes. This method is called as ‘upcycling’ [42, 43]. Upcycling is an effective process altering plastic wastes to high-quality products. Upcycling of waste plastics not only enhance the value of the products by decreasing the production costs but also minimize the carbon footprint in the industry [44]. There is a wide range of waste plastics such as polyethylene (PE), polypropylene (PP), polystyrene (PS), polyethylene

terephthalate (PET), polyamide (PA), textile products, organic wastes and metal wastes used for upcycling [45].

Since reutilization of waste plastics especially PP, PS or PET to produce carbon nanomaterials allow to eliminate waste plastics in huge amounts and to obtain inexpensive sources, attention has been given to produce graphene by upcycling. Moreover, it is possible to synthesize carbon nanotubes, graphene or other carbonaceous from plastic waste materials by using the carbon contents of plastics by upcycling [43, 46]. For graphene production from waste plastics, a substrate is needed. To this end, there are some attempts for the growth of carbon structures on OMMT and zeolites. In one of the work, Gong *et al*. [16] used waste PP as raw material and it was catalyzed by OMMT to realize highly yielding graphene flakes (GFs). As described in the original article, the uniform mixture containing PP (∼89 wt %), talcum (∼11 wt %), and OMMT was placed in a crucible. The mixture was heated up to 700◦C for 15 min to obtain the carbonized char, which was then immersed in HF and HNO_3 after cooling. Impurities (e.g., MMT and talcum additives) were dissolved by HF, and amorphous carbon was oxidized by HNO_3. GFs were obtained after repeatedly centrifuging and isolating from the solution. In another work, Cui *et al*. [47] represented a solid-state CVD method for converting the plastic wastes to valuable graphene foils with high quality, less defects and very high electrical conductivity much higher than that of common free-standing graphene films treated at ultra-high temperatures. This flexible GF's structure was proper and functional for producing an anode for the fabrication of foldable Lithium-Ion Batteries (LIBs). The strategy of generating high-quality free-standing GF from plastic wastes indeed provides a trash-to-treasure way for graphene production and practical applications. Moreover, Jiang *et al.* [48] mixed melted polypropylene with a catalyst, and then heated the mixture to a temperature of 830◦C to obtain CNTs. PP/OMMT/nickel compound mixtures were combusted to synthesize MWCNTs. In this process, different nickel compounds acted as catalyst to synthesize MWCNTs in the presence of OMMT. The combustion temperature, the types, and contents of the nickel catalysts and OMMT had effects on the yield of MWCNTs. In this method, the heat gradually diffused from the surface to the core of the samples, meanwhile the degradation products of PP diffused in a reverse direction of heat diffusion and a part of them were catalyzed to form MWCNTs and hydrogen due to the presence of the degraded OMMT and Ni catalyst. Choi *et al*. [49] successfully converted the "non-carbonizable" linear low-density polyethylene (LLDPE) into an ordered carbon

by using thermal oxidation as a degradation pathway for plastics. Also, the conversion yield of this transformation reached to 50%. The graphitized LLDPE based carbon has an exceptional electrical performance, which makes it an applicable material for lithium-ion battery fabrication. In another work, Song *et al.* [50] investigated the effects of both OMMT and Ni_2O_3 on the carbonization of polypropylene during pyrolysis process. The catalyst H-MMT (montmorillonite (MMT)) that contains hydrogen protons) have an important influence on the degradation and the carbonization behavior of PP and the formation of multiwalled carbon nanotubes (MWNTs). The higher yields of MWNTs obtained by combination of OMMT and the nickel catalyst during pyrolysis process due to the acidic sites upon the H-MMT layers and the metallic Ni formed in situ from the reduction of Ni_2O_3 during the transformation of PP into MWNTs. The presence of carbenium ions as intermediates in the catalytic degradation of PP promotes the formation of MWNTs from the degradation products as carbon sources, especially those with higher carbon content. Liu *et al.* [41] provided a potential way to convert waste plastics into carbon nanomaterials and hydrogen by demonstrating a newly developed process to continuously convert PP to hydrogen and carbon materials. HZSM-5 zeolite and NiO were used as catalysts in a screw kiln reactor for degrading PP and a moving-bed reactor for decomposing the pyrolysis gas separately. The highest yield of MWNTs obtained at the decomposition temperature of 700 °C. The graphitization degree and thermal stability of the MWNTs synthesized at high decomposition temperature were higher than those at low decomposition temperatures. Bajad *et al.* [51] studied synthesis of CNTs from waste plastic by a combustion technique and using Ni/Mo/MgO as a catalyst. The amount of obtained carbon product measured the catalytic activity of three components Ni, Mo, MgO. The activity of the components is observed to be interdependent, and the component Ni is found to be more effective. Additionally, in a recent review, Berktas *et al.* concluded that upcycling of PP can yield high value products such as graphene [52].

As mentioned above, OMMT or MMT was used as a substrate for graphene production by upcycling where a waste plastic was used as a carbon source. Beyond MMT, talc can also be utilized as a substrate in upcycling process. Talc is a clay mineral which does not contain any ionic groups in its structure. It has a hydrophobic surface thus it is difficult to make a homogenous distribution of talc in polymer matrix. At low concentrations (less than 3 wt %), talc acts as a nucleating agent, reduces spherulite size and shortens processing time. On the other hand, at high loadings (10-40 wt %) it acts as a reinforcing

filler by increasing tensile modulus and stiffness, but reducing strain-to break and impact strength [53]. It has been highlighted that the nature of talc influences its reinforcement ability, depending on the surface activity, particle size, surface area, and surface functional groups [54]. The most importantly, talc is a cost-effective filler in polymer matrices compared to the other substrate materials [55]. In order to enhance the usability, performance, and efficiency of talc, some surface modifications either chemical or physical should be conducted [56].

Up to now, there is no reported paper and report about the development of graphene or fullerene or other carbon nanostructures on talc by using different waste plastic sources. The nature of talc and clay are different from each other. Carbon nanostructures are produced by replacing cations in the interlayer of montmorillonite (MMT) with cationic surfactants (such as alkyl ammonium). In the present study, talc was used as an exchanger having no ionic group. In addition, completely pure and charged talc has a hydrophobic surface chemistry, making it difficult to distribute into the polymer matrix. However, when both the surface chemistry and aspect ratio of talc are controlled, it improves the mechanical properties of commodity polymers as a reinforcement. With this study, the dimension of carbon nanostructures is tailored regarding the size of talc. The effect of chemical activation of talc with $FeCl_3$ was also considered for the upcycled graphene formation on talc surface. The obtained graphene/hybrid structures were characterized by several spectroscopic, morphologic characterizations and mechanical testing and the results were compared and explained in detail.

3.2 EXPERIMENTAL

3.2.1. Materials

Micron talc with the particle size of D_{50}=12 μm and fine talc with the particle size of D_{50}=1.9 μm and were purchased from Micron'S company (Turkey) and Imerys company (France), respectively. To fabricate graphene/talc hybrid additives, iron chloride ($FeCl_3$ (≥ 97 %)), hydrofluoric acid (HF (≥ 37 %), nitric acid (HNO_3(≥ 65%),) were purchased from Sigma-Aldrich. Polypropylene sources were provided from Ravago Company (Turkey).

3.2.2. Surface activation of talc

The performance of polymer/inorganic composites is highly dependent on the interface adhesion between the polymer and the inorganic additive. Talc, whose surface is not modified, shows insufficient physical performance when used as an additive in polymer composites. For this reason, various coupling agents (such as silanes, titanium esters, phosphates, aluminates, zirconates) are used for interface modification in the production of talc/polymer composites. In addition, there is not any ionic group in the structure of the talc additive. Completely pure talc has a hydrophobic surface chemistry, making it difficult to disperse into the polymer matrix. However, it is known that talc improves the mechanical properties of commode polymers as a reinforcing agent when both surface chemistry and aspect ratio are controlled [10]. Therefore, chemical functionalization of talc surface is very important to improve its performance and dispersion in polymer composites.

In order to activate the talc surface and initiate graphene growth, talc (30 g) was treated with 0.5 M $FeCl_3$ aqueous solution (500 ml) through refluxing at 80°C for 24 h. At the end of reaction, the temperature of reaction mixture was cooled down and vacuum filtration was applied to obtain iron treated talc samples. Then, the samples were dried at 80°C for 24 h. The same treatment procedure was applied for both fine talc and micron talc.

3.2.3. Conversion of polypropylene waste into upcycled graphene on talc surface

At this stage, iron treated talc samples were mixed with polypropylene (PP) waste at melt-phase by high shear thermokinetic mixer (Dusatec) at the temperature of 180°C and the shear rate of 4000 rpm. In order to monitor the effect of surface functionalization and talc size on the quality of graphene growth, untreated and iron treated talc samples were used to produce graphene/talc hybrid additives. After melt-mixing process, talc reinforced granules were applied by heat treatment process starting from the room temperature to 1000°C by the heating rate of 15°C/min under Argon atmosphere and the samples were kept at 1000°C for 5 min to reach efficient pyrolysis temperature for the deposition of carbon atoms in PP onto iron surface [57, 58]. After carbonization, the colors of hybrid additive from neat talc and iron treated talc became gray and black, respectively. Table 1 shows graphene/talc hybrid additives by using different talc sources.

Table 1. Graphene/talc hybrid additives by using different talc sources.

Sample	Talc type	Process type
Hybrid-1	Non-treated micron talc	Direct carbonization
Hybrid-2	Fe-treated micron talc	Catalytic carbonization
Hybrid-3	Non-treated fine talc	Direct carbonization
Hybrid-4	Fe-treated fine talc	Catalytic carbonization

In order to verify the graphene growth on the surface of each talc, acid treatment was applied as a separation technique on hybrid additives to eliminate talc from hybrid structure. The hybrid graphene/talc structure was treated with 20 wt% hydrofluoric acid mixtures for 48 h at room temperature. Then, filtration was applied to attain the treated samples and drying process was applied at 50°C for 30 min. The dried material was treated with the mixture of HNO_3: distilled water (1:2, v: v) at 110°C for 3 h through refluxing. At the end of reaction, the mixture was cooled down to room temperature and centrifugation process was applied at 7500 rpm for 15 min and samples were washed with water several times. Finally, the obtained black materials were dried at 80°C overnight.

3.2.4. Characterization

Neat and functionalized talc samples, hybrid graphene/talc additives and the separated graphene samples were characterized in detail by using spectroscopic and microscopic techniques. Fourier transform infrared spectroscopy (FT-IR) method was used to determine the surface functional groups in the graphene. The thermal properties of the samples were analyzed by TGA instrument using Mettler Toledo TGA / DSC 3+ under nitrogen atmosphere between 25°C and 1000°C to compare thermal decomposition rates and weight loss.

Raman spectroscopy was performed by using a Renishaw inVia Reflex Raman Microscope with 532 nm edge laser to investigate the molecular structure and vibrational properties of talc structures and upcycled hybrid graphene structures. X-Ray Diffraction (XRD) characterization technique was used by using a Bruker D2 Phaser diffractometer with a CuKα radiation source. Elemental analysis and chemical composition of the samples were investigated by using X-ray Photoelectron Spectroscopy (XPS, Thermo Scientific, Waltham, Massachusetts, USA) technique. Surface topography and morphology were investigated by using a Leo Supra 35VP Field Emission Scanning

Electron Microscope (SEM, Carl Zeiss AG, Jena, Germany) and Transmission Electron Microscopy (TEM, JEOL, Japan).

3.3. RESULTS and DISCUSSION

3.3.1. Structural characteristics of upcycled graphene produced by direct and catalytic carbonization processes

Figure 1 presents FTIR spectra of (a) micron talc and its graphene hybrids and (b) fine talc and its graphene hybrids after direct and catalytic carbonizations. Comparative FTIR spectra of micron talc, fine talc and their graphene hybrids are given in Figure 1. Strong bands around 963-972 cm^{-1} are associated with the stretching vibration of Si-O, which is often taken as evidence of the three-dimensional amorphous silica phase [59]. Sharp peak at 3359 cm^{-1} formed due to occurrence of -OH functional groups [60]. After the direct and catalytic carbonization, two major peaks were revealed. The sharp peaks at around 1070 cm^{-1} corresponds to the formation of Si-O-C peak after the carbonization process [61]. This appearance is evident the fact that the carbon from PP was attached to the surface of talc.

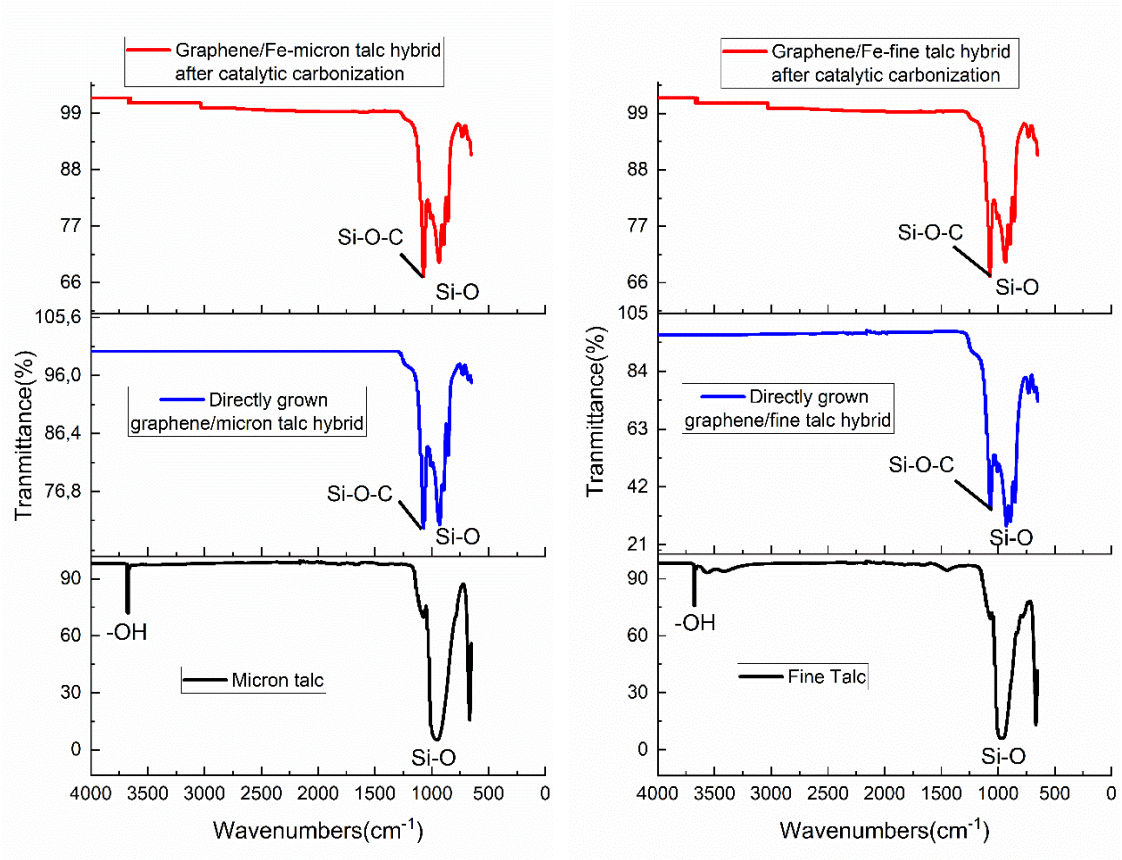

(a) **(b)**

Figure 1. FTIR spectra of (a) micron talc and its graphene hybrids and (b) fine talc and its graphene hybrids after direct and catalytic carbonizations.

Figure 2 shows comparison Raman spectra of micron talc and fine talc, their directly grown graphene/micron talc hybrid additives and graphene/Fe-micron talc hybrids after catalytic carbonization. In the Raman spectrum, D and G peaks are seen after carbonization process. It is possible to examine the change in graphene and carbon structures effectively by Raman spectroscopy. In basic principle, graphite has three basic peaks at 1348 cm^{-1}, 1577 cm^{-1}, and 2715 cm^{-1}, respectively, called as D, G and 2D. D peak is related to the irregularity caused by the errors in the structure, and the intensity of the peak increases with the number of defects in the structure [62]. G peak shows the in-plane vibrations of the sp^2 bonded carbon atoms, and the peak intensity differs according to the changes in the graphene layers. As D and G peak intensity ratios (I_D/I_G) increase, sp^2 bonds are broken, which shows that more sp^3 bonds are formed in the structure and the errors in the structure increase [28].

In the Raman spectrum of micron talc, there are four main distinct peaks at 109 cm^{-1}, 193 cm^{-1}, 361 cm^{-1} and 675 cm^{-1} with different intensities. After the carbonization process,

D peak at 1334 cm^{-1} and G peak at 1578 cm^{-1} of graphene appeared prominently and it was observed that the 2D peak also formed at 2685 cm^{-1}. The intensity of D peak increases with the increase in irregularities of graphitic materials and shifts in its conditions can be seen [63]. The quality and the number of graphene layers can be determined by the position and width of 2D peak [64]. In the Raman spectrum of fine talc, three distinct peaks at 192 cm^{-1}, 359 cm^{-1} and 674 cm^{-1} were seen. However, after carbonization process, characteristic peaks of fine talc disappeared and weak D and G peaks at 1321 cm^{-1} and 1596 cm^{-1} occurred, respectively.

HF acid treatment was applied to the graphene/Fe-micron talc hybrid after catalytic carbonization and graphene/Fe-fine talc hybrid after catalytic carbonization. After HF acid treatment to graphene/Fe-micron talc hybrid after catalytic carbonization, it was observed that the intensity of G peak increased dramatically and 2D peak became more visible. The presence and intensity of 2D peak was a proof of the successful generation of upcycled graphene. The other critical point for the comparison of structural changes after acid treatment is the disorder amount. For instance, as the structure changes from graphite to nanocrystalline graphite, I_D/I_G ratio of the crystalline structures increases. That means that it varies inversely with the size or the interdefect distance [65]. It was confirmed that multilayer graphene sheets were fabricated on Fe-micron talc after carbonization and acid treatment process via Raman spectroscopy. In addition, both in Raman spectroscopy of graphene/Fe-micron talc hybrid after catalytic carbonization and graphene obtained from HF acid treatment of graphene/Fe-fine talc hybrid after catalytic carbonization, 2D peak was clearly seen. As a result of HF acid treatment of graphene/Fe-fine talc hybrid after catalytic carbonization, the intensity of D and G peaks increased, and they existed at 1353 cm^{-1} and 1577 cm^{-1}. Moreover, 2D peak, which was a significant proof of the graphene formation, occurred at 2703 cm^{-1}. By the help of Raman spectroscopy, it can be fairly declared that multilayer graphene was generated from the pyrolysis of HomoPP/Fe-fine talc [66].

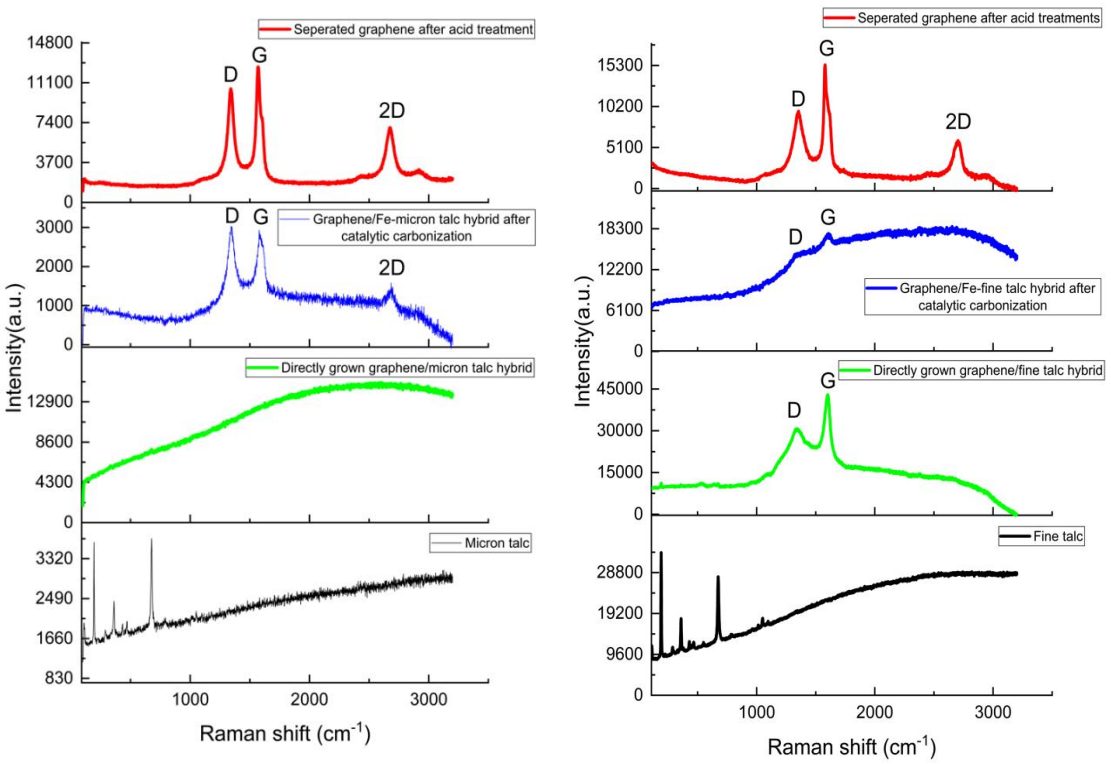

(a) (b)

Figure 2. Comparison Raman spectra of (a) micron talc, hybrid graphene/micron talc additives after direct carbonization and catalytic carbonization and its separated graphene after acid treatments and (b) fine talc, hybrid graphene/fine talc additives after direct carbonization and catalytic carbonization and its separated graphene after acid treatments.

XRD analysis was also conducted to monitor the changes in the talc structure and verify the formation of graphene by addressing main graphite peaks. XRD patterns of micron talc and fine talc, its hybrid additives and after direct carbonization and catalytic carbonization processes and their separated graphene after acid treatments are given comparatively in Figure 3. In the XRD patterns shown in Figure 3(a) and 3(b), basal planes of (001), (002), (003), (004) and (005) belong to micron talc occurred at 9◦, 18◦, 28◦, 37◦ and 48◦, respectively [67, 68]. XRD pattern of graphene/Fe-micron talc hybrid after catalytic carbonization resulted in (002) crystal peak [69] which belongs to graphene occurred at 28◦ and weak graphene peaks of (100) [70] and (004) [71] were seen at 43◦ and 54◦, respectively. In addition, the low-intensity peak seen at 43.8◦ shows the

formation of Fe-C bond. The most importantly, the formation of (002) basal plane was observed after carbonization. In the XRD pattern of the hybrid additives, the shift of the main talc peaks, the reduction of their intensities and the formation of new diffraction planes confirm the structural change. The formation of (002) peak was also observed in the XRD pattern of directly grown graphene/fine talc hybrid. As a result of carbonization, the main talc peak, (001), disappeared and high temperature let the crystalline talc to have amorphous structure. Additionally, the low-intensity (100) peak occurring at 43^{o} indicates the formation of turbostratic graphene [47].

After HF acid treatment, in the XRD patterns shown in Figure 3(a) and 3(b), the intensity of the (002) peak increased dramatically. However, it was also seen that some talc remained in the structure. This is due to the strong chemical interactions happened during carbonization and causes the talc not to be completely removed from the structure. In the XRD pattern of graphene/Fe-fine talc hybrid after catalytic carbonization, the main talc peak (001) disappeared, and the crystalline structure of talc turned to be amorphous. The low-intensity (100) peak at 43° indicated the formation of turbostratic graphene [72]. Moreover, after HF acid treatment, the characteristic (002) peak of graphene peak was seen at 29◦ indicating that the obtained upcycled graphene structure was crystalline. However, new compounds based on Mg and Si were formed due to the excessive binding of fluorine to the structure. Moreover, the crystal structures of the particles were studied to predict both the crystal phase and texture and understand whether the graphene planes run parallel to the substrate surface. After acid treatment, it was observed that (002) peak belonging graphene was appeared in the XRD of separated graphene. The intensities of the (002) peak of graphene/Fe-micron talc hybrid after HF acid treatment was determined as 192 while it was 5.65 for graphene/Fe-fine talc hybrid after HF acid treatment. It showed that Fe-micron talc supplied more possibility for the graphene growth on it compared to Fe-fine talc surface.

Layer numbers of graphene/ talc hybrids can be calculated by using Debye-Scherer equation [73].

$$D = \frac{0.89\,\lambda}{\beta_{002}\,cos\theta_{002}} \tag{1}$$

$$n = \frac{D}{d_{002}} + 1 \tag{2}$$

In the equation, D (nm) means the average crystallite size whereas λ (Å) is X-ray wavelength, K is Scherrer constant, β (°) is FWHM (Full Width at Half Maximum) of XRD peak and n is the number of layers.

XRD result revealed that graphene obtained from the acid treatment of graphene/Fe-micron talc hybrid after catalytic carbonization had a d-spacing of 3.40 nm at 2θ ~ 26(⁰). The graphene layer number was calculated as 17 layers of graphene sheets for graphene/Fe-micron talc, whereas graphene obtained from the acid treatment of graphene/Fe-fine talc hybrid after catalytic carbonization revealed 13 layers of graphene sheets.

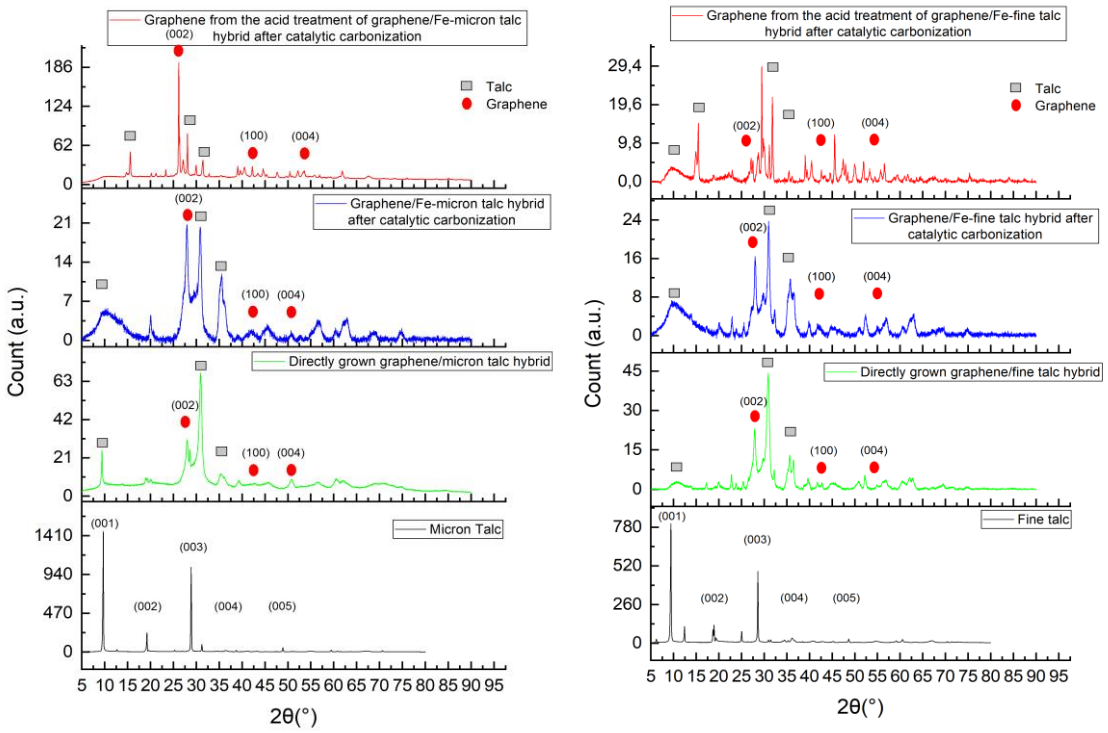

(a) (b)

Figure 3. Comparison XRD patterns of (a) micron talc and its hybrid additive and (b) fine talc and its hybrid additive after direct carbonization and catalytic carbonization and their separated graphenes after acid treatments.

3.3.2. Investigation of chemical compositions of hybrid and separated graphene sheets

XPS is a useful technique for analyzing the molecular structure and elemental composition of the samples. In Table 2 and Table 3, XPS characterization results of

micron talc, directly grown graphene/micron talc hybrid, graphene/Fe-micron talc hybrid after catalytic carbonization and fine talc, directly grown graphene/fine talc hybrid and graphene/Fe-fine talc hybrid after catalytic carbonization, respectively. In micron talc, the percentage of oxygen (O) and silicon (Si) were high. An increase in the carbon (C) ratio was determined after mixing HomoPP with talc by thermokinetic mixer. When the direct carbonization and catalytic carbonization conducted in the presence of iron, it was seen that C ratio in the hybrid structures obtained by catalytic carbonization was higher than the one produced by direct carbonization. This showed that catalytic carbonization triggered the accumulation of carbon atoms from the plastic source on iron and the formation of planar carbon structures [64].

Table 2. XPS elemental analysis of neat micron talc, hybrid graphene/talc additives and graphene obtained from the acid treatment of hybrids.

Sample	**C (at%)**	**O (at%)**	**Si (at%)**	**Fe (at%)**	**Mg (at%)**	**Ca (at%)**	**Others (at%)**
Micron talc	-	52.72	21.66	-	18.69	6.93	-
Directly grown graphene/micron talc hybrid	8.71	56.67	28.20	-	6.42	-	-
Graphene/Fe-micron talc hybrid after catalytic carbonization	24.23	48.46	20.35	1.21	3.10	-	-
Graphene from graphene/Fe-micron talc hybrid after acid treatment	56.89	12.49	-	-	6.6	2.95	21.06

Table 3. XPS elemental analysis of neat fine talc, hybrid graphene/talc additives and graphene obtained from the acid treatment of HomoPP/Fe-fine talc.

Sample	**C (at%)**	**O (at%)**	**Si (at%)**	**Fe (at%)**	**Mg (at%)**	**Ca (at%)**	**Others (at%)**
Fine talc	-	58.97	23.90	-	17.12	-	-
Directly grown graphene/fine talc hybrid	10.46	56.23	27.17	-	6.15	-	-
Graphene/Fe-fine talc hybrid after catalytic carbonization	7.81	56.44	26.90	1.86	6.99	-	-
Graphene from graphene/Fe-fine talc hybrid after catalytic carbonization	51.55	20.77	2.54	-	6.28	-	18.87

C1s, O1s and Fe2p signals were measured for the detection of functional groups on the surface of the samples, and the type of bonds according to their binding energies and their atomic percentage distribution were determined. Figure 4 reveals XPS deconvolution peaks of directly grown graphene/micron talc hybrid, (a) C1s, (b) O1s and graphene/Fe-micron talc hybrid after catalytic carbonization (c) C1s, (d) O1s, and (e)Fe2p. Four main C1s peaks in Figure 4(a), illustrated C1s spectrum of directly grown graphene/micron talc hybrid revealing three main peaks at around 284 eV, 285 eV, and 287 eV which corresponds to the sp^2, sp^3 hybridization, and C=O functional groups, respectively. In Figure 4(b), O1s spectrum showed that formation C-O and C=O bonding occurred at binding energies of 532.3 eV, and 531.8 eV, respectively. Moreover, Figure 4(d), O1s signal displayed the O-C, C-O, and C=O bonds at 533 eV, 532.2 eV, and 531.2 eV, respectively. Figure 4(e), various iron bondings were occurred after catalytic carbonization. Graphene/Fe-micron talc hybrid after catalytic carbonization revealed iron bondings as Fe^{+2} at 710 eV, Fe-$2p_{3/2}$ at 712 eV, Fe^{+3} at 715 eV, $Fe2p_{1/2}$ at 724 eV[74].

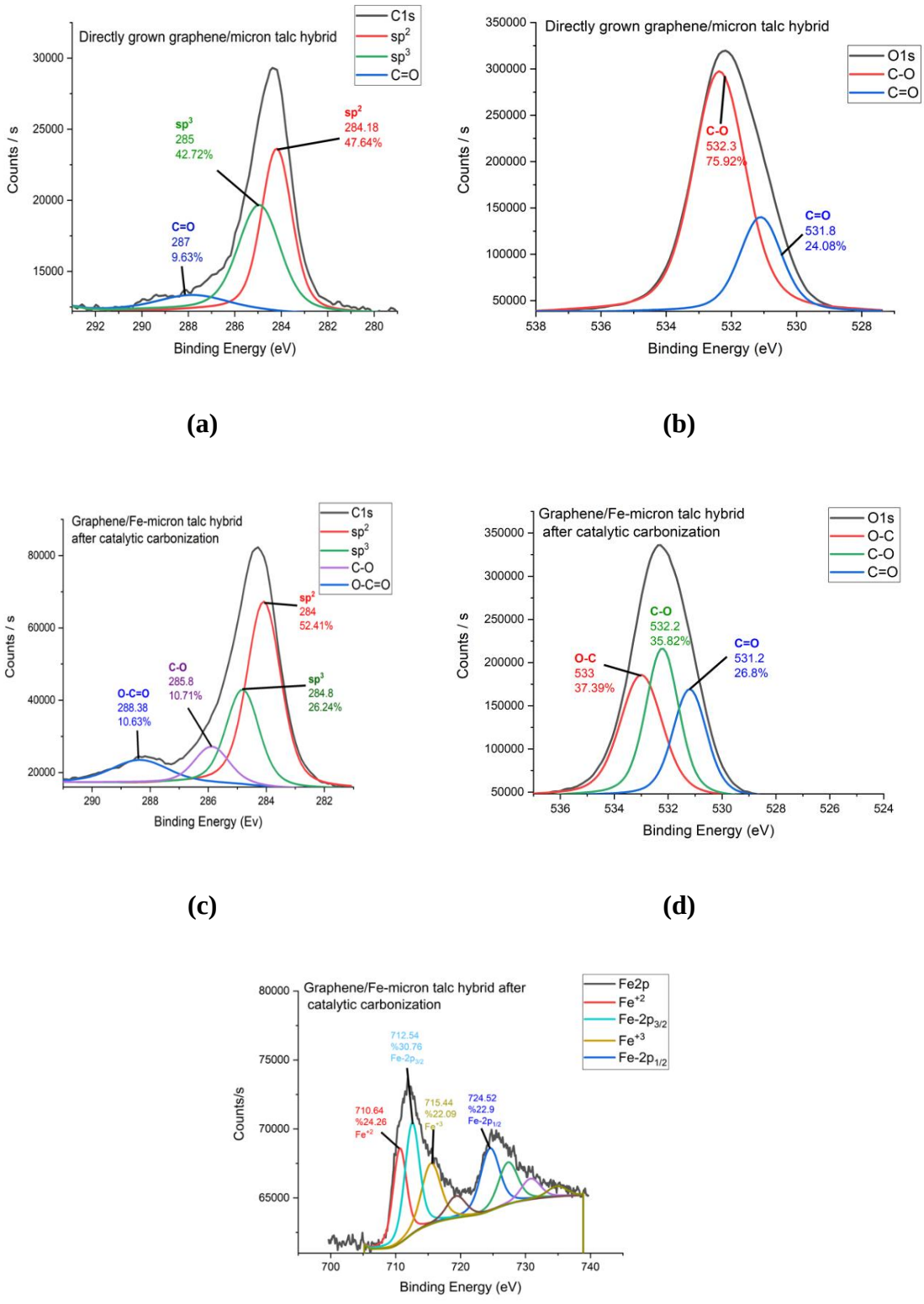

Figure 4. XPS deconvolution peaks of (a) C1s, (b) O1s directly grown graphene/micron talc hybrid and (c) C1s, (d) O1s, and (e) Fe2p graphene/Fe-micron talc hybrid after catalytic carbonization.

Figure 5 represents the C1s and O1s XPS deconvolution peaks of directly grown graphene/fine talc hybrid and graphene/Fe-fine talc hybrid after catalytic carbonization. Figure 5(a) illustrates C1s spectrum of directly grown graphene/fine talc hybrid resulting in three peaks at 284.34 eV, 285.78 eV, and 288.81 eV corresponding to the sp^2 hybridization, C-O, and O-C=O functional groups [75]. Moreover, Figure 5(b), illustrates that O1s spectrum of directly grown graphene/fine talc hybrid of three peaks at around 530 eV, 531 eV, and 532 eV belonging to the O-C, C=O, and C-O functional groups. In C1s spectrum of graphene/Fe-fine talc hybrid after catalytic carbonization, there were three peaks of 284.34 eV, 285.76 eV, and 288.53 eV corresponding to the sp^2 hybridization, C-O, and O-C=O functional groups. In addition, Figure 5(d), pointed the formation of C-O-Fe bonding at 531.03 eV, and C-O bonding formation at 532.29 eV. Moreover, Figure 5(e), Fe2p spectrum demonstrated that, $Fe^{+2}2p^{3/2}$ at 711 eV, Fe^{3+} $2p^{3/2}$ at 713 eV, $Fe2p^{3/2}$ at 724 eV occurred for graphene/Fe-fine talc hybrid after catalytic carbonization [74]. Therefore, it can be concluded that, Fe attached to the surface of the talc.

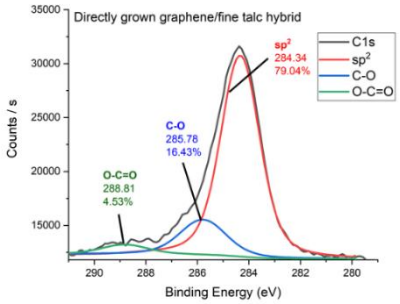

(a)

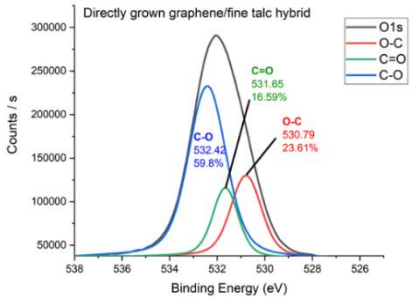

(b)

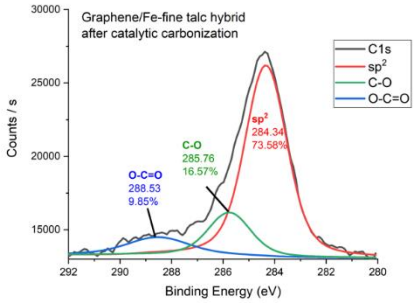

(c)

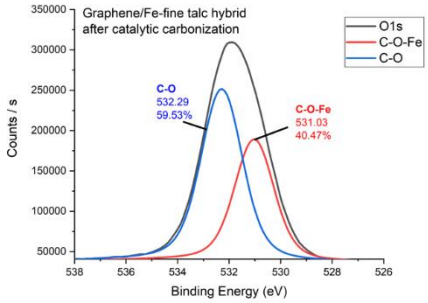

(d)

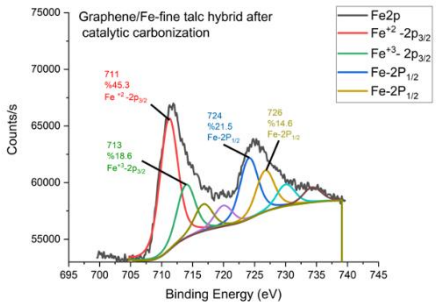

(e)

Figure 5. XPS deconvolution peaks (a) C1s and (b) O1s of directly growngraphene/fine talc hybrid, (c) C1s, (d) O1s, and (e) Fe2p of graphene/Fe-fine talc hybrid after catalytic carbonization.

Figure 6 demonstrates XPS deconvolution peaks of graphene from the acid treatment of graphene/Fe-micron talc hybrid after catalytic carbonization (a) C1s and (b) O1s, and graphene obtained from the acid treatment of graphene/Fe-fine talc hybrid after catalytic carbonization (c) C1s and (d) O1s. C1 spectrum demonstrated that, graphene obtained from the acid treatment of graphene/Fe-micron talc hybrid after catalytic carbonization had two main peaks of sp^2, and one sp^3 hybridization with values of 31.66%, 26.17%, and 18.1% as well as C-O-C, O-C=O functional groups with the values of 11.81% and 9.02% [75]. In addition, an excess amount of C-F bonding formation obtained. Peaks at around 285.9 eV, 288 eV, and 291 eV revealed the occurrence of functional groups of C-O, O-C=O, and C-F, respectively. Furthermore, O1s showed the formation of C-O, and C=O at 532.8 eV, and 531.2 eV [76, 77]. Moreover, XPS deconvolution peaks of graphene obtained from acid treatment of graphene/Fe-fine talc hybrid after catalytic carbonization. The formation of sp^2, sp^2, and sp^3 hybridization were observed at 283.8 eV,284.29 eV, and 284.8 eV, respectively. Moreover, peaks at around 284 eV, 285.76 eV, and 288.53 eV displayed the occurrence of functional groups of C-O, O-C=O. Moreover, oxygen bonding of C=O, and C-O were seen.

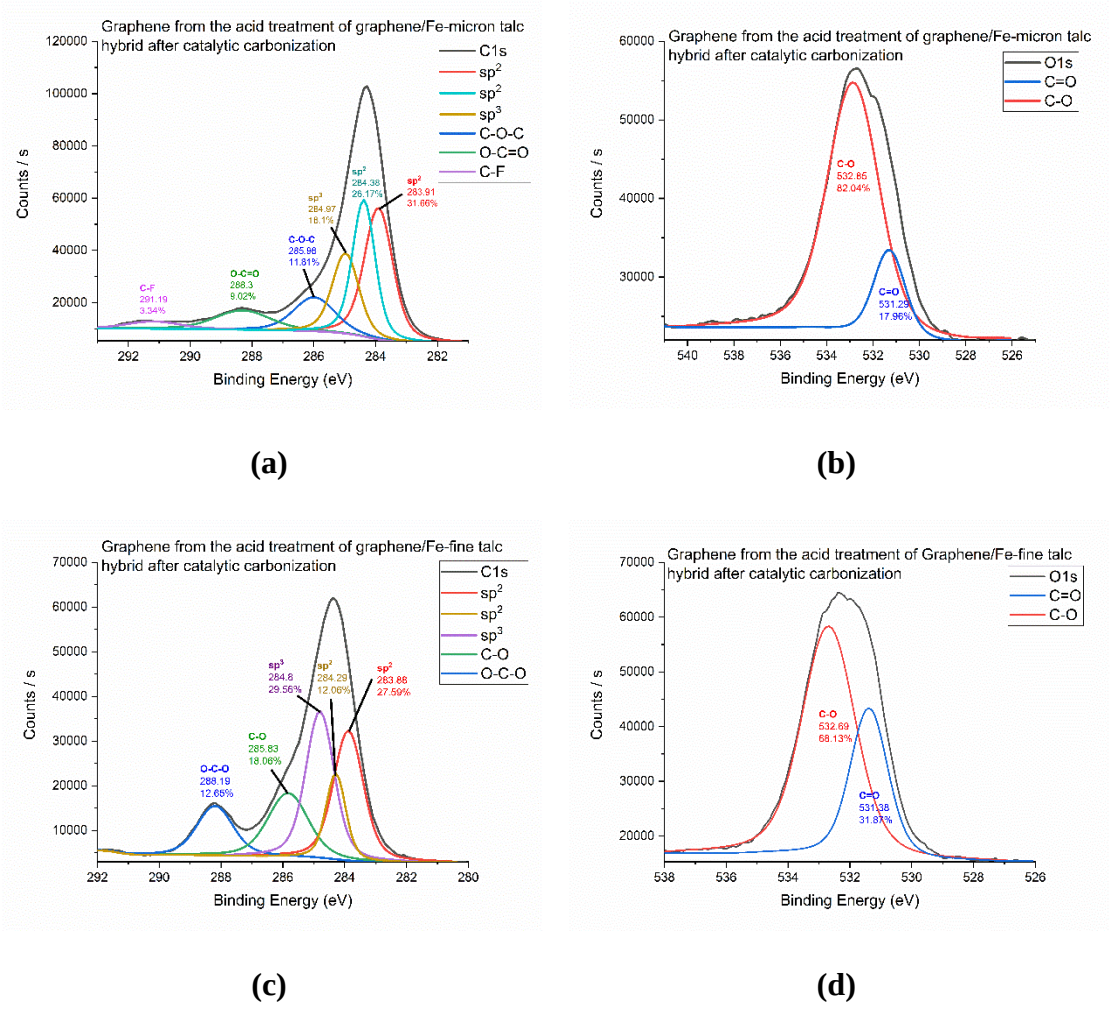

Figure 6. XPS deconvolution peaks of (a) C1s and (b)O1s graphene from the acid treatment of graphene/Fe-micron talc hybrid after catalytic carbonization and (c) C1s and (d) O1s graphene obtained from the acid treatment of graphene/Fe-fine talc hybrid after catalytic carbonization.

3.3.3. Morphological properties of 2D and 3D grown graphene on talc substrates

The morphological features of upcycled graphene/talc hybrid additives and separated graphene structures after acid treatments were investigated systematically by SEM and TEM in order to monitor the graphene growing mechanisms on the different size of talc substrates. Figure 7 and 8 represents SEM images of untreated micron talc and fine talc, its graphene hybrid additives after direct and catalytic carbonization processes. There is no difference in the morphological structure of hybrids between direct carbonization and virgin form. It was clear that the lamellar structure of talc was preserved after carbonization process.

As seen in SEM images, both SEM images of micron talc and fine talc have the lamellar structures. The only difference on the morphology of micron talc and fine talc was the particle size.

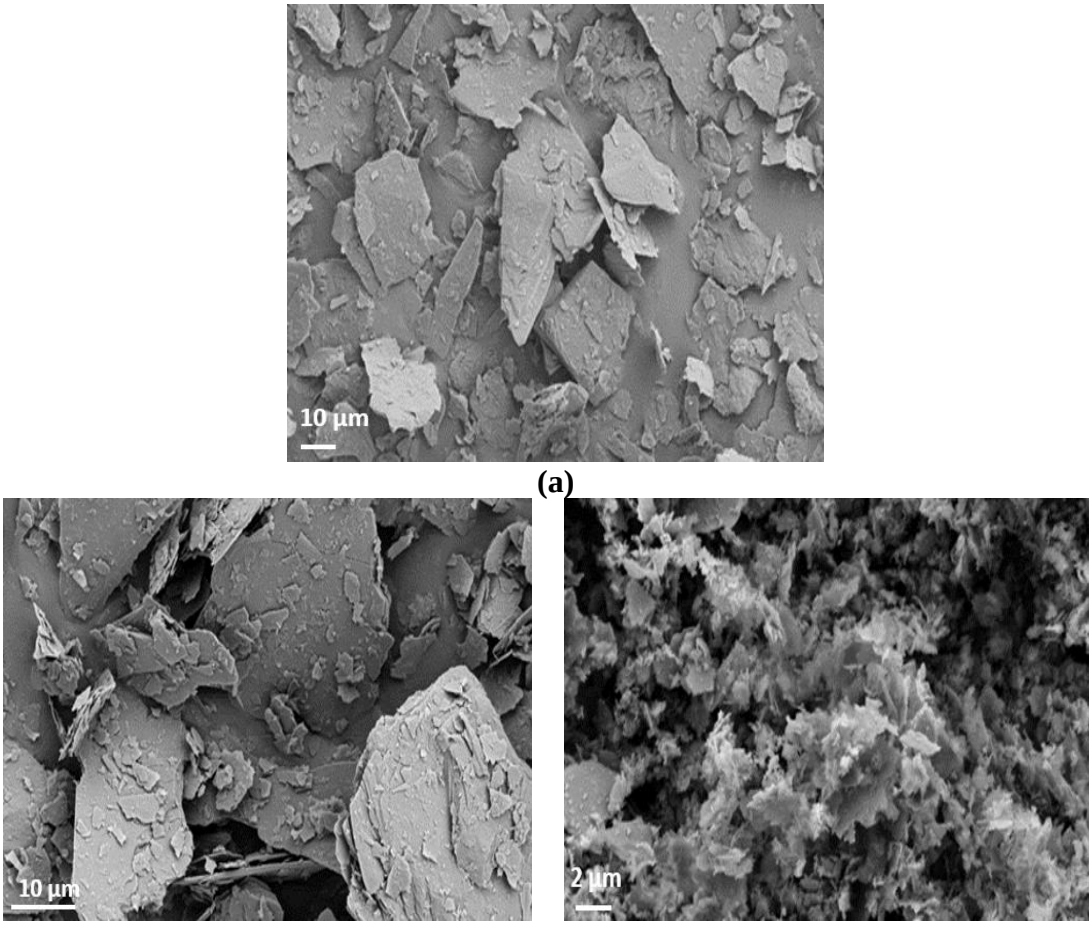

Figure 7. SEM images of (a) untreated micron talc, (b) upcycled graphene/micron talc hybrid material after direct carbonization, and (c) upcycled graphene/talc hybrid materials after catalytic carbonization.

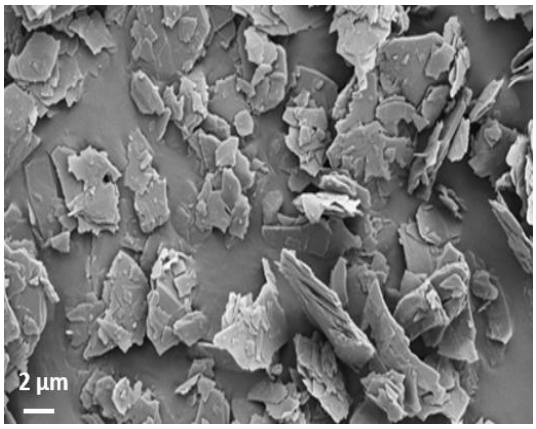

(a)

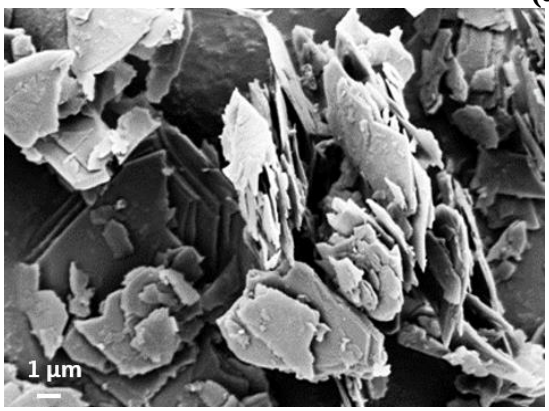

(b)

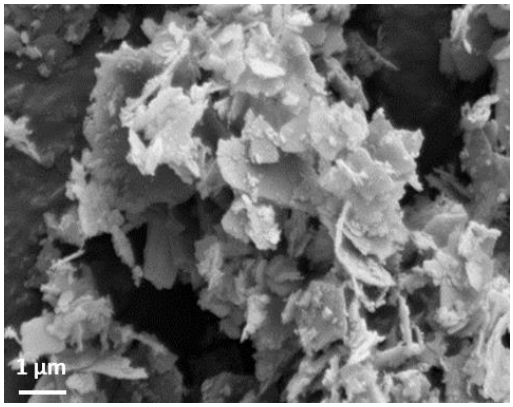

(c)

Figure 8. SEM images of (a) untreated fine talc, (b) upcycled graphene hybrid/fine talc from direct carbonization, and (c) upcycled graphene hybrid/fine talc after catalytic carbonization.

In addition to that, SEM images of upcycled graphene after HF acid treatment of graphene/Fe-micron talc hybrid after catalytic carbonization and graphene after HF acid treatment of graphene/Fe-fine talc hybrid after catalytic carbonization are given in Figure 9. It was seen from the SEM images that the upcycled graphene obtained from the acid treatment of graphene/Fe-fine talc hybrid after catalytic carbonization, had a clustered and spherical structure whereas upcycled graphene obtained from the acid treatment of graphene/Fe-micron talc hybrid after catalytic carbonization was in a layered form.

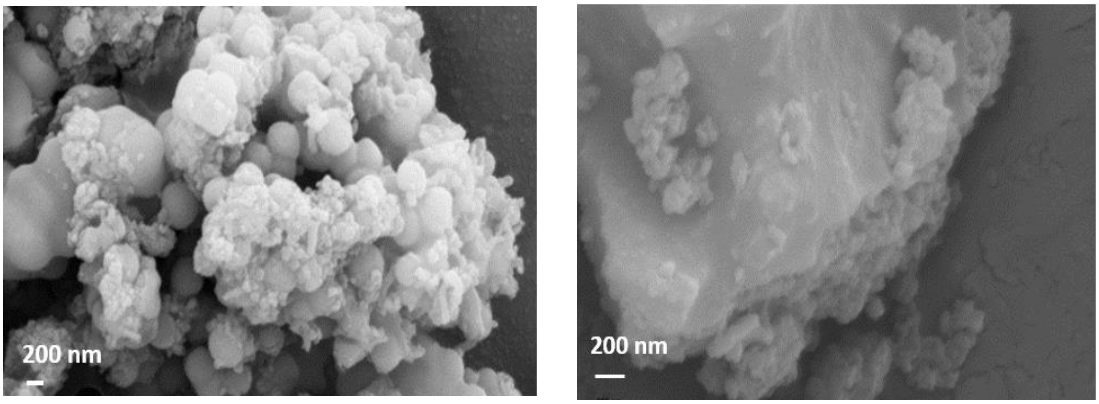

(a) **(b)**

Figure 9. SEM images of separated graphene structures from (a) graphene/Fe-fine talc and (b) graphene/Fe-micron talc after acid treatments.

In order to understand and explain the size and morphological features of the produced nanostructures, TEM characterization was applied to graphene structures obtained after HF acid treatment of micron talc and fine talc-based hybrid additives. TEM images of upcycled graphene layers grown on Fe-micron talc surface and lattice fringes at different magnifications and upcycled graphene spheres grown on Fe-fine talc surface and lattice fringes at different magnifications are given in Figure 10 and Figure 11, respectively. TEM can also be used to determine the planes existing perpendicular to substrate surface and to measure the interplanetary spacing of the lattice fringes which were in crystalline particles [78]. Figure 11 reveals that the graphene has plate like structure. The size of the graphene was calculated as 200-400 nm by using Image program while the distance between the graphene sheets was approximately 0.21 nm. However, this value was calculated as 0.34 nm by considering the peak (002) existing in XRD. On the other hand, Figure 12, reveals TEM images of 3D graphene spheres grown on Fe-fine talc by PP waste revealed spherical shape graphene formation where distance between the graphene sheets was approximately 0.18 nm and the diameters of the spheres varies from 0.2 μm to 0.4 μm.

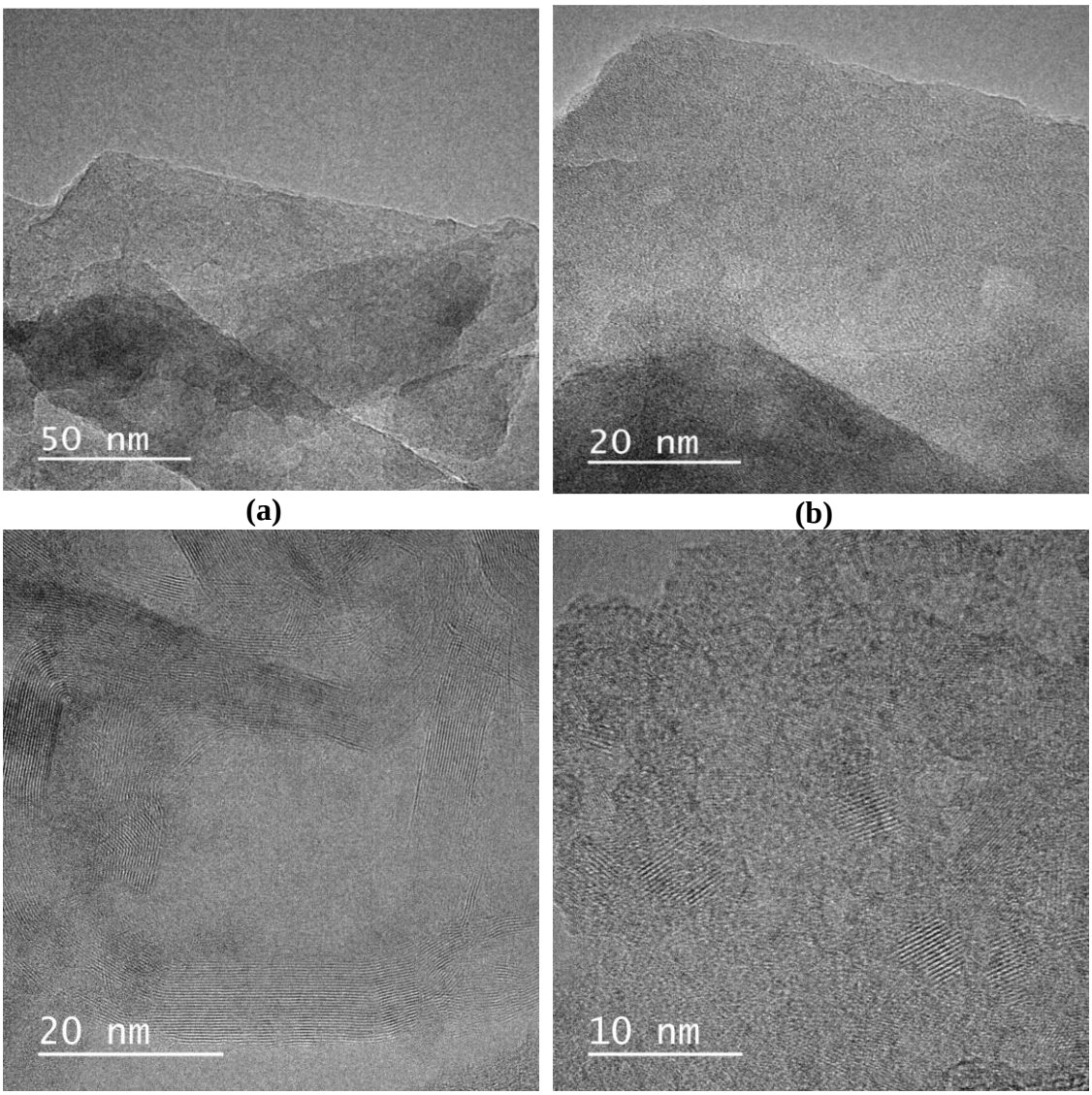

Figure 10. (a) and (b) TEM images of 2D graphene sheets grown on Fe-micron talc by PP waste; (c) and (d) lattice fringes at different magnifications.

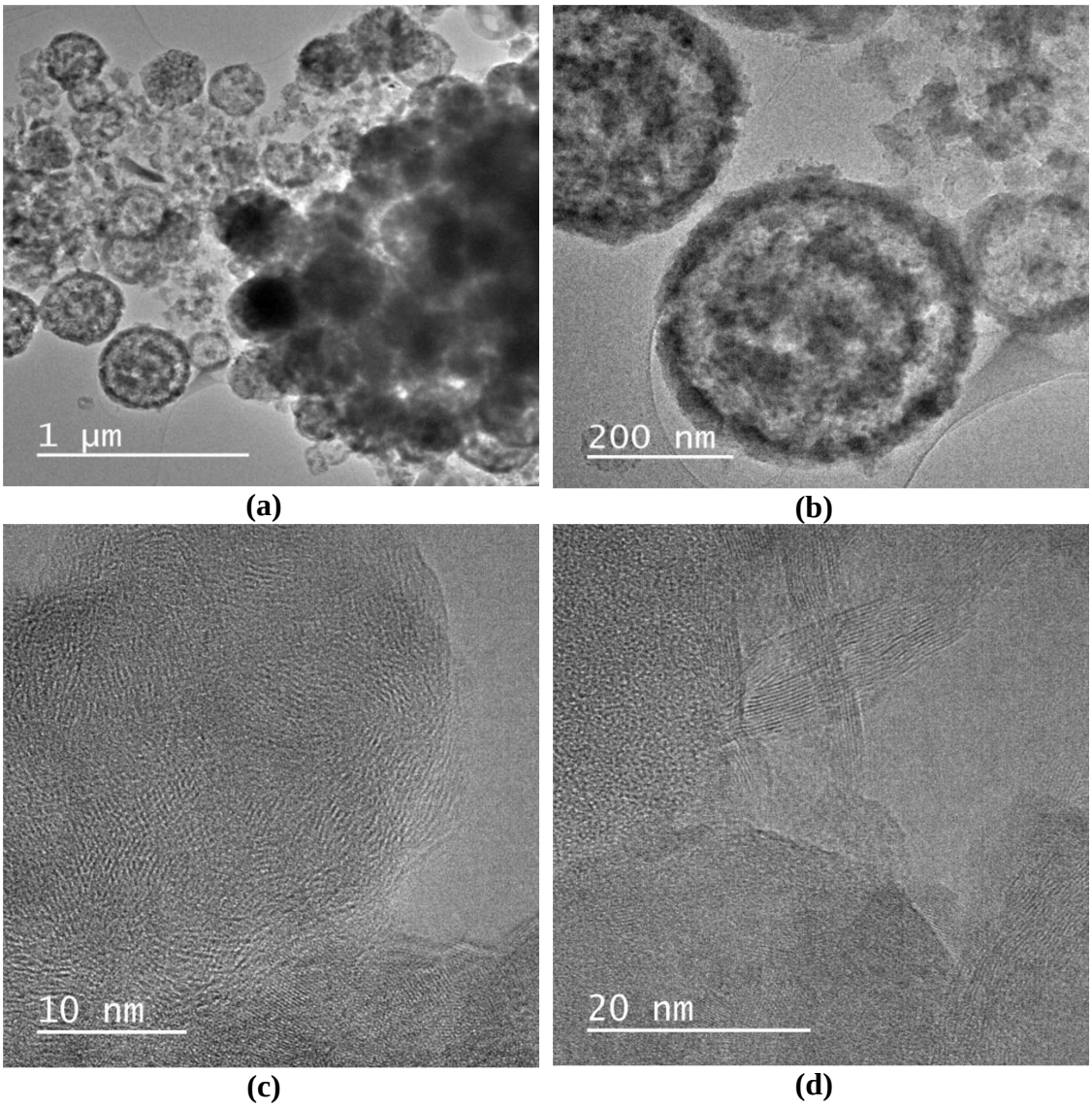

Figure 11. (a) and (b) TEM images of 3D graphene spheres grown on Fe-fine talc by PP waste; (c) and (d) lattice fringes at different magnifications.

3.3.4. Thermal properties of graphene grown on talc surface

Figure 12 shows TGA curves of (a) micron talc and its graphene hybrid additives and (b) fine talc and its graphene hybrid additives after direct and catalytic carbonizations. No weight lost occurred for micron talc at 500^{o}C, while a 4.1% decrease occurred at 1000^{o}C and fine talc lost 0.1% of its weight at 500^{o}C, and 7.2% at 1000^{o}C. Although directly grown graphene/micron talc hybrid and directly grown graphene/fine talc hybrid lost 0.2% and 0.3% its weight at 1000^{o}C, respectively, no loss of weight was observed after the graphene/Fe-micron talc hybrid after catalytic carbonization and graphene/Fe-fine talc hybrid after catalytic carbonization. The increase in the weight in Figure 12 can be explained as the oxidation of the graphene/Fe-micron talc hybrid after catalytic

carbonization, and graphene/Fe-fine talc hybrid after catalytic carbonization might occurred during heating or nitrogen might reacted with graphene/ Fe-talc hybrids and caused the formation of some compounds.

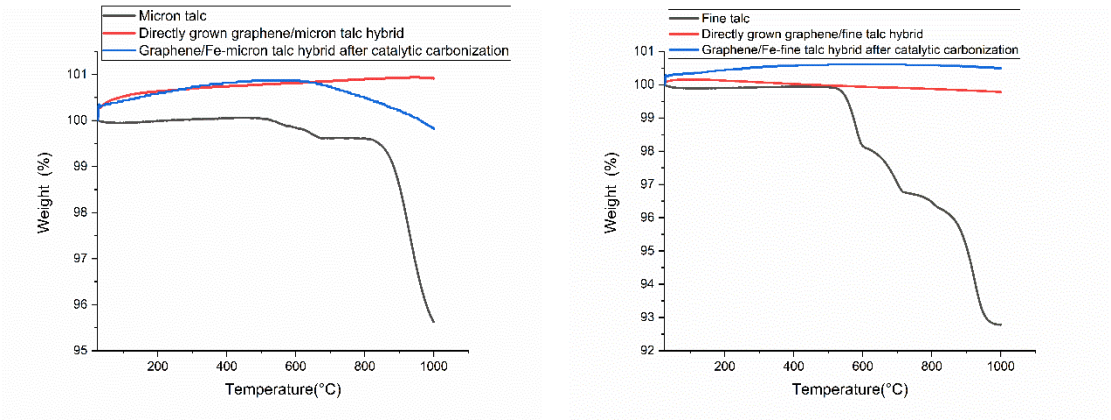

(a) **(b)**

Figure 12. TGA curves of (a) micron talc and its graphene hybrid additives and (b) fine talc and its graphene hybrid additives after direct and catalytic carbonizations.

3.4. CONCLUSION

In this study, upcycled graphene growth on different size of talcs, micron talc and fine talc, was achieved by the application of thermal treatment. In the literature, graphene growth on MMT, OMMT or other substrates was performed. However, the novelty of this study was performing the graphene growth on talc surface instead of the substrates used in the previous studies and examine the effect of talc size on the performance of graphene production. In order to enhance the graphene growth on talc surface, it was activated by $FeCl_3$ chemically since the natural talc surface is hydrophobic. By the activation, the homogeneous dispersion of talc could be achieved in polymer matrices. The activated and non-activated micron talc and fine talc were blended with waste PP, separately in the ratio of 20:80 wt % and subjected to pyrolysis for 5 min at 1000°C. Moreover, for graphene separation after pyrolysis, acid treatment was applied to graphene/talc hybrids. For the verification of upcycled graphene production, several characterization techniques were used. In the XRD patterns, it was seen that characteristic graphene plane of (002) was observed after both catalytic and direct carbonization. Moreover, the intensity of prominent the (002) peak increased after HF acid treatment of

upcycled graphene/talc hybrids. In addition to Debye-Scherrer equation, it was approved that multilayer graphene sheets were obtained after carbonization processes. The number of graphene layers was calculated as 17 for graphene/Fe-micron talc and 13 for graphene/Fe-fine talc. The formation of graphene was also seen via Raman characterization. Raman spectra of all graphene/talc hybrids revealed three prominent D, G, and 2D graphene bands after carbonization process. Furthermore, 2D bands of graphene/talc hybrids became more visible after HF acid treatment and the intensity of G and 2D peak increased dramatically in graphene/Fe-micron talc hybrid after HF acid treatment. XPS elemental analysis revealed the sp^2 band formation of upcycled graphene. SEM and TEM images revealed the plate like and sphere formation of graphene/Fe-micron talc and graphene/Fe-fine talc, respectively. The distance between the graphene layers was calculated as 0.21 while the size of the spheres was changed between 200-400 nm.

CHAPTER 4. THE EFFECT OF HEAT TREATMENT AND PROCESS TYPE ON THE CHARACTERISTICS OF GRAPHENE GROWN ON TALC

In this study, upcycled graphene production from waste PP on Fe-micron talc surface by using both direct carbonization (in chamber furnace) and flash pyrolysis (in rotary furnace) was conducted, and the effect of heat treatment and polymer processing techniques before carbonization on the resultant graphene was evaluated. The carbonization temperature was adjusted as 1000°C for both direct and flash carbonization. Afterward, the separation of upcycled graphene from Fe-micron talc surface, graphene/Fe-micron talc hybrids, obtained from direct and flash carbonization, were subjected to HF acid treatment. Graphene/Fe-micron talc hybrids and separated graphene were analyzed by XRD and Raman characterization, spectroscopically and by SEM, morphologically. According to the characterization results, it was observed that flash pyrolysis was much more effective than the direct carbonization process for the graphene formation on Fe-micron talc surface.

4.1. INTRODUCTION

As a versatile two-dimensional material, Graphene has attracted great interest in the research community due to its high mechanical stiffness, great flexibility, and stable chemical properties [5]. Based on the properties of graphene and its nano-scale thickness, it has been selected as an appropriate material for various applications in electrical, chemical, mechanical, optical, and catalysis industries. However, high production cost and energy consumption are main drawbacks in large scale graphene production [79]. There are various ways to facilitate graphene production such as top-down, mechanical exfoliation, and bottom-up approaches, chemical synthesis [15]. In the literature, there are various attempts to produce GO sheets from graphite by using Hummers' technique [80] and modify the reaction steps to increase the yield of GO. Kaur *et al.* used a facile method of breaking the weak Van der Waals forces between graphite flakes by using concentrated H_2SO_4 and $KMnO_4$ resulting in high yield GO production [81]. In addition, Alam *et al.* synthesized GO with high yield and lower toxic emissions by using modified Hummers' method in the presence of H_2SO_4, $KMnO_4$, and H_3PO_4 [82].

Instead of the aforementioned methods, graphene is also synthesized from waste plastics by applying upcycling methods. For the conversion of plastics wastes into carbon based nanomaterials, pyrolysis [83] and CVD methods [25] are the most preferred production methods. For instance, Pandey *et al.* synthesized graphene nanosheets from upcycled waste plastics by slow-rate pyrolysis followed by heat treatment where bentonite nano clay used as a graphene growth template [84]. In addition, Ruan *et al.* demonstrated the graphene growth on copper foil from waste polystyrene by using CVD technique in quartz tube reactor at 1050^{o}C [21]. Essawy *et al.* synthesized graphene from waste PET bottles by applying pyrolysis at 800^{o}C for 1 h [85]. However, long-time pyrolysis process is not convenient for large-scale graphene manufacturing due to high energy and time consumption. On the other hand, flash pyrolysis becomes a more facile, scalable, and cheap production method for scaling up graphene in a short time [86].

In this section, the effect of heat treatment process on the formation of graphene on the Fe-micron talc surface was investigated to get an ideal graphene production by upcycling technology. Flash pyrolysis by the rotary furnace and direct carbonization by the chamber furnace were applied to increase the yield of production. In addition, the effects of polymer processing techniques before carbonization process and the shear rates on the characteristics of upcycled graphene grown on the surface of Fe-micron talc were examined to monitor the changes in crystalline planes of the produced hybrid additives. A detailed characterization and comparison study was carried out to explain the properties of upcycled graphene on Fe-micron talc surface.

4.2. EXPERIMENTAL

4.2.1. Materials

Micron talc with the particle size of D_{50}=12 μm was purchased from Micron'S company (Turkey). To fabricate graphene/talc hybrid additives, iron chloride ($FeCl_3$ (≥ 97 %)), hydrofluoric acid (HF (≥ 37 %), nitric acid (HNO_3 (≥ 65%),) were purchased from Sigma-Aldrich. Polypropylene sources were provided from Ravago Company (Turkey). Custom made three-zone rotary furnace purchased from Protherm company (USA) was used for the carbonization.

4.2.2. Surface activation of talc

Surface activation of talc was achieved by chemical functionalization of micron talc with $FeCl_3$. 30 g of micron talc was treated with 500 ml of $FeCl_3$ aqueous solution through

refluxing at 80ºC for 24 h. At the end of reaction, the temperature of reaction mixture was cooled down and vacuum filtration was applied to obtain iron treated talc samples. Then, the samples were dried at 80°C for 24 h. Surface activation carries significant importance during graphene growth process on the iron treated talc surface to increase the selectivity of three-dimensional nano- or submicron-sized graphene structures.

4.2.3. Conversion of polypropylene waste into upcycled graphene on talc surface

Iron treated talc samples were mixed with polypropylene (PP) waste at melt-phase by a twin-screw extruder at the temperature of 228◦C and the screw speed of 349 rpm. In order to monitor the effect of surface functionalization of the talc on the quality of graphene growth, iron treated talc samples were used to produce graphene/talc hybrid additives. After extrusion process, the resulting compound was subjected to ball milling to convert the compound into powder form for ease of feeding to rotary furnace. Two different heat treatment processes were applied on the samples obtained from thermokinetic mixer and twin-screw extrusion processes: catalytic carbonization by chamber furnace and flash pyrolysis by rotary furnace. Talc reinforced granules were applied to heat treatment process starting from the room temperature to 1000◦C by the heating rate of 15◦C/min under Argon atmosphere and the samples were kept at 1000◦C for 5 min in chamber furnace to reach efficient pyrolysis temperature for the deposition of carbon atoms in PP onto iron surface [57, 58]. Moreover, talc reinforced granules were subjected to flash pyrolysis where they were fed to the three-zone rotary furnace at 1000◦C under argon atmosphere and the samples were kept at 1000◦C for 10 min.

Figure 13 illustrates the images of chamber and rotary furnaces. Rotating chamber and adjustable incline ability of the rotary furnace allow more iron treated talc sample feeding to the furnace and continuous graphene/talc hybrid additives production. Table 4 shows graphene/talc hybrid additive production by using different furnaces.

Table 4 indicates the carbonization of Graphene/ Fe-micron talc hybrid (raw material was obtained from extruder) in the rotary and the chamber furnace.

Table 4. Graphene/talc hybrid additives by using different furnaces.

Sample	Furnace type	Duration at 1000°C (min)
Graphene/ Fe-micron talc hybrid (raw material was obtained from extruder)	Rotary furnace	10 min
Graphene/Fe-micron talc hybrid (raw material was obtained from extruder)	Chamber furnace	5 min

(a) (b)

Figure 13. Photographs of (a) chamber furnace and (b) rotary furnace.

Moreover, the effect of polymer processing on the formation of graphene structures during carbonization was evaluated. At this step, HomoPP and Fe-micron talc samples were mixed in the ratio of 80:20 wt% by using a thermokinetic mixer and an extruder, then carbonized at 1000◦C for 5 min in the chamber furnace. Table 5 summarizes the graphene/Fe-micron talc hybrids using different polymer processing techniques.

Table 5. Graphene/Fe-micron talc hybrids by using different polymer processing techniques.

Sample	Furnace type	Duration at 1000ºC (min)
Graphene/Fe-micron talc hybrid (raw material was obtained from thermokinetic mixer)	Chamber furnace	5
Graphene/Fe-micron talc hybrid (raw material was obtained from twin-screw extruder)	Chamber furnace	5

In order to verify the graphene growth on the surface of talc, acid treatment was applied as a separation technique on hybrid additives to eliminate talc from the hybrid structure. The hybrid graphene/talc structure was treated with 20 wt% HF mixtures for 48 h at room temperature. Then, filtration was applied to attain the treated samples, and drying process was applied at 50°C for 30 min. The dried material was treated with the mixture of HNO_3: distilled water (1:2, v: v) at 110°C for 3 h through refluxing. At the end of reaction, the mixture was cooled down to room temperature, and centrifugation process was applied at 7500 rpm for 15 min, and samples were washed with water several times. Finally, the obtained black materials were dried in an oven at 80°C overnight.

4.2.4. Characterization

Hybrid graphene/talc additives and the separated graphene samples were characterized in detail by using spectroscopic and microscopic techniques. Raman spectroscopy was performed using a Renishaw inVia Reflex Raman Microscope with 532 nm edge laser to investigate the molecular structure and vibrational properties of talc structures and upcycled hybrid graphene structures. X-Ray Diffraction (XRD) characterization technique was performed by using a Bruker D2 Phaser diffractometer with a CuKα radiation source. Elemental analysis and chemical composition of the samples were investigated by using X-ray Photoelectron Spectroscopy (XPS, Thermo Scientific, Waltham, Massachusetts, USA) technique. Surface topography and morphology were investigated using a Leo Supra 35VP Field Emission Scanning Electron Microscope

(SEM, Carl Zeiss AG, Jena, Germany) and Transmission Electron Microscopy (TEM, JEOL, Japan).

4.3. RESULTS and DISCUSSION

4.3.1. Structural characteristics of upcycled graphene/talc hybrid additives produced by catalytic and flash pyrolysis processes

Raman spectroscopy is a practical, sensitive, and fast characterization technique for the determination of graphene formation, functional groups, structural changes, number of graphene layers, properties, quality, and by-products of the obtained graphene [87, 88].The G and 2G modes are the significant bands for interpreting the graphene formation, whereas 2G band is mostly referred as 2D band [88]. In addition, D band is also important for the evaluation of structural defects in the graphene [16, 89]. The Raman D band originates from partially disordered sp^2 bonded carbon atoms, and the intensity of D band increases by the increase in the irregularity and that are exist in the structure [63]. The G peak belongs to the first-order scattering of the in-plane vibrations of the sp^2 carbon atoms and the degree of graphitization [16].The 2D band is the second-order of zone-boundary phonons, and it is a fingerprint for the number of graphene layers [89]. Indeed, the band intensities and variations in the positions are affected by the number of graphene layers, doping, and laser excitation energy. In particular, the 2D band is influenced significantly by the C-C bond strength and electron-electron interactions [88]. Figure 14 (a) shows Raman spectra of micron talc, carbonized HomoPP/Fe-micron talc after thermokinetic mixing, in chamber furnace, and carbonized HomoPP/Fe-micron talc after extrusion, in chamber furnace. In basic principle, graphite has three peaks at 1348 cm^{-1}, 1577 cm^{-1}, and 2715 cm^{-1}, respectively, called as D, G and 2D.

After the thermokinetic mixing, the carbonization in the chamber furnace revealed the D peak at 1343 cm^{-1} and G peak at 1583 cm^{-1} of graphene prominently, and it was observed that the 2D peak also formed at 2675 cm^{-1}. On the other hand, after extrusion, the carbonization in the chamber furnace revealed the D peak at 1345 cm^{-1}, and the G peak at 1586 cm^{-1} of graphene appeared prominently, and it was observed that the 2D peak also formed at 2680 cm^{-1}. The intensity of the D peak increases with the increase in irregularities of graphitic materials, and shifts in its conditions can be seen [63]. I_D/I_G ratio of carbonization of HomoPP/Fe-micron talc after thermokinetic mixing calculated as 1

whereas after carbonization of HomoPP/Fe-micron talc after extrusion it was 1.34. The quality and the number of graphene layers can be determined by the position and width of 2D peak [64]. I_{2D}/I_G ratio of carbonization of HomoPP/Fe-micron talc after thermokinetic mixing was calculated as 0.54 whereas after carbonization of HomoPP/Fe-micron talc after extrusion, it was 0.47. When examined, it is understood from the I_{2D}/I_G ratios that both HomoPP/Fe-micron talc carbonized after extrusion and HomoPP/Fe-micron talc carbonized after thermokinetic mixer have a multilayer graphene structure [66]. It is seen that the defects in the structure of HomoPP/Fe-micron talc carbonized after thermokinetic mixing are less than the defects in the structure of HomoPP/Fe-micron talc carbonized after extrusion. In summary, differences were also detected in the Raman spectrum of the hybrid produced with the raw material obtained from different polymer processing techniques. The fact that the rpm speeds in the twin-screw extruder was very low compared to the thermokinetic mixer preserved the crystal structure of the talc, and it was determined that the 2D peak was more prominent. Figure 14(b) shows Raman spectrums of micron talc, carbonized HomoPP/Fe-micron talc in chamber furnace, and carbonized HomoPP/Fe-micron talc in rotary furnace. As can be seen from Figure 14(b), prominent D, G, and 2D peaks of graphene appeared at 1339 cm^{-1}, 1597cm^{-1} and 2694 cm^{-1} [26]. Although, after the carbonization process carried out in the rotary furnace, it is seen that the G peak is higher in intensity than the D peak in the Raman spectrum; The situation is opposite in the Raman spectrum resulting from the carbonization process carried out in the chamber furnace. As it is mentioned before, the D band shows the defects in the structure, while the G band shows the sp^2 planar configuration of graphene. In other words, higher intensity G band formation can be interpreted as the carbons being bonded to form a graphene structure. I_D/I_G ratio of carbonization of HomoPP/Fe-micron talc in rotary furnace calculated as 0.94, whereas after carbonization of HomoPP/Fe-micron talc in the chamber furnace, it was 1.37. I_{2D}/I_G ratio of carbonization of HomoPP/Fe-micron talc in rotary furnace calculated as 0.43 whereas after carbonization of HomoPP/Fe-micron talc in chamber furnace it was 0.49.

XRD analysis was also conducted to monitor the changes in the talc structure and verify the formation of graphene by addressing prominent graphite peaks. XRD patterns of micron talc, carbonized HomoPP/Fe-micron talc after thermokinetic mixing, chamber furnace, and carbonized HomoPP/Fe-micron talc after extrusion in chamber furnace are given comparatively in Figure 14(b). In the XRD patterns shown in Figure 14(c), basal

planes of (001), (002), (003), (004), and (005) belong to micron talc occurred at 9◦, 18◦, 28◦, 37◦, and 48◦, respectively [67, 68]. XRD pattern of carbonized HomoPP/Fe-micron talc hybrid resulted in (002) crystal peak [69] which belongs to graphene occurred at 28◦ and weak graphene peaks of (100) [70] and (004) [71] were seen at 43◦ and 54◦, respectively . In addition, the low-intensity peak seen at 43.8◦ shows the formation of Fe-C bond. In the XRD pattern of the hybrid additives, the shift of the main talc peaks, the reduction of their intensities and the formation of new diffraction planes confirm the structural change. Additionally, the low-intensity (100) peak occurring at 43◦ indicates the formation of turbostratic graphene [47].

It is clearly seen that the intensity of the (002) basal plane of graphene is higher in the XRD pattern of the material obtained as a result of the carbonization of the compound produced by the thermokinetic mixer. On the other hand, after the carbonization process of HomoPP/Fe-micron talc produced with the twin-screw extruder, it was determined that the characteristic peaks of the talc were seen more clearly. In particular, the peak of talc (001) appears to be prominent in the hybrid additive produced by the extruder. In the hybrid obtained from the raw material produced with a thermokinetic mixer, the (001) peak disappeared. In this case, it was determined that during the mixing of talc with polymer at high shear rates, the talc was also exfoliated, and its planar structure changed, and the peak intensities were reduced compared to those of produced after extrusion. As a result, the lamellar and layered structure of talc exfoliates like graphite at high shear speeds. This causes the structure to become thinner. Figure 14(d) illustrates the XRD characterization of micron talc, carbonized HomoPP/ Fe-micron talc in chamber furnace, and carbonized HomoPP/ Fe-micron talc in rotary furnace. Carbonized HomoPP/Fe-micron talc in the chamber furnace, (002) crystal peak of graphene occurred at 28°, and weak graphene peaks at 43° and 54° (100), and (400) formed respectively. In the carbonization process performed in the rotary furnace, the peak appeared at 43°, indicating the formation of turbostratic graphene. In addition, a sharp and intense peak belonging to micron talc is observed at 9° in the carbonization process carried out in the rotary furnace. This peak indicates that the micron talc structure is not completely disintegrated. It can be clearly seen from Figure 14(d) that in the carbonization process carried out in the rotary furnace, the intensity of the (002) graphene peak is higher. At the same time, the intensity of the (001) peak belonging to micron talc was increased after the carbonization process in the rotary furnace.

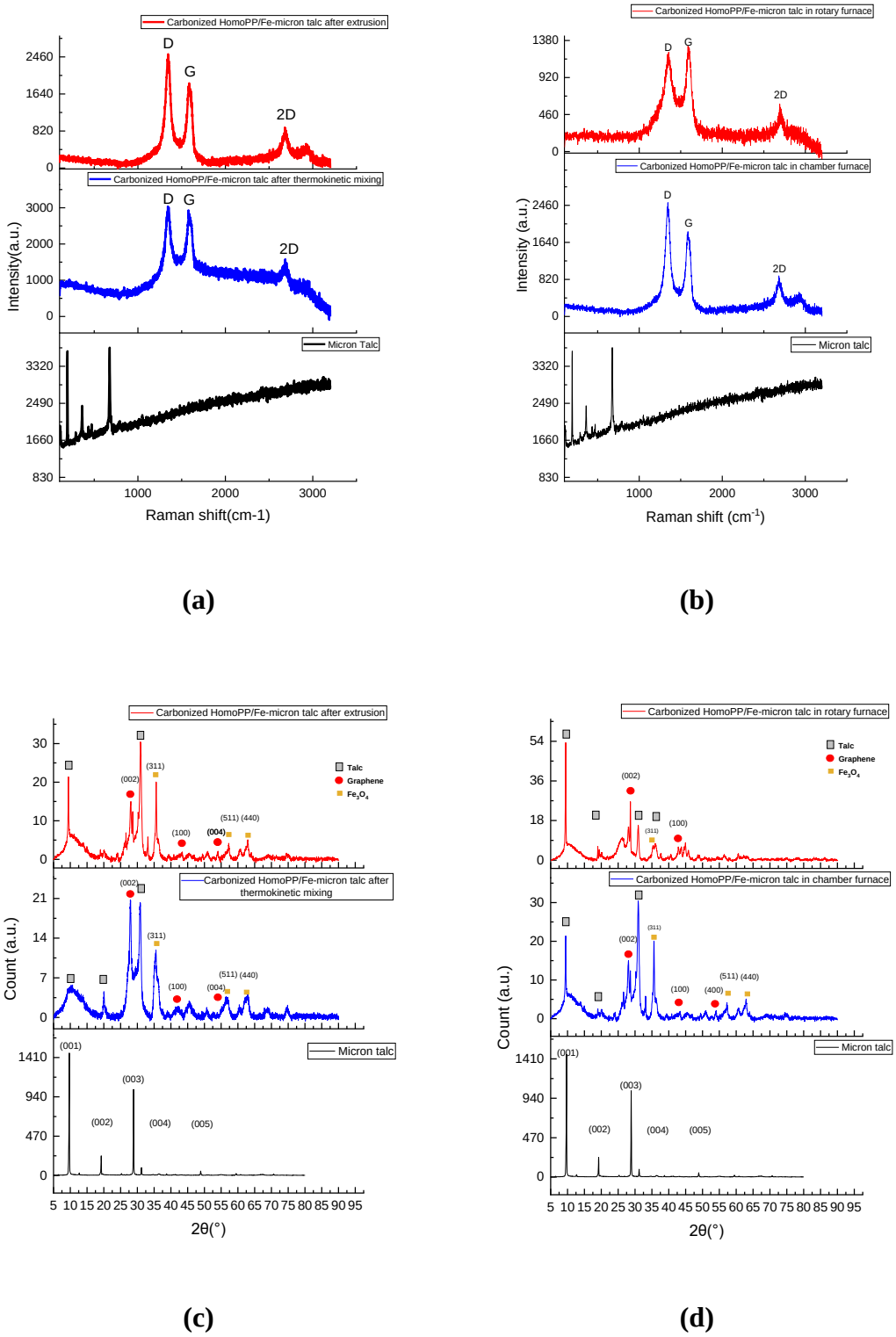

Figure 14. Comparison Raman spectra of (a) micron talc, carbonized HomoPP/ Fe-micron talc after thermokinetic mixing, in chamber furnace, and carbonized HomoPP/ Fe-micron talc after extrusion, in chamber furnace, and (b) micron talc, carbonized HomoPP/ Fe-micron talc in chamber furnace, and carbonized HomoPP/ Fe-micron talc in rotary furnace, XRD patterns of (c) micron talc, carbonized HomoPP/ Fe-micron talc

after thermokinetic mixing, in chamber furnace, and carbonized HomoPP/ Fe-micron talc after extrusion, in chamber furnace, and (d) micron talc, carbonized HomoPP/ Fe-micron talc in chamber furnace, and carbonized HomoPP/ Fe-micron talc in rotary furnace.

4.3.2. Morphological properties of hybrid graphene/talc additives obtained by different heat treatments

The morphological properties of separated graphene structures from Fe-micron talc-based hybrid additives after acid treatment were investigated by SEM characterization as given in Figure 15. Graphene growth mechanisms were evaluated regarding the heat treatment types. After catalytic carbonization in chamber furnace, lamellar structures are densely observed in Figures 15(a) and 15(b). On the other hand, spherical and tubular structures were formed after flash pyrolysis process as seen in Figures 15(c) and 15(d), but there are some platelet structures in SEM images. This indicates that the acid treatment process is not effective in eliminating the talc from the hybrid structure completely. To sum up, the fast pyrolysis process leads to the formation of 3D structures, whereas catalytic carbonization started at room temperature and heated up to 1000^{o}C with the controlled heating ramp rate preserves 2D structure of talc and graphene growth is occurred in 2D forms.

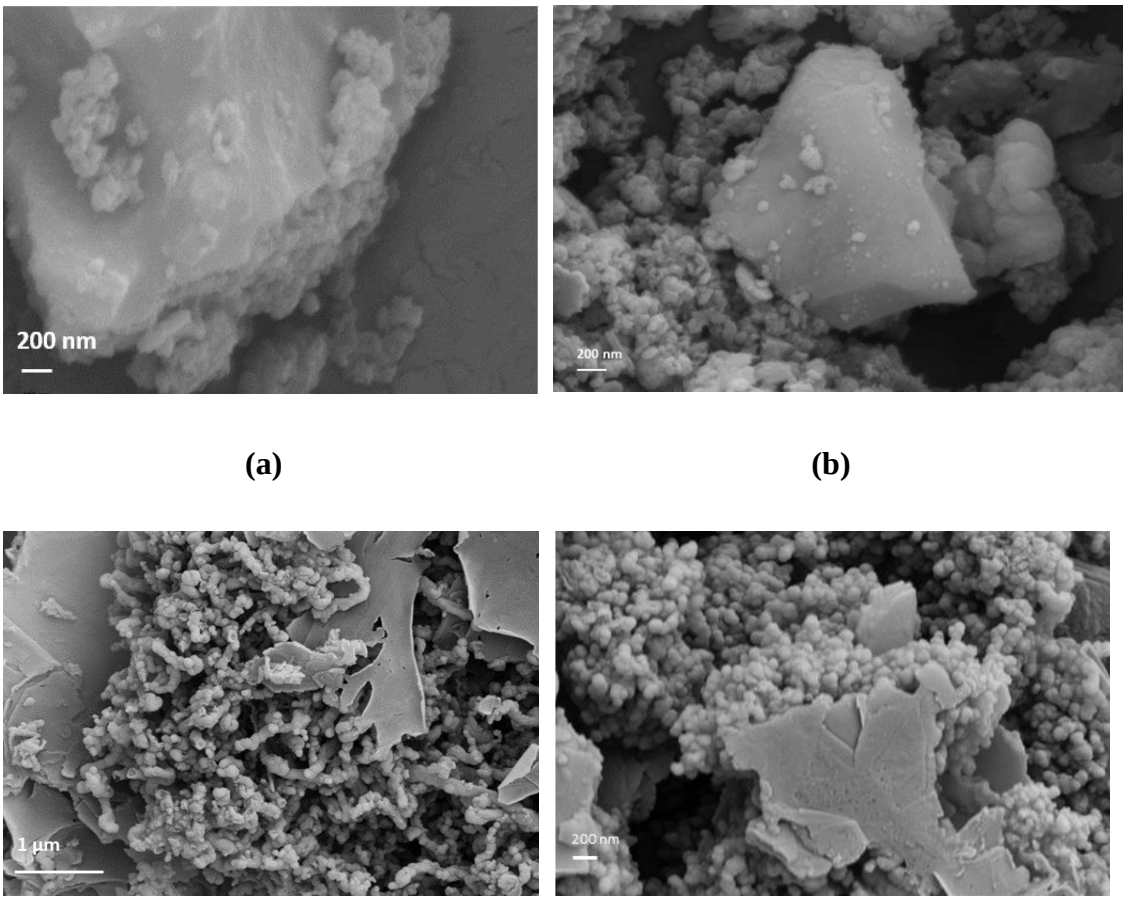

Figure 15. SEM images of separated graphene structures from Fe-micron talc-based hybrid additives obtained by (a) and (b) catalytic carbonization in chamber furnace, and (c) and (d) flash pyrolysis in rotary furnace.

4.4. CONCLUSION

In this study, upcycled graphene growth on Fe-micron talc from waste PP was achieved by both direct and flash pyrolysis at 1000◦C and the influence of heat treatment process on the resultant graphene yield was evaluated. Furthermore, the effect of polymer processing techniques the formation of upcycled graphene on Fe-micron talc in chamber furnace was examined. Prior to carbonization in chamber furnace, HomoPP and Fe-micron talc were mixed in the ratio of 80:20 wt% by using two processing techniques: thermokinetic mixing at 4000 rpm and 180◦C, and twin-screw extrusion at 349 rpm and 228◦C. The upcycled graphene formation was proved by XRD, Raman, and SEM characterizations.

CHAPTER 5. FABRICATION OF GRAPHENE/TALC HYBRID ADDITIVE REINFORCED POLYPROPYLENE THERMOPLASTIC COMPOSITES

In this study, micron talc, fine talc, and their graphene/talc hybrid additives obtained by catalytic carbonization and using polymer sources coming from thermokinetic mixer were mixed with CopoPP and HomoPP polymers at different loading ratios by thermokinetic mixer. Herein, CopoPP and HomoPP polymers were selected based on automotive OEM standards and the selected parts. The details of target compounds used in serial part production are given in Table 6.

Table 6. The details of target compounds used in serial part production.

Parts	**Compound used in serial production**	**Details**
Part 1-exterior part	%20 talc reinforced HomoPP	The amount of use of this type of raw material per vehicle is approximately 4 kg.
Part 2-interior part	%15 talc reinforced CopoPP	The amount of use of this type of raw material per vehicle is approximately 7 kg.

A detailed comparison was carried out to investigate the effect of neat talc addition and hybrid graphene/talc reinforcement on tensile and flexural properties of HomoPP and CopoPP polymer matrices with various filler ratios.

5.1. INTRODUCTION

Polypropylene is a semicrystalline thermoplastic polymer that has been utilized in a variety of applications, including packaging, automotive components, and electronics [3]. PP polymers have taken attention in various industrial applications due to their easy and inexpensive manufacturing process, recyclability, low density, and strong mechanical and chemical characteristics [4], and PP production accounts for 60% of all polyolefin that are produced [90]. Also, PP polymer can be mixed with different additives for the development of compound formulations. Blending techniques such as melt-mixing [91], solid state shear mixing [92] of PP with several fillers affect the final mechanical properties the resultant compound and also the production cost [93]. Fillers such as talc, calcium carbonate ($CaCO_3$), and glass fibers are the most widely used in PP blends.

Among them, platelet-like geometry and nucleating effect of talc make it a favorable reinforcer [94]. If the talc is added to the polymer matrix in the amount of 10-40 wt %, it is considered as a reinforcing agent, while it acts as a nucleating agent when it is incorporated into polymer matrix less than 3% [95]. While the talc addition into polymer matrix is compatible, the other fillers, like carbon-based materials has some limitations on compatibility, which means that the resultant compound suffers from low homogeneity in mixing and poor interfacial adhesion between the nanomaterial and matrix of the polymer [27]. Although filler addition is advantageous for mechanical improvements, there are other ways to increase polymers' mechanical properties by co-monomer addition. Randomly oriented addition of Co-monomers such as ethylene is used to produce copolymers. Co-monomer addition to polypropylene is advantageous due to properties such as moderate to low impact strength, relative softness, and lower sealing temperatures [96]. The length and inclusion of side chains has a significant impact on chain entanglement, crystallization of backbone, and mechanical properties [97]. Therefore, addition of co-monomers and fillers has been performed to produce PP with enhanced mechanical properties. Among these additions for mechanical improvement, the mixing techniques become crucial. Solution mixing, in situ polymerization, and melt compounding are just a few of the composite manufacturing processes that have been utilized to make PP/graphene composites. In addition to that, an increasing amount of interest has been given to using high-quality/functional carbon-based nanofillers such as graphene, carbon nanotubes, and micro-scale fillers such as carbon fibers to reinforce the PP [98].

Graphene is a 2D material formed by sp^2 hybridization of carbon atoms as one atom thick layer as a hexagonal shape [99]. Having superior mechanical properties (modulus of elasticity ~1TPa) [100], high thermal conductivity (5000 W/mK) [101], large surface area (2630 m^2/g) [102], and outstanding electron mobility (250,000 cm2/V s) [103] properties of graphene led the graphene to be one of the most studied material in decades. There have been studies that indicate the graphene nanoplatelets (GNPs) enhance the mechanical properties such as tensile strength and tensile modulus of PP [104][105][106]. Zanjani *et al.* obtained an increase of Chord modulus and flexural strength with 33.6%, and 22.5 %, respectively, with an addition of 5 wt% GNP to HomoPP matrix. Furthermore, an increase of Chord modulus and flexural strength with 31.9%, and 20.8 %, respectively, were obtained with an addition of 5 wt% GNP to Copolymer PP(Copo-

PP) matrix [27]. In addition, Ghasemi *et al.* elucidate that although the addition of talc increases the tensile properties of the polymer, it decreases the impact strength. Moreover, the addition of GNPs with 0.75 wt% enhances the tensile properties. After that amount, the increase did not obtain because of the agglomeration of GNPs [93].

In this chapter, the composites are produced by high-shear mixing technique by blending talc with PP and blending Graphene/talc hybrid additives with PP by adding various filling ratios to elucidate the increase in the mechanical properties. A detailed comparison of the effect of talc addition and graphene reinforcement to HomoPP and CopoPP with various filling ratios for tensile, flexural properties is performed. The novelty of the study is that the graphene growth on talc surface was performed by carbonization of PP, and the resulting graphene/talc hybrid was blended with polypropylene directly.

5.2. EXPERIMENTAL

5.2.1. Materials

CAPILENE® TR 50 Copo PP and BUPLEN® Homo PP were received from Ravago Petrochemical Company.

5.2.2. Fabrication of PP composites by thermokinetic mixing

In order to make a comparative study, neat fine talc and neat micron talc and their hybrid additives were mixed with HomoPP and CopoPP at four different loading rates of 5, 10, 15, and 20 wt % by using high shear thermokinetic mixer (Dusatec) at the temperature of 180◦C and the shear rate of 4000 rpm. Table 7 summarizes the details of graphene/talc hybrid additives produced from micron talc and fine talc.

Table 7. The details of graphene/talc hybrid additives produced from micron talc and fine talc.

Sample	Additive type
Hybrid-1	Graphene/Fe-micron talc hybrid after catalytic carbonization
Hybrid-2	Graphene/Fe-fine talc hybrid after catalytic carbonization

5.2.3. Characterization

For mechanical testing, the test specimens were prepared by injection moulding (Xplore, Sittard, The Netherlands). For the mechanical test analysis of HomoPP and CopoPP composites prepared with a thermokinetic mixer, tensile and flexural test specimens were prepared in accordance with ISO 527-2 and ISO 178, respectively. For ISO 527-2 tensile and ISO 178 flexural tests, a 5982 Static Universal Testing Machine (UTM, Instron, Norwood, MA, USA) with a 5 kN load cell was used.

5.3. RESULTS and DISCUSSION

5.3.1. Flexural and tensile test results of Homo PP composites reinforced by micron talc and its hybrid graphene/talc hybrid additives

Flexural and tensile test results of the additive produced in the presence of micron talc and the presence of iron are given in Tables 8, 9, 10, and 11. It has been determined that hybrid-1 reinforcement with untreated talc positively affects their modulus and strength values. Table 8 reveals that with the addition of 20 wt% micron talc to HomoPP, flexural strength and flexural modulus were improved by 33% and 92.7%, respectively. On the other hand, Table 9 indicates that in the flexural strength values of hybrid-1 (Graphene/Fe-micron talc hybrid after catalytic carbonization), the highest value was achieved with 10% and 15% hybrid-1 additive ratio. For the flexural modulus analysis, as the amount of filling increased, an increase in the amount of modulus value was observed. Furthermore, A close look at the tensile values in Table 10 reveals an increase in tensile strength by 17.2% with an addition of 10 wt% micron talc ratio an increase in tensile modulus of 74.3% achieved. On the other hand, as shown in Table 11, very similar results were obtained in tensile strengths at 5 wt% and 10 wt% filling ratios with hybrid-1 additive. A directly proportional increase in tensile modulus of hybrid-1 reinforced PP composites for an increase in filling ratio was observed. In Figure 16, comparative flexural modulus and flexural strength graphs at different loadings in the HomoPP matrix of micron talc and Hybrid 1 are given. The results revealed that when we look at micron talc addition and the developed hybrid-1 additive on HomoPP, hybrid-1 produced from micron talc did not make a big difference on mechanical properties. However, the addition of hybrid-1 to HomoPP revealed higher flexural strength and flexural modulus than neat HomoPP.

Table 8. Summary of flexural test results of HomoPP composites reinforced by micron talc.

Sample	Flexural Strength (MPa)	Improvement in Flexural Strength (%)	Flexural Modulus (MPa)	Improvement in Flexural Modulus (%)	Flexural Strain (%)
HomoPP	46	-	1733	-	6.6
HomoPP+ %5 micron talc	58.9	28.0	2493	43.9	6.0
HomoPP+ %10 micron talc	60.4	31.3	2770	59.8	5.4
HomoPP+ %15 micron talc	61.0	32.6	3080	77.7	5.2
HomoPP+ %20 micron talc	61.2	33.0	3340	92.7	4.9

Table 9. Summary of flexural test results of HomoPP composites reinforced with Hybrid 1 (Graphene/Fe-micron talc hybrid after catalytic carbonization).

Sample	Flexural Strength (MPa)	Improvement in Flexural Strength (%)	Flexural Modulus (MPa)	Improvement in Flexural Modulus (%)	Flexural Strain (%)
HomoPP	46	-	1733	-	6.6
HomoPP+ %5 hybrid 1	55.4	20.4	2100	21.2	6.4
HomoPP+ %10 hybrid 1	57.5	25	2193	26.5	6.3
HomoPP+%15 hybrid 1	57.4	24.7	2405	38.8	5.7

HomoPP+%20 hybrid 1	56.5	22.8	2453	41.5	5.4

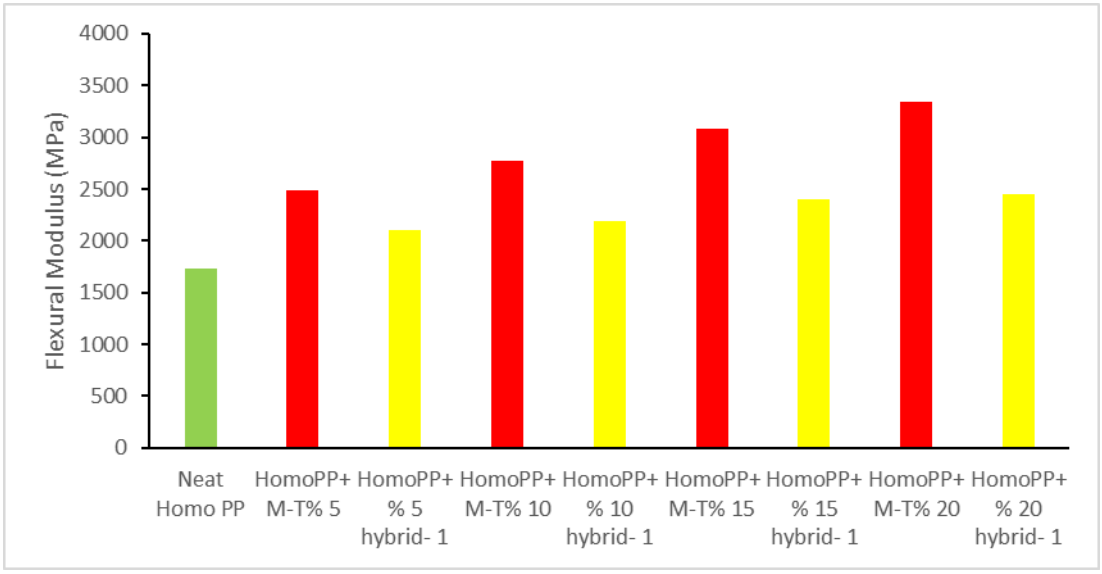

(a)

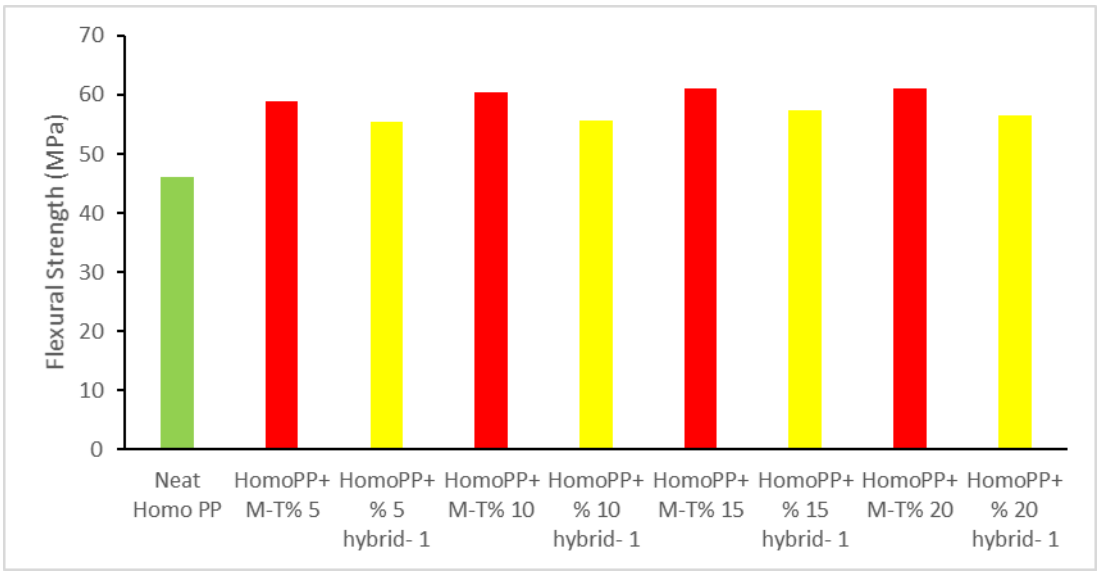

(b)

Figure 16. Flexural modulus (a) and flexural strength (b) comparison graphs of micron talc and Hybrid 1 (Graphene/Fe-micron talc hybrid after catalytic carbonization) reinforced HomoPP composites at different loadings.

Table 10. Summary of tensile test results of micron talc reinforced HomoPP composites.

Sample	Tensile Strength (MPa)	Improvement in Tensile Strength (%)	Tensile modulus (MPa)	Improvement in Tensile Modulus (%)	Tensile Strain at break (%)
HomoPP	34.3	-	1905	-	282.5
HomoPP+ %5 micron talc	38.5	12.3	2720	42.8	243.3
HomoPP+ %10 micron talc	40.2	17.2	3321	74.3	40.3
HomoPP+ %15 micron talc	37.8	10.2	3701	94.3	22.6
HomoPP+ %20 micron talc	40.2	17.2	4110	115.7	28.0

Table 11. Summary of tensile test results of Hybrid 1 (Graphene/Fe-micron talc hybrid after catalytic carbonization) reinforced HomoPP composites.

Sample	Tensile Strength (MPa)	Improvement in Tensile Strength (%)	Tensile modulus (MPa)	Improvement in Tensile Modulus (%)	Tensile Strain at break (%)
HomoPP	34.3	-	1905	-	282.5
HomoPP+ %5 hybrid 1	38.1	11.1	2582	35.5	265
HomoPP+ %10 hybrid 1	38.2	11.4	2700	42	138
HomoPP+ %15 hybrid 1	36.9	7.6	2759	45	61
HomoPP+ %20 hybrid 1	37.5	9.3	3052	60	42

5.3.2. Mechanical characterization of HomoPP composites reinforced by fine talc and its hybrid graphene/talc hybrid additives

In this chapter, the tensile and flexural test results of the Hybrid-2 (Graphene/Fe-fine talc hybrid after catalytic carbonization) additive and fine talc are given. Tables 12, 13, 14, and 15 demonstrate the comparison of flexural and tensile test values. Table 12 reveals that fine talc addition increased 37.2% in flexural strength and 82.9% in flexural modulus with a filling ratio of 15 wt%. On the other hand, Table 13 reveals that for the hybrid-2 additive reinforcement, there was a 27% increase in flexural strength with 10 wt% filling ratios, while the highest increase in flexural modulus was achieved with a 20 wt% filling ratio. As shown in Table 14, tensile test results reveal that an improvement of 99.7% was achieved in the tensile module with 20 wt% fine talc addition and 17.3% tensile strength with 15 wt% fine talc additions. In addition, looking at the effect of hybrid-2 additive on tensile properties, the increase in tensile strength is 8.5% with 15 wt% hybrid-2 additive ratio, and the increase in tensile modulus with 20 wt% hybrid-2 additive ratio is around 60.2%. In summary, hybrid produced using fine talc has improved the mechanical properties in different loadings compared to neat HomoPP. However, neat fine talc addition, which we compared with the hybrid additive, provided a greater improvement than the hybrid-2. Figure 17 shows the comparative graphs of the tensile modulus and tensile strength of fine talc and hybrid-2 additive reinforced HomoPP composites.

Table 12. Summary of flexural test results of fine talc reinforced HomoPP composites.

Sample	Flexural Strength (MPa)	Improvement in Flexural Strength (%)	Flexural Modulus (Mpa)	Improvement in Flexural Modulus (%)	Flexural Strain (%)
HomoPP	46	-	1733	-	6.60
HomoPP+ %5 fine talc	58.3	26.7	2497	44.1	5.50
HomoPP+ %10 fine talc	61.2	33.0	2828	63.2	5.72
HomoPP+ %15 fine talc	63.1	37.2	3170	82.9	5.11
HomoPP+ %20 fine talc	61.1	32.8	3205	84.9	5.07

Table 13. Summary of flexural test results of Hybrid 2 (Graphene/Fe-fine talc hybrid after catalytic carbonization) reinforced HomoPP composites.

Sample	Flexural Strength (MPa)	Improvement in Flexural Strength (%)	Flexural Modulus (MPa)	Improvement in Flexural Modulus (%)	Flexural Strain (%)
HomoPP	46	-	1733	-	6.6
HomoPP+ %5 hybrid 2	55.2	20	2257	30.2	6.1
HomoPP+ %10 hybrid 2	58.4	27	2537	46.4	6.0
HomoPP+ %15 hybrid 2	53.3	16	2368	36.6	5.5
HomoPP+ %20 hybrid 2	56.8	24	2640	52.3	5.4

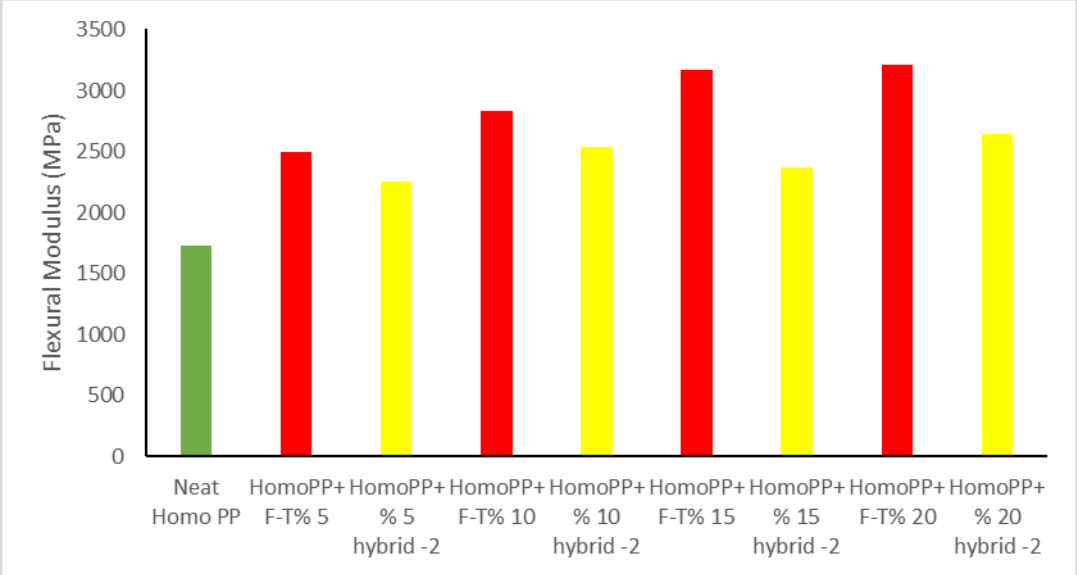

(a)

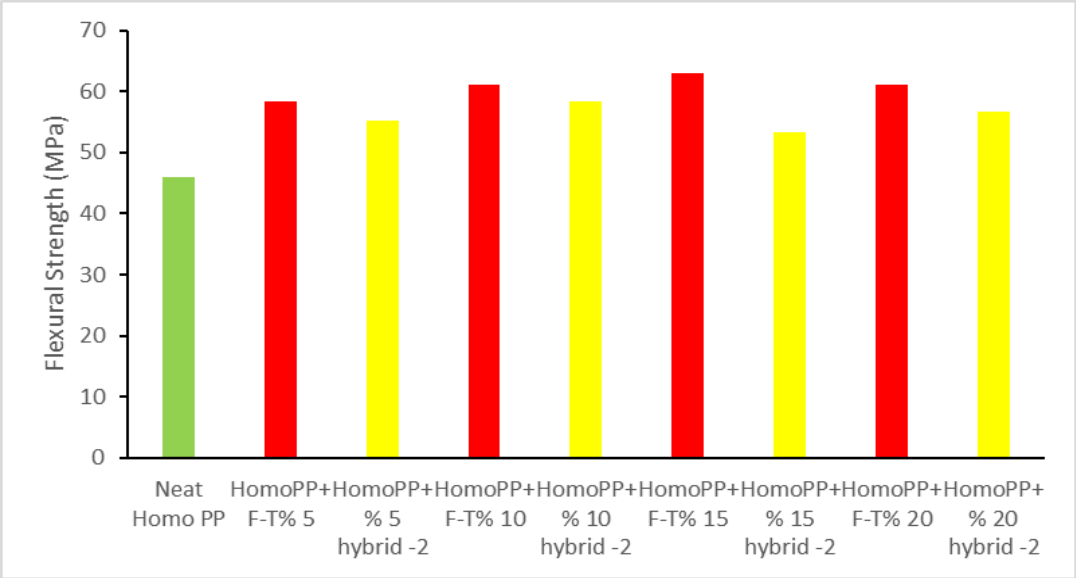

(b)

Figure 17. Flexural modulus (a) and flexural strength (b) comparison graphs of fine talc and Hybrid-2 (Graphene/Fe-fine talc hybrid after catalytic carbonization) reinforced HomoPP composites at different loadings.

Table 14. Summary of tensile test results of fine talc reinforced HomoPP composites.

Sample	Tensile Strength (Mpa)	Improvement in Tensile Strength (%)	Tensile modulus (Mpa)	Improvement in Tensile Modulus (%)	Tensile Strain at break (%)
HomoPP	34.3	-	1905	-	282.5
HomoPP+ %5 fine talc	38.2	11.4	2753	44.5	105
HomoPP+ %10 fine talc	40.0	16.6	3055	60.3	113
HomoPP+ %15 fine talc	40.3	17.3	3389	77.9	33
HomoPP+ %20 fine talc	39.3	14.6	3804	99.7	25

Table 15. Summary of tensile test results of Hybrid 2 (Graphene/Fe-fine talc hybrid after catalytic carbonization) reinforced HomoPP composites.

Sample	Tensile Strength (MPa)	Improvement in Tensile Strength (%)	Tensile modulus (MPa)	Improvement in Tensile Modulus (%)	Tensile Strain at break (%)
HomoPP	34.3	-	1905	-	282.5
HomoPP+ %5 hybrid 2	36.9	7.6	2364	24.1	97
HomoPP+ %10 hybrid 2	36.5	6.4	2564	34.6	43
HomoPP+ %15 hybrid 2	37.2	8.5	2910	52.8	47
HomoPP+ %20 hybrid 2	36.0	5.0	3051	60.2	161

5.3.3. Mechanical characterization of CopoPP composites reinforced by micron talc and its hybrid graphene/talc hybrid additives

In this part of the chapter, the effect of micron talc and Graphene/Fe-micron talc hybrid after catalytic carbonization addition on the performance of the CopoPP matrix was analyzed at 5, 10, 15, and 20 wt% loading rates. A summary of the flexural test results of CopoPP composites reinforced with micron talc is given in Table 16. With the addition of 10 wt% micron talc ratio, 39.4% improvement in flexural strength, and 95.3% improvement in flexural modulus obtained in CopoPP based composites. A slight decrease in flexural strength was observed when the loading amount increased by more than 10 wt% micron talc. Table 17 reveals the flexural test results of CopoPP composites reinforced with hybrid-1 (Graphene/Fe-micron talc hybrid after catalytic carbonization). The hybrid graphene/talc additive addition has significantly improved flexural strengths at different loadings than micron talc reinforced composites. With the 5 wt% hybrid-1 additives, 75.8% increase was achieved in the flexural strength of CopoPP, and 88.2% improvement was observed in the flexural modulus. In the flexural modulus, 105% increase was achieved with 20 wt% hybrid-1 additive ratio, and thus, the most significant mechanical improvement was provided. Especially when compared with the micron talc additive ratio, it has been seen that a high improvement is achieved in the structure of the composite with a lower hybrid additive ratio. This result is a significant finding for

mitigation studies. In Figure 18, the graphs comparatively illustrate the flexural strength and flexural modulus of micron talc and hybrid-1 based CopoPP composites. Herein, it is clearly seen that the hybrid additive provides an advantage in CopoPP compared to micron talc in terms of strength and modulus. Similar behavior was observed when we looked at the tensile properties. Table 18 shows the effect of micron talc on tensile strength and tensile modulus at different loadings. A 16.4% increase in tensile strength and a 77.8% increase in tensile modulus were achieved with 10wt% micron talc. In Table 19, a summary of the tensile test results of CopoPP composites reinforced with hybrid-1 (Graphene/Fe-micron talc hybrid after catalytic carbonization) is given. The 5% hybrid-1 additive results were quite good compared to the performance results obtained with the micron talc reinforced composites. With 5% hybrid-1 additive loading, a 37.8% increase in tensile strength was achieved, and a seven-fold increase was achieved compared to the increase of CopoPP composite reinforced with 5 wt% micron talc. The highest tensile modulus value was reached with an addition of 15 wt% hybrid-1 and 20 wt% hybrid-1.

Table 16. Summary of flexural test results of micron talc reinforced CopoPP composites.

Sample	Flexural Strength (MPa)	Improvement in Flexural Strength (%)	Flexural Modulus (MPa)	Improvement in Flexural Modulus (%)	Flexural Strain (%)
CopoPP	25.6	-	1015	-	6.2
CopoPP+ %5 micron talc	29.2	14.0	1405	38.4	5.5
CopoPP+ %10 micron talc	35.7	39.4	1983	95.3	5.0
CopoPP+ %15 micron talc	30.1	17.6	1756	73.0	5.4
CopoPP+ %20 micron talc	30.8	20.3	1960	93.1	5.2

Table 17. Summary of flexural test results of Hybrid 1 (Graphene/Fe-micron talc hybrid after catalytic carbonization) reinforced CopoPP composites.

Sample	Flexural Strength (MPa)	Improvement in Flexural Strength (%)	Flexural Modulus (MPa)	Improvement in Flexural Modulus (%)	Flexural Strain (%)
CopoPP	25.6	-	1015	-	6.2
CopoPP+ %5 hybrid- 1	45.0	75.8	1910	88.2	5.8
CopoPP+ %10 hybrid- 1	39.8	55.5	1658	63.3	5.7
CopoPP+ %15 hybrid- 1	40.7	59.0	1843	81.5	5.5
CopoPP+ %20 hybrid- 1	42.4	65.6	2080	105.0	4.8

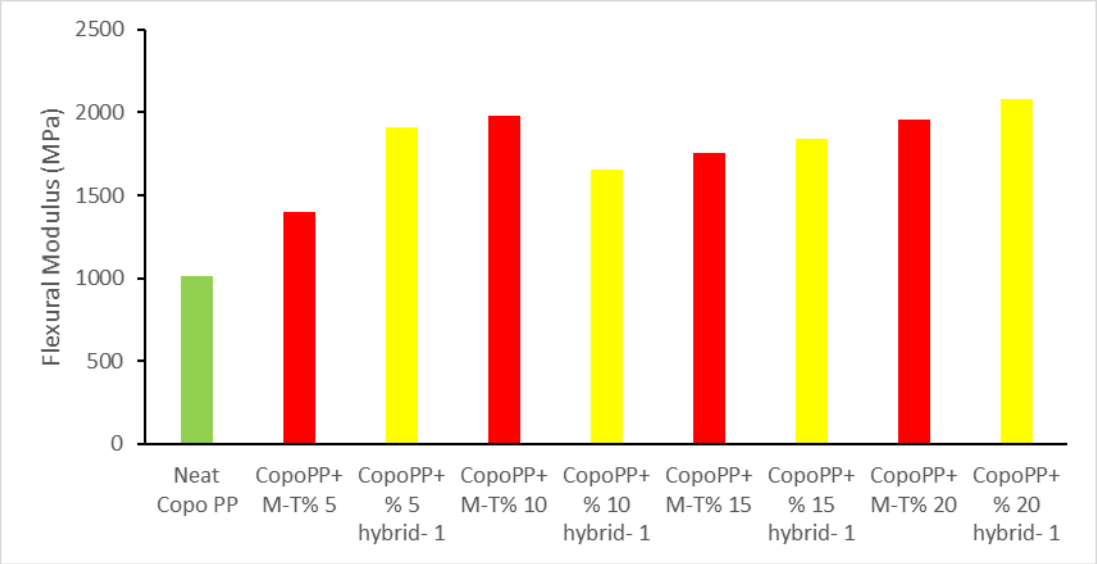

(a)

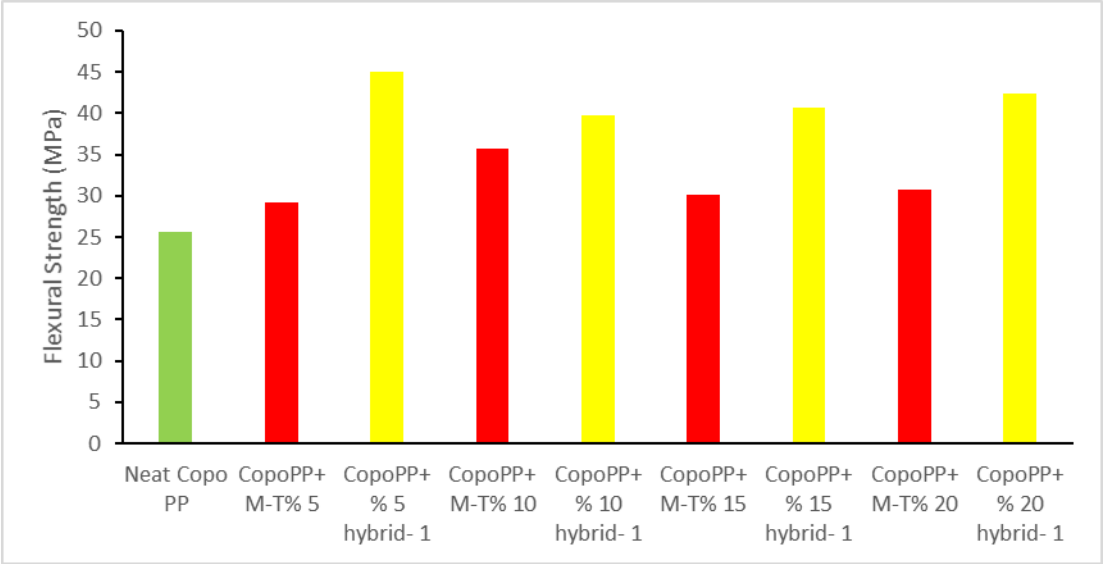

(b)

Figure 18. Flexural modulus (a) and flexural strength (b) comparison graphs of micron talc and Hybrid 1 (Graphene/Fe-micron talc hybrid after catalytic carbonization) reinforced CopoPP composites at different loadings.

Table 18. Summary of tensile test results of micron talc reinforced CopoPP composites.

Sample	Tensile Strength (MPa)	Improvement in Tensile Strength (%)	Tensile modulus (MPa)	Improvement in Tensile Modulus (%)	Tensile Strain at break (%)
CopoPP	20.1	-	1189	-	325
CopoPP+ %5 micron talc	21.2	5.1	1850	55.6	142
CopoPP+ %10 micron talc	23.4	16.4	2114	77.8	22
CopoPP+ %15 micron talc	20.8	3.5	2064	73.6	225
CopoPP+ %20 micron talc	21.6	7.5	2369	99.2	76

Table 19. Summary of tensile test results of Hybrid 1 (Graphene/Fe-micron talc hybrid after catalytic carbonization) reinforced CopoPP composites

Sample	Tensile Strength (MPa)	Improvement in Tensile Strength (%)	Tensile modulus (MPa)	Improvement in Tensile Modulus (%)	Tensile Strain at break (%)
CopoPP	20.1	-	1189	-	325
CopoPP+ %5 hybrid- 1	27.7	37.8	1861	56.5	137.2
CopoPP+ %10 hybrid- 1	27.4	36.3	2114	77.8	111.5
CopoPP+ %15 hybrid- 1	28.2	40.3	2181	83.4	22.5
CopoPP+ %20 hybrid- 1	28.2	40.3	2244	88.7	29.2

5.3.4. Mechanical characterization of CopoPP composites reinforced by fine talc and its hybrid graphene/talc hybrid additives

At this part of the chapter, the performance of hybrid-2 (Graphene/Fe-fine talc hybrid after catalytic carbonization) produced from fine talc and polypropylene source in CopoPP has been compared. Table 20 summarizes the flexural test results of CopoPP composites reinforced with fine talc. With 20% loading of fine talc, the highest increases in CopoPP were obtained, an increase of 20% in flexural strength and an increase in flexural modulus of 86.5%. Table 21 shows the flexural test results of CopoPP composites reinforced with Hybrid -2 (graphene / Graphene/Fe-fine talc hybrid after catalytic carbonization). A close look at the results of Hybrid -2, the flexural strength increased by 17.7% with 20% loading, while the flexural modulus increased by 46.1%. Hybrid -2 and fine talc provided very similar values for an increase in the improvement of mechanical properties at 10% loading. Although hybrid-2 is not seen to be superior to fine talc in flexural values, the addition of hybrid-2 has provided a moderate amount of increase in the properties of neat CopoPP. In Figure 19, the flexural values of fine talc and hybrid-2 are also compared with comparative graphs. On the other hand, hybrid-2 provided higher performance than fine talc in tensile values. A summary of the tensile test results of CopoPP composites reinforced with fine talc is given in Table 22. With 20% fine talc loading, an increase in the amount of 8.9% in tensile strength and 84.2% in tensile modulus was achieved. In Table 23, the change in tensile values of CopoPP of hybrid-2

is given. An increase of 15.4% in flexural strength and 30.8% increase in flexural modulus were obtained with 15% hybrid-2 filling ratio. The highest tensile modulus value was achieved with 20% hybrid-2 filler ratio.

Table 20. Summary of flexural test results of fine talc reinforced CopoPP composites.

Sample	Flexural Strength (MPa)	Improvement in Flexural Strength (%)	Flexural Modulus (MPa)	Improvement in Flexural Modulus (%)	Flexural Strain (%)
CopoPP	25.6	-	1015	-	6.2
CopoPP+ %5 fine talc	28.6	11.7	1276.6	25.8	5.58
CopoPP+ %10 fine talc	28.7	12.1	1360	34	5.57
CopoPP+ %15 fine talc	30.2	18.0	1700	67.5	5.43
CopoPP+ %20 fine talc	30.7	20.0	1893.3	86.5	5.16

Table 21. Summary of flexural test results of Hybrid 2 (Graphene/Fe-fine talc hybrid after catalytic carbonization) reinforced CopoPP composites.

Sample	Flexural Strength (MPa)	Improvement in Flexural Strength (%)	Flexural Modulus (MPa)	Improvement in Flexural Modulus (%)	Flexural Strain (%)
CopoPP	25.6	-	1015	-	6.2
CopoPP+ %5 hybrid- 2	28.1	9.8	1175	15.8	5.91
CopoPP+ %10 hybrid- 2	29.1	13.7	1298	27.8	5.72
CopoPP+ %15 hybrid- 2	29.7	16.0	1407	38.6	5.49
CopoPP+ %20 hybrid- 2	30.1	17.7	1483	46.1	5.63

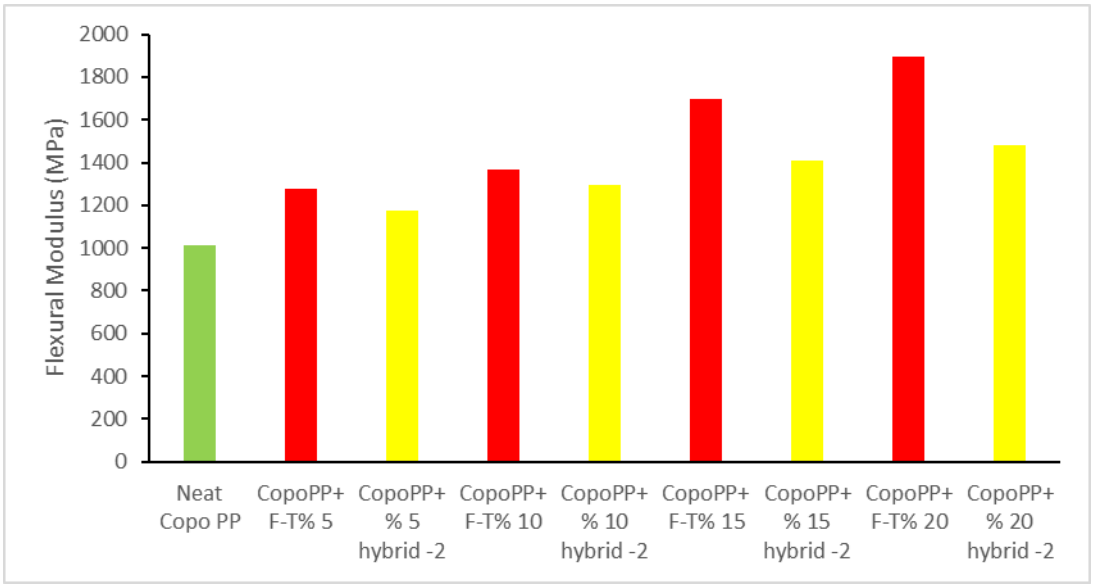

(a)

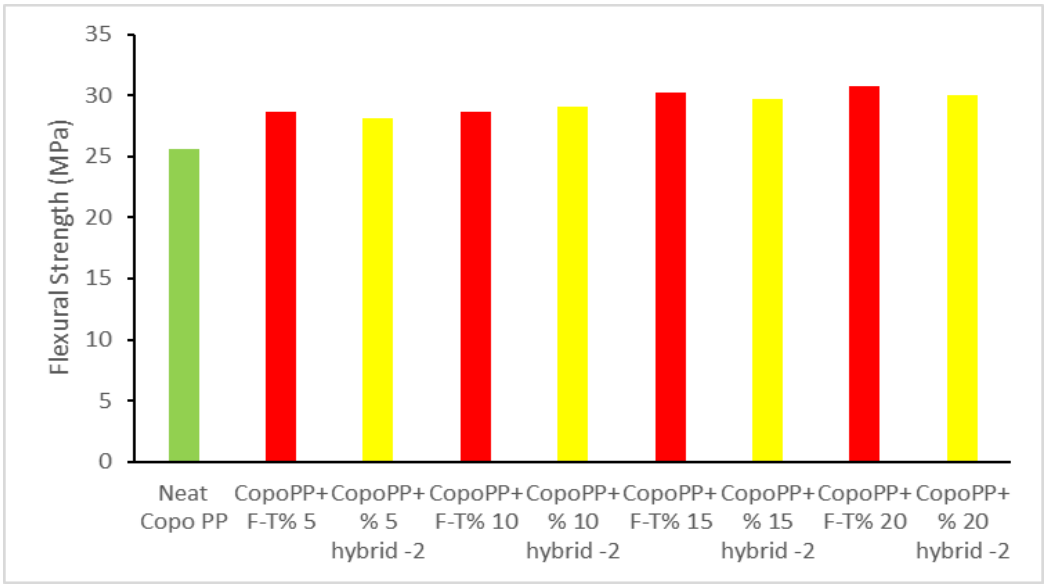

(b)

Figure 19. Flexural modulus (a) and flexural strength (b) comparison graphs of fine talc and Hybrid 2 (graphene/Fe-fine talc) at different loadings in the CopoPP matrix.

Table 22. Summary of tensile test results of fine talc reinforced CopoPP composites.

Sample	Tensile Strength (MPa)	Improvement in Tensile Strength (%)	Tensile modulus (MPa)	Improvement in Tensile Modulus (%)	Tensile Strain at break (%)
CopoPP	20.1	-	1189	-	325
CopoPP+ %5 fine talc	20.3	0.9	1411	18.7	221
CopoPP+ %10 fine talc	21.5	7.0	1551	30.4	121
CopoPP+ %15 fine talc	21	4.5	1997	68.0	110
CopoPP+ %20 fine talc	21.9	8.9	2191	84.2	104

Table 23. Summary of tensile test results of Hybrid 2 (Graphene/Fe-fine talc hybrid after catalytic carbonization) reinforced CopoPP composites.

Sample	Tensile Strength (MPa)	Improvement in Tensile Strength (%)	Tensile modulus (MPa)	Improvement in Tensile Modulus (%)	Tensile Strain at break (%)
CopoPP	20.1	-	1189	-	325
CopoPP+ %5 hybrid- 2	22	9.5	1421	19.5	95
CopoPP+ %10 hybrid- 2	21.6	7.5	1501	26.2	48
CopoPP+ %15 hybrid- 2	23.2	15.4	1555	30.8	26
CopoPP+ %20 hybrid- 2	22.7	12.9	1696	42.6	18

5.3.5. Cross-sectional analysis of hybrid additive reinforced composites

The thickness of these crystal lamellae determines the intrinsic deformation behavior (yield stress and strain hardening) of the material [107]. Direction of the injection flow is also affects the mechanical properties of the thermoplastics and homogeneity of the graphene nanomaterials. In Figure 20, SEM images reveal ordering formation in the cross-section of the deformed part after tensile testing of CopoPP+10% Hybrid -1.

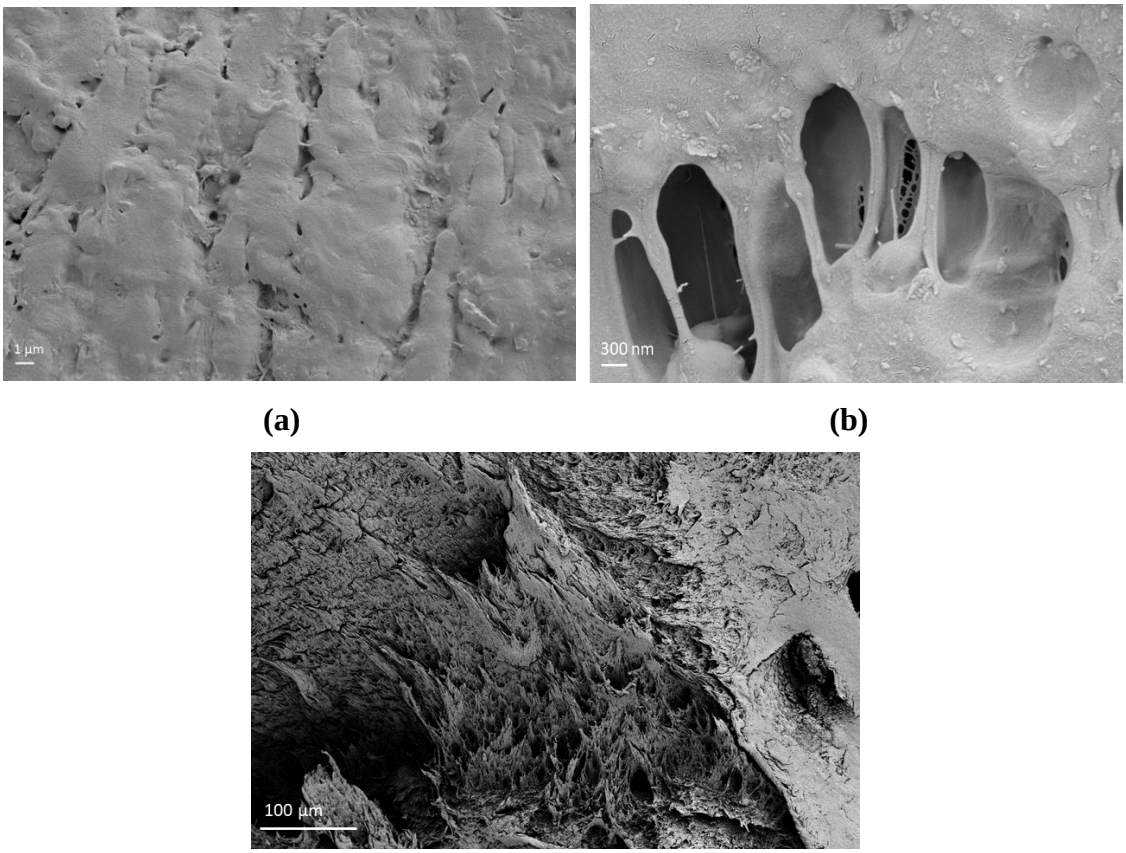

Figure 20. SEM images of fractured surfaces of a) neat CopoPP b) 10wt% micron talc reinforced CopoPP, and c) 10 wt% hybrid graphene/Fe-micron talc reinforced CopoPP composites.

5.3.6. Thermal and crystallinity properties of graphene/micron talc hybrid reinforced CopoPP composites

It is known that the integration of carbon-based materials such as graphene and carbon nanotubes into the PP matrix acts as a nucleating agent on the surface of the polymer, forming a crystalline structure, thereby increasing the crystallization temperature, crystallization rate, and degree of crystallinity [27]. In order to examine the effect of the hybrid additive on the crystallization degree of PP, a Differential Scanning Calorimetry (DSC) was performed. The effect of the hybrid additives obtained within this study on the mechanical properties was investigated. Flexural properties are critical parameters for

evaluating the mechanical performance of composite structures and understanding the interactions between the matrix and the reinforcing additive due to the complex strain profile induced in the tested samples. Figure 21 reveals the cooling and heating cycle thermograms of PP, PP/micron talc, and PP/Hybrid-1 composites. As it can be seen, the addition of Hybrid-1 increased the crystallization temperature. In addition, micron talc addition resulted in a slight increase in crystallization temperature than the hybrid-1 addition.

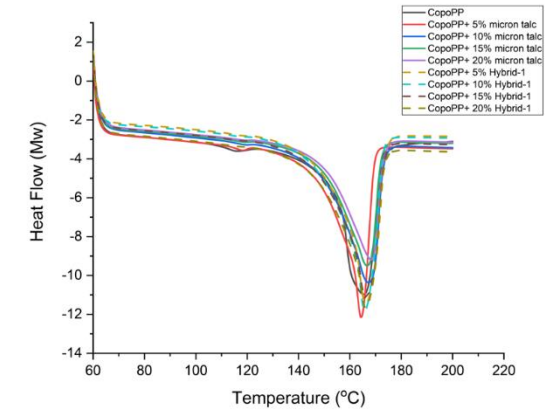

(a)

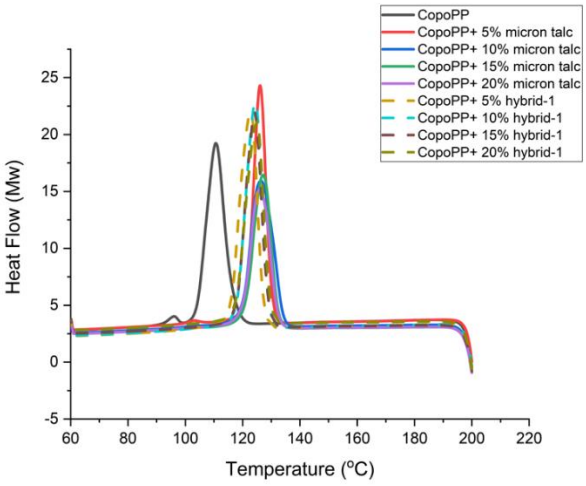

(b)

Figure 21. First cooling cycle (a) and second heating cycle (b) thermograms of PP, PP/micron talc, and PP/Hybrid-1 composites.

Thermal parameters of neat CopoPP, CopoPP/micron talc composites, and CopoPP/hybrid-1 composites are given in Table 24. As it can be seen in Table 24, the addition of both micron talc and hybrid-1(Graphene/Fe-micron talc hybrid after catalytic carbonization) increased the crystallization temperature. Hybrid-1 acted as a nucleating

agent and started an early crystallization, providing the crystals with more time to form and boost overall crystallinity since crystallization begins early [108].

Table 24. Melting and crystallization parameters of neat CopoPP, CopoPP/micron talc composites, and CopoPP/hybrid-1 composites.

Sample	Melting Onset Temperature (°C)	Melting Peak Temperature (°C)	Melting Integral, ΔH_M (J/g)	Crystallization Onset Temperature (°C)	Crystallization Peak Temperature (°C)	Crystallization Integral ΔH_C (J/g)
Neat Copo PP	154.2	165.3	-82.8	116.6	110	78.6
CopoPP+ 5%micron talc	156.7	164.15	-76.6	130.1	126.4	73.9
CopoPP+ 10%micron talc	151	167	-78.4	134.1	126.5	73.6
CopoPP+ 15%micron talc	150.5	166.6	-68.1	132.2	127.3	64.3
CopoPP+ 20%micron talc	148.9	168	-66.3	132.2	126	63.6
CopoPP+ 5%hybrid-1	157.4	165.9	-90.4	127.2	123.1	87.6
CopoPP+ 10%hybrid-1	147.4	165.6	-89.3	128.9	124.6	85.5
CopoPP+ 15%hybrid-1	156.7	166	-84.5	128.9	124.4	81.6
CopoPP+ 20%hybrid-1	156.3	165.9	-85.5	129.5	125.1	82.6

Equation 3 illustrates the degree of crystallinity(X_C) where ΔH_M is the enthalpy of melting of CopoPP, and CopoPP compounds, whereas the $\Delta {H_M}^{100\%}$ melting enthalpy of 100% CopoPP [109]. The melting enthalpy of crystalline PP was taken as 183 J/g[110].

$$X_C = \left(\frac{\Delta H_M}{\Delta H_M{}^{100\%}} \right) x\ 100 \qquad (3)$$

Table 25 indicates the crystallinity degrees of CopoPP, CopoPP/micron talc compounds, and CopoPP/hybrid-1 composites. The crystallinity degree of neat CopoPP was calculated as 45.2%, and the addition of micron talc resulted in a slight decrease in the amount of crystallinity degree. On the other hand, hybrid-1 addition resulted in a more crystalline structure; hence, the mechanical properties of CopoPP/Hybrid-1 composites increased. In addition, when the loading ratio of the micron talc increased, a decrease in the crystallinity of CopoPP/micron talc hybrids occurred. Moreover, the same phenomena also occurred for the CopoPP/hybrid-1 composites. The highest crystallinity degree was obtained after 5% hybrid-1 addition to the CopoPP.

Table 25. Crystallinity degrees of neat CopoPP, CopoPP/micron talc compounds, and CopoPP/hybrid-1 composites.

Sample	**Crystallinity (%)**	**Amorphous (%)**
Neat Copo PP	45.2	54.8
CopoPP+ 5%micron talc	41.8	58.2
CopoPP+ 10%micron talc	42.8	57.2
CopoPP+ 15%micron talc	37.2	62.8
CopoPP+ 20%micron talc	36.2	63.8
CopoPP+ 5%hybrid-1	49.4	50.6
CopoPP+ 10%hybrid-1	48.8	51.2
CopoPP+ 15%hybrid-1	46.2	53.8
CopoPP+ 20%hybrid-1	46.7	53.3

5.4. CONCLUSION

In this part of the study, micron talc, fine talc, Graphene/Fe-micron talc hybrid after catalytic carbonization, and Graphene/Fe-fine talc hybrid additives after catalytic carbonization were successfully mixed at high shear rates with HomoPP and CopoPP polymers by using a custom made thermokinetic mixer. Then, the addition of various filling ratios of micron talc, fine talc, and their hybrids to polymer matrices was

performed to observe the improvement in the mechanical properties of the composites. Hence, tensile and flexural tests were performed to elucidate the strength and modulus improvements on HomoPP and CopoPP. Furthermore, DSC analysis was performed to demonstrate the increase of the crystallinity degrees after graphene/talc hybrid additions CopoPP. It was determined that the graphene hybrid additive growth on micron talc produced from polypropylene plastic source resulted in higher mechanical properties than hybrid additive growth on fine talc. In addition to that, the micron talc and hybrid-1 (graphene grown on Fe-micron talc) addition resulted in more significant mechanical improvements compared to the fine talc and hybrid-2 (graphene growth on Fe-fine talc). Moreover, a directly proportional increase in tensile modulus and flexural modulus for an increase in filling ratio was observed after the micron talc and hybrid-1 addition. Furthermore, HomoPP revealed superior mechanical properties as a polymer matrix compared to the CopoPP. However, the highest improvement was achieved after adding 5 wt% hybrid-1 additive ratio to CopoPP, which was a 75.8% increase in the flexural strength and 88.2% improvement in the flexural modulus of CopoPP. Moreover, with 5% hybrid-1 additive loading, a 37.8% increase in tensile strength was achieved, and a seven-fold increase was achieved compared to the percent increase in the CopoPP composite reinforced with 5 wt% micron talc. DSC analysis revealed that the addition of hybrid-1 enhanced the crystallinity degree of the polymer, whereas micron talc addition slightly decreased that and an increase in the filler ratio decreased the crystallinity degree. Overall, at low loading ratio of Hybrid-1, addition to CopoPP revealed the highest mechanical improvement, and such improvement will be useful for the future of the car part production.

CHAPTER 6. A CONSEQUENTIAL PROCESS ORIENTED LIFE CYCLE ANALYSIS (LCA) OF PRODUCTION ROUTES OF UPCYCLED GRAPHENE GROWN ON TALC

In this study, a consequential process-oriented LCA study of upcycled graphene production from waste polypropylene on talc surface was reported. Environmental impact evaluation of conducted processes was investigated, and a comparison of global warming potential of graphene/talc/hybrids, reduced graphene oxide, and neat polypropylene was discussed. In addition, the environmental impact of batch and continuous production routes of graphene from waste plastics were compared. Life cycle inventory and impact assessment methods were used to elucidate the carbon footprint of these production processes.

6.1. INTRODUCTION

Graphene has been employed in compound production as a nucleating and reinforcing agent due to its exceptional mechanical properties and large surface area. Despite the fact that graphene has unique features for engineering plastics, traditional production methods are difficult to operate, low yield, and expensive, making the large-scale production impractical. There are three common production routines patented for the graphene formation such as exfoliation, chemical vapor deposition (CVD), and epitaxial growth [111]. In addition, flash pyrolysis and carbonization of hydrocarbons are some other thermal treatment methods to produce graphene [112]. Impacts of graphene production are highly dependent on the production routine [113], and these negative impacts result from the energy and chemicals used in the production processes and the toxic effect of graphene as a product [114]. To identify and eliminate the hazardous emissions of greenhouse gasses, life cycle assessment is a convenient method.

Life cycle assessment (LCA) is a technique that comprehensively analyses and elucidates the effects of the productions, processes, and related technologies on human health and environmental impacts from the cradle-to-grave approach. LCA allows the manufacturers and scientists to identify and find the environmental hotspots [115] to design their processes to alleviate the hazardous impact on crucial environmental and human health issues [116]. An LCA is to be carried out in compliance with ISO 14040 (2006a) and ISO 14044 (2006) through the stages of goal and scope definition followed by life cycle

inventory analysis (LCI), life cycle impact assessment (LCIA), and interpretation of outcomes. The first step of an LCA study is goal and scope definition, which indicates the system boundaries, types of impacts considered, and functional units practiced [117]. LCI part indicates the data of resources that have been used, processes that followed, and emissions as a result of the processes [118]. After identifying the inputs and processes, LCIA is performed to evaluate the impact by analyzing the data necessary to measure both inputs and outputs found relevant to the processes occurring within the boundaries of the whole commodity system [119]. Characterization factor selection plays a vital role in selecting the impact assessment method while calculating the potential impacts on various subjects such as human health and the environment. Global warming potential (GWP) is one of the most studied methods as an impact indicator [120]. Moreover, climate change, ozone depletion, human toxicity, respiratory inorganics, ionizing radiation, photochemical ozone formation, acidification, eutrophication, ecotoxicity, land use, and resource depletion are some impacts identified by International Reference Life Cycle Data System (ILCD) standard methodology. In the European context, the ILCD handbook on the LCIA methods provides essential sources for the scope of the study [121]. Subsequently, at the last step, the outcomes of studies are interpreted in the manner of data and assumptions that have been made, and eventually, it results in a conclusion that describes the whole system [117]. Despite the advances and growing interest, LCA analysis of graphene and related materials is currently challenging due to the lack of a standardized method for the production process and quality of the products [113, 122].

6.2. EXPERIMENTAL

6.2.1. Materials

Talc/graphene hybrid and graphene grown on talc were mentioned in chapter 3 and chapter 4. rGO produced by modified hummers method, and PP life cycle inventory (LCI) data from ecoinvent inventory. LCA analysis was performed using the Ecoinvent 3-Classification allocation by cutting databases with the help of SimaPro (version 9.1.1.1). Completed LCA findings were calculated by using the ReciPe 2016 v1.1 midpoint hierarchical version impact approach to show all eighteen impact groups.

6.2.2. Environmental impact of graphene production from plastics and raw graphite by LCA analysis

Life cycle assessment methodologies examine the environmental consequences and consequent sustainability of a particular manufacturing process and the overall product. Comparative studies on talc/ graphene hybrid production routes, reduced graphene oxide (rGO), graphene growth on talc surface, and PP were investigated using process-oriented consequential life cycle assessment methods. Ecoinvent 3- Allocation cut off by classification & cut off by unit, and Swiss input & output databases used the life cycle inventory (LCI). The unit of the analysis covered only one batch of graphene production from waste PP and talc/ graphene hybrid. Moreover, one batch production of rGO by modified hummers method and PP. According to the landfill disposal scenario, the end life of the products was selected as municipal solid waste. The system evaluates materials entered in the mass units because volume units are not considered during the waste disposal scenario. The LCA study covers the life cycle analysis of the processes starting from the carbonization of waste plastic to produce graphene, talc/graphene hybrid for the reinforcement purpose, production of rGO by modified hummers method, commercial PP production, and disposal of them as waste. Graphene production by thermal treatment and chemical synthesis method was compared to investigate which method has more influence on environmental pollution. Since waste PP is used for graphene production, for the PP input, only the transportation of waste PP was taken into consideration. Global warming potential and human health categories, which were considered the two most important effect factors, were taken into the consideration for the scope of this LCA study [120].

6.2.3. Environmental impact of batch and continuous production routes of graphene from waste plastics by LCA analysis

Life cycle assessment methodologies examine the environmental consequences and consequent sustainability of a specific manufacturing process and the overall product. Comparative study on the production routes by thermal treatment of talc/ graphene hybrid, graphene growth on talc surface was investigated using process-oriented consequential life cycle assessment methods. Two types of furnaces: chamber furnace (batch production) and custom-made rotary furnace (continuous production) were compared by considering variables such as the feeding capacity, carbonization time, and energy consumption. Ecoinvent 3- Allocation cut off by classification, and Swiss input

& output databases were used for the life cycle inventory (LCI). The unit of the analysis covered only one batch of graphene production from waste PP and talc/ graphene hybrid by using a chamber furnace and rotary furnace. According to the landfill disposal scenario, the end life of the products was selected as municipal solid waste. The system evaluates materials that are entered in units of the mass because volume units are not taken into account during the waste disposal scenario. The LCA study covers the life cycle analysis of the processes starting from the carbonization of waste plastic to produce graphene and talc/graphene hybrid for the large-scale production applications and disposal of them as waste. Graphene production by thermal treatment method was compared to investigate which method has more influence on environmental pollution. Since waste PP is used for graphene production, for the PP input, only the transportation of waste PP was taken into consideration. Global warming potential and human health categories, which were considered the two most crucial effect factors, were taken into consideration for the scope of this LCA study [120].

6.3. RESULTS and DISCUSSION

6.3.1. Environmental impact of graphene production from plastics and raw graphite by LCA analysis

The environmental impact factors from graphene production on the talc surface, rGO, talc/graphene hybrid, and PP are given in Table 26. When the environmental impact factors were evaluated according to the global warming potential, it was seen that the production of reduced graphene oxide (rGO) has a value of 16.0 kg CO_2 eq. The global warming potential of talc/graphene hybrid and PP was lower than the rGO, and their values were 3.29 kg CO_2 eq and 0.18 kg CO_2 eq. The strong acids used in the separation of graphene and the additional energy (reflux heater, oven, centrifuge) expenditures could be considered the reason for harmful emissions to the environment caused during the separation process. Additionally, it can be said that the production of graphene/talc hybrid structures process was more environmentally friendly on the protection of the ozone layer than the rGO production. It was seen from Table 26 that the carbonization process conducted at 1000°C under argon atmosphere for upcycled graphene production on talc surface yielded a high value of CO_2 emission. It was seen that the PP production process had little effect on these characterizations. Similarly, its effects on human health and ozone formation also showed a low risk.

Table 26. Environmental impact factors from the production of graphene grown from talc, rGO, talc/graphene hybrid additive and PP.

Impact Category	Unit	Graphene grown from talc surface	rGO	Talc/Graphene hybrid	PP
Global warming	kg CO_2 eq	11.5	16.0	3.29	0.18
Stratospheric ozone depletion	kg CFC11 eq	1.28×10^{-5}	3.68×10^{-5}	9.65×10^{-7}	3.75×10^{-9}
Ionizing radiation	kBq Co-60 eq	0.14	0.33	0.04	0.0002
Ozone formation, Human health	kg NO_x eq	0.022	0.030	0.006	0.0003
Fine particulate matter formation	kg PM2.5 eq	0.072	0.063	0.018	0.0001
Ozone formation, Terrestrial ecosystems	kg NO_x eq	0.021	0.030	0.006	0.0004
Terrestrial acidification	kg SO_2 eq	0.05	0.06	0.01	0.0004
Freshwater eutrophication	kg P eq	0.0095	0.0087	0.0025	6.14×10^{-6}
Marine eutrophication	kg N eq	0.0009	0.0083	0.0004	9.62×10^{-6}
Terrestrial ecotoxicity	kg 1,4-DCB	6.93	21.2	1.8	0.07
Freshwater ecotoxicity	kg 1,4-DCB	0.605	1.3	0.34	0.01
Marine ecotoxicity	kg 1,4-DCB	0.809	1.8	0.45	0.018
Human carcinogenic toxicity	kg 1,4-DCB	0.54	0.59	0.15	0.003
Human non-carcinogenic toxicity	kg 1,4-DCB	13.7	32.8	7.46	0.20
Land use	m^2a crop eq	0.04	7.06	0.01	0.0005
Mineral resource scarcity	kg Cu eq	0.006	0.027	0.0013	3.74×10^{-5}
Fossil resource scarcity	kg oil eq	2.97	3.33	0.77	0.13
Water consumption	m^3	0.07	0.89	0.018	0.001

Figure 22 displays the characterizations of global warming, stratospheric ozone depletion, ionizing radiation, ozone formation, human health, and the rest of the characterizations, which are the impact categories of the production processes of graphene grown on talc surface, talc/graphene hybrid, rGO, and PP.

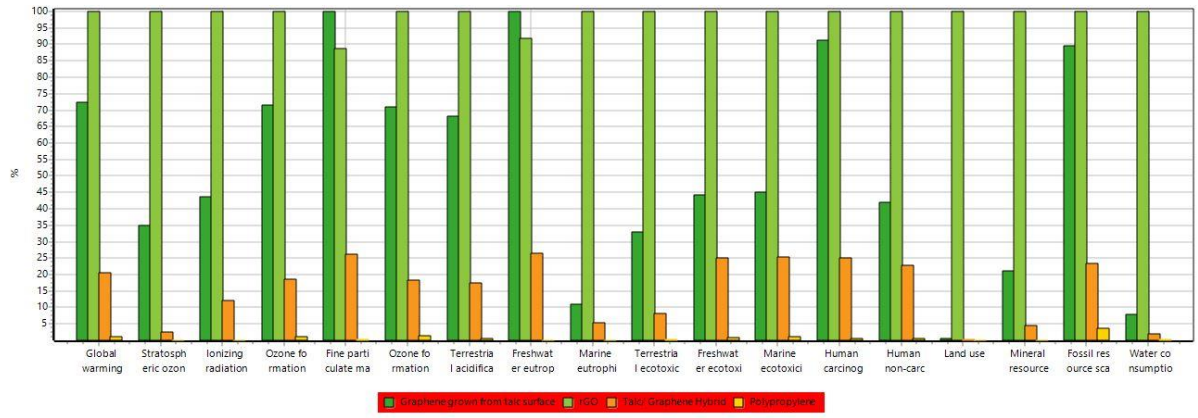

Figure 22. Impact characterization of graphene grown on talc surface, talc/graphene hybrid, rGO and PP.

The comparison of global warming potential of graphene grown on talc surface, talc/graphene hybrid, rGO and PP are given in Figure 23. As explained above, the rGO production process has been the most influential production process on the global warming. Usage of hydrazine and complex production process might be the reason for this high impact.

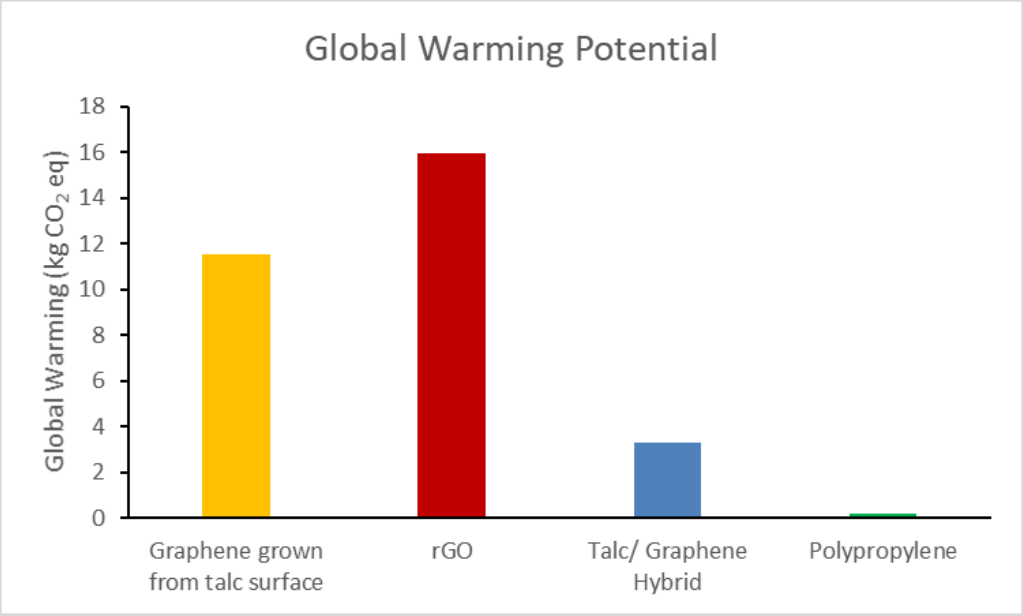

Figure 23. The comparison of global warming potential of graphene grown on talc surface, talc/graphene hybrid, rGO and PP.

In addition, Figure 24 reveals the impact of production processes and inputs on global warming potential. It can be said that the PP production process has the lowest effect

compared to the other production processes. Electricity consumption plays an essential role in global warming, ozone depletion in the stratosphere, ozone formation, and fine particulate matter formation, which are included in the effect characterizations of rGO and the graphene process grown from the talc surface. One of the main reasons the graphene/talc hybrid emits relatively more minor and has less impact on characterizations is that the production technique has a more straightforward process than other production techniques. It is widely used in producing graphene oxide according to the modified Hummer's method, which is one of the most preferred methods recently. In the process, graphite is oxidized with potassium permanganate ($KMnO_4$) by using strong acids such as sulfuric acid (H_2SO_4) and phosphoric acid (H_3PO_4). The use of strong acids directly impact on the global warming potential as it causes CO_2 emissions.

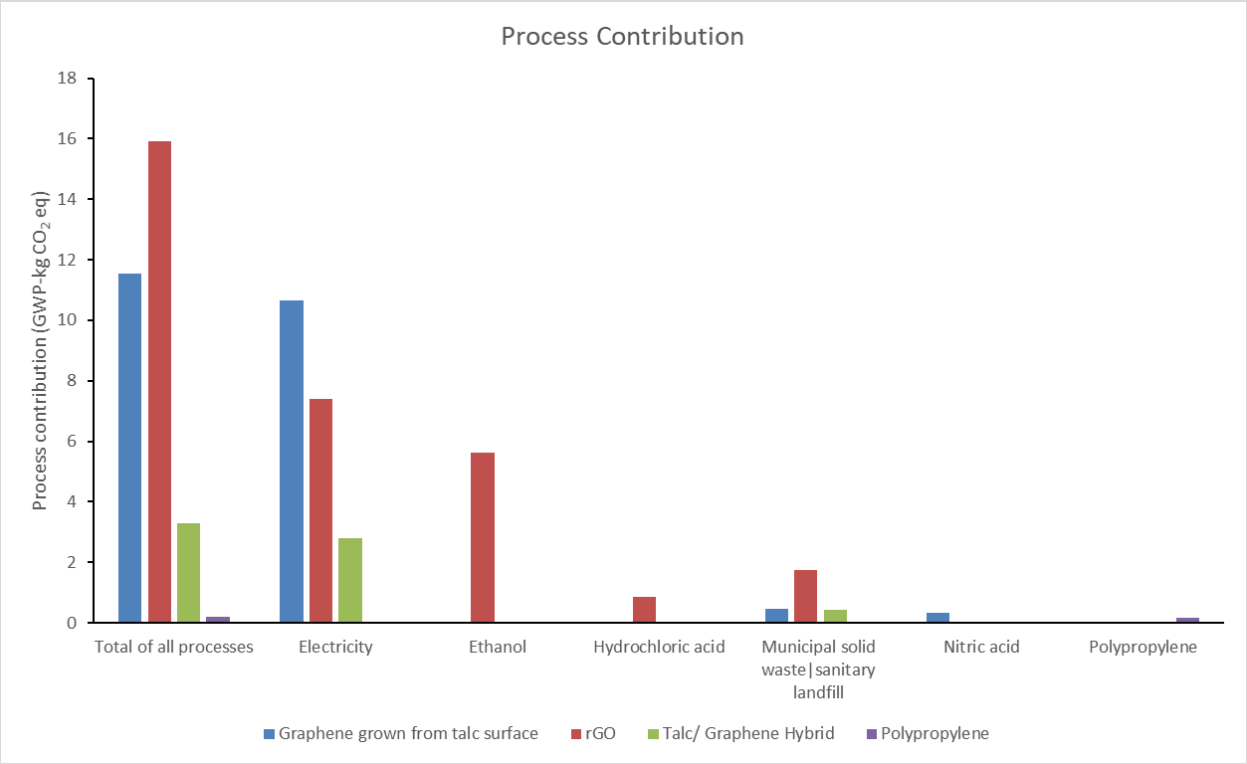

Figure 24. Impact of production processes and inputs on global warming potential.

The hotspots of all these production processes were the electricity consumption during the reactions (heater), high-shear mixing, and thermal treatment. In order to decrease greenhouse gases (GHG) emissions, more energy-efficient devices could be used for future applications. In addition, it should be noted that the life cycle analysis may yield controversial results depending on the regions where the facilities are located and the

places where the data was obtained. Low-efficiency productions are essential parts that need improvement for future LCA studies.

6.3.2. Effect of production routes environmental impact of graphene from plastics

The environmental impact factors from graphene production on the talc surface and talc/graphene hybrid by using chamber furnace and rotary furnace are given in Table 27.

When the environmental impact factors were evaluated according to the global warming potential, it was seen that the production of Graphene grown from talc surface by using chamber furnace has a value of 11.5 kg CO_2 eq. The global warming potential of Talc/Graphene hybrid produced in rotary furnace was lower than the production of the Talc/Graphene hybrid produced in chamber furnace, and the values of them was 0.77 kg CO_2 eq and 3.29 kg CO_2 eq. In addition, the production of graphene grown from talc surface using rotary furnace has a value of 9.1 kg CO_2 eq which is 21% lower than the graphene grown from talc surface by using chamber furnace.

The strong acids used in the separation of graphene and the additional energy (reflux heater, oven, centrifuge) expenditures could be considered the reason for harmful emissions to the environment caused during the separation process. Additionally, it can be said that the production of graphene/talc hybrid structures process was more environmentally friendly than the graphene grown from talc surface regardless of the furnace type. Moreover, the usage of waste plastic instead of virgin plastic decreased the CO_2 emission. It was seen from Table 27 that the carbonization process conducted in chamber furnace at 1000°C under argon atmosphere for upcycled graphene production on talc surface yielded a high value of CO_2 emission. Moreover, the highest impact difference between graphene growth on talc and talc/graphene hybrid was observed in stratospheric ozone depletion.

Table 27. Environmental impact factors from the production of Talc/Graphene hybrid produced in rotary furnace, Talc/Graphene hybrid produced in chamber furnace, Graphene grown from talc surface-Rotary furnace, and Graphene grown from talc surface- Chamber furnace.

Impact Category	**Unit**	**Talc/Graphene hybrid produced in rotary furnace**	**Talc/Graphene hybrid produced in chamber furnace**	**Graphene grown from talc surface-Rotary furnace**	**Graphene grown from talc surface-Chamber furnace**
Global warming	kg CO_2 eq	0.77	3.29	9.1	11.5
Stratospheric ozone depletion	kg CFC11 eq	2.43×10^{-7}	9.65×10^{-7}	1.21×10^{-5}	1.28×10^{-5}
Ionizing radiation	kBq Co-60 eq	0.009	0.04	0.11	0.14
Ozone formation, Human health	kg NO_x eq	0.001	0.006	0.01	0.022
Fine particulate matter formation	kg PM2.5 eq	0.004	0.018	0.05	0.072
Ozone formation, Terrestrial ecosystems	kg NO_x eq	0.001	0.006	0.01	0.021
Terrestrial acidification	kg SO_2 eq	0.003	0.01	0.03	0.05
Freshwater eutrophication	kg P eq	0.0006	0.0025	0.007	0.0095
Marine eutrophication	kg N eq	6.98×10^{-5}	0.0004	0.0005	0.0009
Terrestrial ecotoxicity	kg 1,4-DCB	0.4	1.8	5.6	6.93
Freshwater ecotoxicity	kg 1,4-DCB	0.04	0.34	0.31	0.605
Marine ecotoxicity	kg 1,4-DCB	0.06	0.45	0.42	0.809
Human carcinogenic toxicity	kg 1,4-DCB	0.03	0.15	0.43	0.54
Human non-carcinogenic toxicity	kg 1,4-DCB	1.06	7.46	7.31	13.7
Land use	m^2a crop eq	0.003	0.01	0.03	0.04
Mineral resource scarcity	kg Cu eq	0.0002	0.0013	0.004	0.005
Fossil resource scarcity	kg oil eq	0.2	0.77	2.39	2.97
Water consumption	m^3	0.004	0.018	0.05	0.07

Figure 25 illustrates that production Graphene grown from talc surface using chamber furnace results in the highest emission to the environment whereas the production routine of Talc/Graphene hybrid produced in the rotary furnace was the lowest. Moreover, Talc/Graphene hybrid produced in chamber furnaces had more impact than the Graphene grown from talc surface-Rotary furnace on the impact categories of freshwater ecotoxicity, marine ecotoxicity, human non-carcinogenic toxicity.

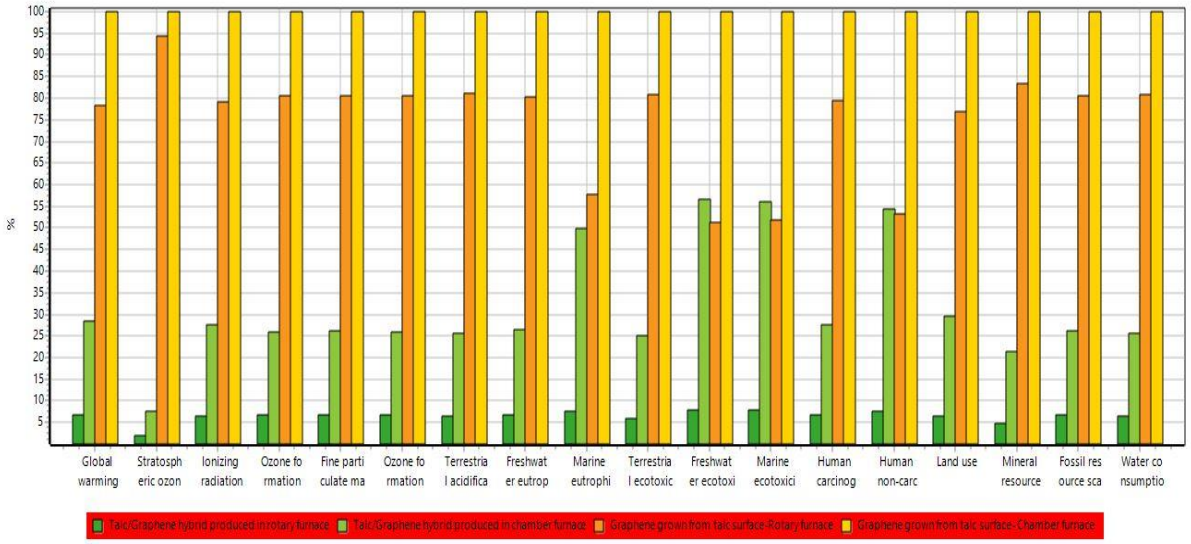

Figure 25. Impact characterization of production processes of talc/graphene hybrids and graphene grown on talc surface.

The comparison of global warming potential of Talc/Graphene hybrid produced in rotary furnace, Talc/Graphene hybrid produced in chamber furnace, Graphene grown from talc surface (Rotary furnace), and Graphene was grown from talc surface (Chamber furnace) is given in Figure 27. As explained above, the Graphene grown from talc surface using the chamber furnace production process has been the most influential production process on global warming. Usage of high electrical consumption and non-continuous feeding ability to the chamber furnace might be the reason for this high impact.

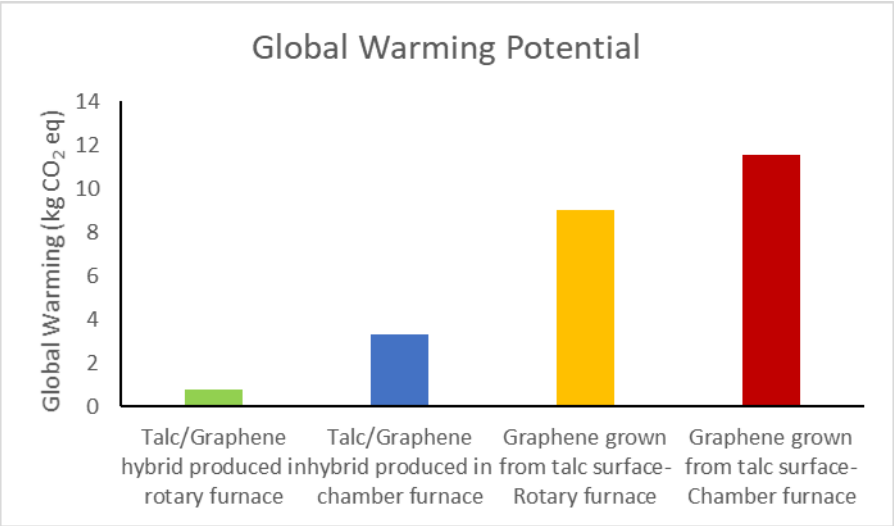

Figure 26. The comparison of global warming potential of Talc/Graphene hybrid produced in rotary furnace, Talc/Graphene hybrid produced in chamber furnace, Graphene grown from talc surface-Rotary furnace, and Graphene grown from talc surface- Chamber furnace talc/graphene hybrid, rGO and PP.

In addition, Figure 27 reveals the impact of production processes and inputs on global warming potential. Electricity consumption plays an essential role in global warming, ozone depletion in the stratosphere, ozone formation, and fine particulate matter formation, which are included in the effect characterizations of graphene process grown from the talc surface and graphene/ talc hybrid additive production. One of the main reasons the production process of graphene/talc hybrid produced in rotary furnaces emits relatively more minor and has less impact on characterizations is the continuous feeding ability of the furnace. One of the main reasons for the low CO_2 emission of production in the rotary furnace is that, while one batch of production occurs in chamber furnace, up to nine batch production can be performed in the rotary furnace, which results in less electricity consumption. Although one batch of material could be carbonized in the chamber furnace, for the same amount of time, nine batches can be carbonized in the rotary furnace; hence more production can be performed for the same amount of energy consumption.

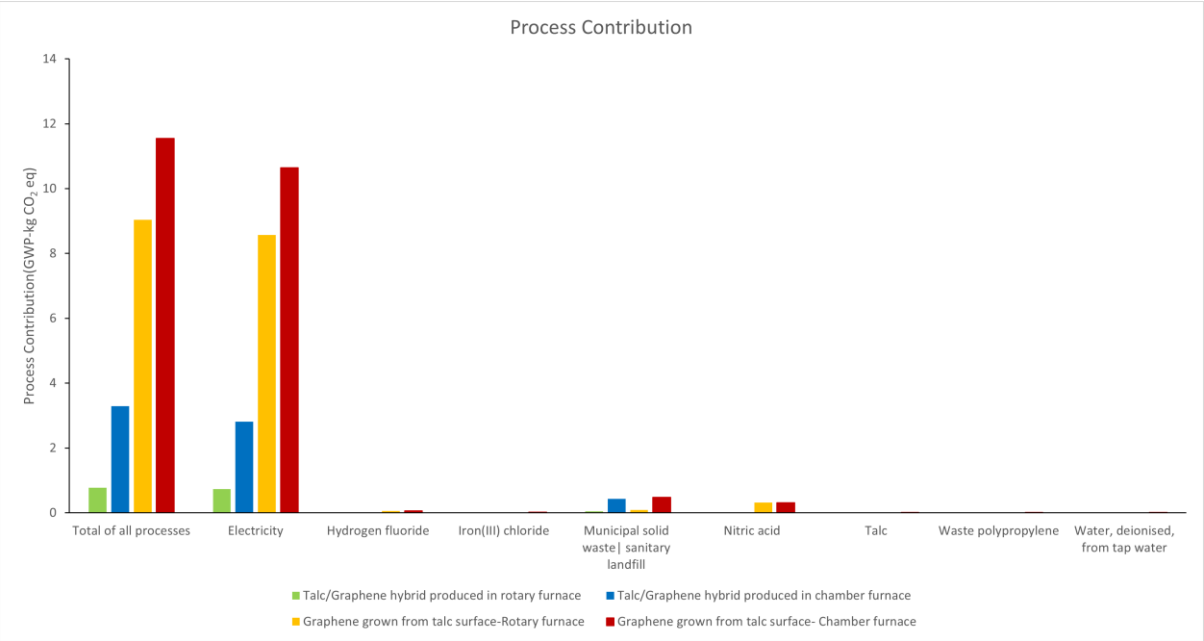

Figure 27. Impact of production processes and inputs on global warming potential.

The hotspots of all these production processes were the electricity consumption during the reactions (heater), high-shear mixing, and thermal treatment. In order to decrease greenhouse gas (GHG) emissions, more energy-efficient devices could be used for future applications. Furthermore, usage of the rotary furnace resulted as a convenient method for large-scale production due to its low CO2 and other environmentally non-friendly emissions. In addition, it should be noted that the life cycle analysis may yield controversial results depending on the regions where the facilities are located and the places where the data was obtained. Low-efficiency productions are essential parts that need improvement for future LCA studies.

6.4. CONCLUSION

In this study, LCA study was performed to investigate the CO_2 emissions of the production processes and to find the hotspots of the processes. Life cycle analyses of graphene grown from talc surface, reduced graphene oxide (rGO), Talc/Graphene Hybrid and polypropylene (PP) production processes were made, and an evaluation of material and energy consumption was made to minimize negative environmental effects. Graphene and Talc/Graphene Hybrid structures grown on the talc surface revealed promising results, especially in increasing production-energy costs and demands. Reduced graphene oxide (rGO), which we used as a parameter to compare the graphene

production routines, has an important place in its electrical and thermal properties. However, the fact that the synthesis of this material is obtained because of two-stage reactions has revealed that it has high emission values in terms of both energy and chemicals used in the production process. After synthesizing graphene oxide (oxidation with strong acids) by Hummer's method, the first step reaction of which has been modified, a reduction is carried out with a hydrazine hydrate chemical. Life cycle analyzes resulted that the production process of rGO can be considered risky due to chemical use and energy expenditure during the synthesis and purification. Furthermore, energy (electricity) consumption is one of the most contributing factors to global warming potential. Carbonization of the process at 1000˚C is the main factor affecting energy consumption. It has been observed that chemicals such as iron (III) chloride, strong acids HF and HNO_3, which are used during the production process, especially affect the global warming potential. In addition, carbonization in rotary furnace and chamber furnace revealed that, rotary furnace is more convenient to perform carbonization because it is environmentally friendly, cost-effective, and time-saving method. Graphene production revealed more CO_2 emissions than graphene/talc hybrid production because of more electricity usage through the production and strong acid usage.

CHAPTER 7. CONCLUSIONS

In the scope of this thesis, graphene formation on talc surface from waste PP was achieved by upcycling process. As a first step, the effect of talc size on upcycled graphene formation was examined, and for this reason, two types of talc, micron talc and fine talc were supplied. According to the talc size and chemical structure of waste polymer (whether the polymer is aliphatic or aromatic), the dimension of carbon nanomaterials obtained on the talc surface can be controlled. Using talc, smaller than micron talc, three-dimensional (3D) spherical graphene structures can be produced instead of two-dimensional (2D) graphene plates. Figure 28 reveals schematically described the production of 3D spherical graphene structures grown on fine talc, and Figure 29 illustrates 2D graphene plates on micron talc from waste plastics.

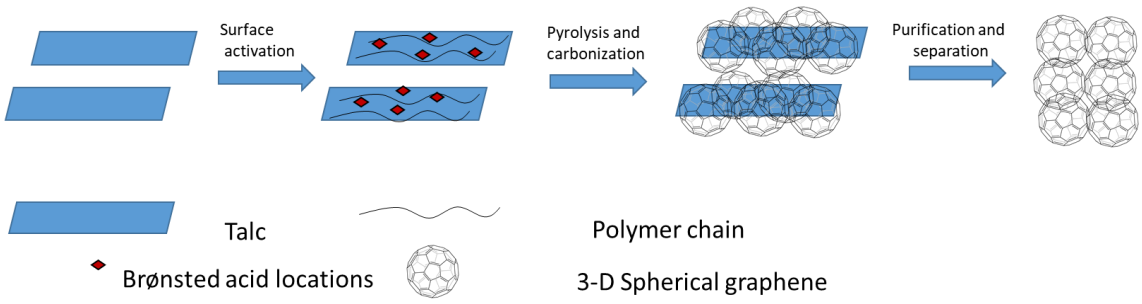

Figure 28. The schematic of the production of 3D spherical graphene structures grown on fine talc from waste platics.

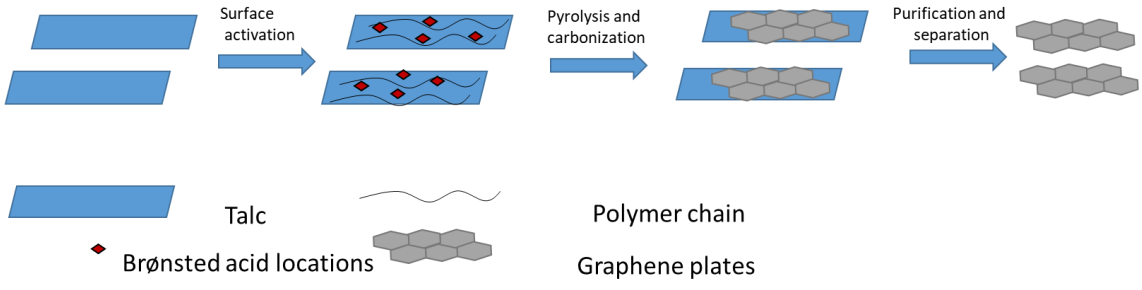

Figure 29. The schematic of the production of 2D graphene plates grown on micron talc from waste platics.

It is known that the talc surface is hydrophobic, which makes it challenging to be homogeneously dispersed in polymer matrices. In order to improve the adhesion between the talc/polymer, surface activation of micron talc and fine-talc were achieved with $FeCl_3$.

In addition, non-functionalized micron talc and fine talc were used in carbonization to compare the impact of surface activation on upcycled graphene formation. To sum up, it can be said that the size of utilized talc and surface activation of talc was the major examined parameters for upcycled graphene formation in the preliminary experiments.

As a second step, before carbonization waste PP (HomoPP) and Fe-talc /non-functionalized talc were mixed with a thermokinetic mixer at a high-shear rate (4000 rpm) in the ratio of 80:20 wt %. Then upcycled graphene formation was conducted by the carbonization at 1000◦C for 5 min in a chamber furnace under Argon atmosphere. The obtained graphene/talc hybrids were then subjected to HF acid treatment to separate graphene from the talc surface. Several microscopic, spectroscopic, and thermal characterizations investigated the graphene/talc hybrids and upcycled graphene structure. Related to the characterization results, it can be said that the production of upcycled graphene on Fe-micron talc, Fe-fine talc, micron talc, and fine talc by using waste PP as a carbon source was well-achieved. In addition, it was mentioned that it was better to use $FeCl_3$ treated talc for graphene formation. 2D graphene plates could be obtained whether the talc size was 10 μm or above, while 3D graphene spheres occurred by using the talc size 2 μm or below. Moreover, carbonization temperature had a direct impact on graphene production. It was determined conducting a carbonization process above 850◦C; efficient graphene formation can be achieved. The desired graphene/talc hybrids could be produced based on these outcomes. The outcomes of the third chapter in this thesis are summarized in the table 28.

Table 28. Summary of graphene growth on the surface of functionalized and non-functionalized talc samples.

Carbon source	The size of talc	Surface activation	Graphene formation	Details
Polypropylene	Micron talc	$FeCl_3$	✅	2D graphene plates were produced. (verification was performed with TEM).
Polypropylene	Micron talc	-	✅	Graphene formation yield was lower than that of Fe-micron talc. Low carbon ratio was detected.
Polypropylene	Fine talc	$FeCl_3$	✅	Spherical 3D graphene fabrication was performed (verified by TEM)
Polypropylene	Fine talc	-	✅	Graphene formation was proved, but the graphene yield was less than that of Fe-treated fine talc (according to XRD results).

The number of graphene layers was also calculated by considering the data from XRD and using Debye-Scherer equations (shown below) in the thesis.

$$D = \frac{0.89\,\lambda}{\beta_{002}\,cos\theta_{002}} \tag{4}$$

$$n = \frac{D}{d_{002}} + 1 \tag{5}$$

Where, L_a is stacking height, β is full-width at half-maximum and d_{002} is the distance between the layers.

In the table shown below, the number of graphene layers was given, and it was observed that as the talc size decreases, the number of graphene layers also decreases.

Table 29. The number of graphene layers obtained from different hybrid structures.

Sample	Layer Number
Graphene from Hybrid-2 (thermokinetic mixing , Fe-micron talc, catalytic carbonization in chamber furnace)	17
Graphene from Hybrid-4 (thermokinetic mixing , Fe-fine talc, direct carbonization in chamber furnace)	13

In addition to carbonization in the chamber furnace, flash pyrolysis in the rotary furnace was also conducted using HomoPP/Fe-micron talc. Prior to flash pyrolysis in the rotary furnace, HomoPP, and Fe-micron talc (in the ratio of 80:20 wt %) were mixed with extruder at 349 rpm and 228◦C. Then, HomoPP/Fe-micron talc was subjected to ball-milling to supply the compound in powder form and subsequently sent to the rotary furnace for flash pyrolysis at 1000°C. Completing this research made it possible to compare heat treatment and polymer processing effects on upcycled graphene formation. It was seen that flash pyrolysis was advantageous in terms of time and yield of graphene. Furthermore, mixing HomoPP and Fe-micron talc in an extruder conserved the crystal structure of talc, while thermokinetic mixing was not so successful in that. Below, heat treatment and polymer processing methods for graphene formation from waste PP were detailed.

Table 30. Summary of the effects of polymer processing types and heat treatments on the growth of graphene.

Graphene/talc hybrid	**Polymer processing type prior to carbonization**	**Carbonization process**	**Result**
Hybrid 1	Thermokinetic mixer/twin-screw extruder	Flash pyrolysis/direct carbonization in chamber furnace	Twin-screw extruder and flash pyrolysis were selected the best polymer processing methods and heat treatment process

The obtained graphene/talc hybrids were used to reinforce HomoPP and CopoPP to enhance the mechanical features of neat HomoPP and CopoPP. The hybrid was incorporated into the HomoPP and CopoPP by a thermokinetic mixer at a high shear rate in 5, 10, 15, and 20 wt %. Both Fe-functionalized and non-functionalized talcs were utilized for compound preparation. The addition of hybrid structures into HomoPP and CopoPP significantly increased the flexural and tensile modulus of the compounds.

A life-cycle assessment (LCA) allows for an investigation of the CO_2 emissions of the manufacturing processes and identifying their hotspots. To eliminate negative environmental consequences, life cycle analyses can be performed. Therefore, LCA of the production routes of graphene/talc hybrids was conducted to see the hazardous effects on the environment and human health. Furthermore, the global warming potential of the

obtained hybrids was evaluated and compared to the conventional graphene production methods. The assessment was considered for both catalytic and flash carbonization in detail.

References

[1] Rahimi, A.R. and Garciá, J.M. (2017). Chemical recycling of waste plastics for new materials production. *Nature Reviews Chemistry*, *1*,: 1–11, doi: 10.1038/s41570-017-0046.

[2] World Economic Forum. (2016). The new plastics economy: Rethinking the future of plastics. *Ellen MacArthur Foundation*, (January),: 120.

[3] Ahleitner, M.A.G. and Gmbh, B.P. , Borealis Polyolefine GmbH, Linz, Austria C.

[4] Iwamoto, S. Yamamoto, S. Lee, S.H. and Endo, T. (2014). Mechanical properties of polypropylene composites reinforced by surface-coated microfibrillated cellulose. *Composites Part A: Applied Science and Manufacturing*, *59*,: 26–29, doi: 10.1016/j.compositesa.2013.12.011.

[5] Geim, A.K. and Novoselov, K.S. (2009). The rise of grapheneIn: Nanosci. Technol. A Collect. Rev. from Nat. Journals. *World Scientific*; pp 11–19.

[6] Mohan, V.B. Lau, K. tak. Hui, D. and Bhattacharyya, D. (2018). Graphene-based materials and their composites: A review on production, applications and product limitationsCompos. Part B Eng. 142:200–220.

[7] C. Backes, A. Abdelkader, C.A. et al. (2020). Production and processing of graphene and related materials. *2D Materials*, *7*(2), doi: 10.1088/2053-1583/ab1e0a.

[8] Finnveden, G. Hauschild, M.Z. Ekvall, T. Guinée, J. Heijungs, R. Hellweg, S. Koehler, A. Pennington, D. and Suh, S. (2009). Recent developments in Life Cycle Assessment. *Journal of Environmental Management*, *91*(1),: 1–21, doi: 10.1016/j.jenvman.2009.06.018.

[9] Basset, J.M. Zhou, L. and Enakonda, L.R. (2018). Treated iron ore catalysts for production of hydrogen and graphene.

[10] Tiwari, S.K. Sahoo, S. Wang, N. and Huczko, A. (2020). Graphene research and their outputs: Status and prospect. *Journal of Science: Advanced Materials and Devices*, *5*(1),: 10–29, doi: 10.1016/j.jsamd.2020.01.006.

[11] Zhong, Y.L. Tian, Z. Simon, G.P. and Li, D. (2015). Scalable production of graphene via wet chemistry: Progress and challenges. *Materials Today*, *18*(2),: 73–78, doi:

10.1016/j.mattod.2014.08.019.

[12] Gurzęda, B. Buchwald, T. Nocuń, M. Bąkowicz, A. and Krawczyk, P. (2017). Graphene material preparation through thermal treatment of graphite oxide electrochemically synthesized in aqueous sulfuric acidRSC Adv. 7:19904–19911.

[13] Bohm, S. Ingle, A. Bohm, H.L.M. Fenech-Salerno, B. Wu, S. and Torrisi, F. (2021). Graphene production by cracking. *Philosophical Transactions of the Royal Society A: Mathematical, Physical and Engineering Sciences*, *379*(2203), doi: 10.1098/rsta.2020.0293.

[14] Adetayo, A. and Runsewe, D. (2019). Synthesis and Fabrication of Graphene and Graphene Oxide: A Review. *Open Journal of Composite Materials*, *09*(02),: 207–229, doi: 10.4236/ojcm.2019.92012.

[15] Shams, S.S. Zhang, R. and Zhu, J. (2015). Graphene synthesis: A Review. *Materials Science- Poland*, *33*(3),: 566–578, doi: 10.1515/msp-2015-0079.

[16] Gong, J. Liu, J. Wen, X. Jiang, Z. Chen, X. Mijowska, E. and Tang, T. (2014). Upcycling waste polypropylene into graphene flakes on organically modified montmorillonite. *Industrial and Engineering Chemistry Research*, *53*(11),: 4173–4181, doi: 10.1021/ie4043246.

[17] Tan, H. Wang, D. and Guo, Y. (2018). Thermal growth of graphene: A review. *Coatings*, *8*(1), doi: 10.3390/coatings8010040.

[18] Chung, T.F. Shen, T. Cao, H. Jauregui, L.A. Wu, W. Yu, Q. Newell, D. and Chen, Y.P. (2013). Synthetic graphene grown by chemical vapor deposition on copper foils. *International Journal of Modern Physics B*, *27*(10), doi: 10.1142/S0217979213410026.

[19] Yi, M. and Shen, Z. (2015). A review on mechanical exfoliation for the scalable production of graphene. *Journal of Materials Chemistry A*, *3*(22),: 11700–11715.

[20] Akhavan, O. Bijanzad, K. and Mirsepah, A. (2014). Synthesis of graphene from natural and industrial carbonaceous wastes. *RSC Advances*, *4*(39),: 20441–20448, doi: 10.1039/c4ra01550a.

[21] Ruan, G. Sun, Z. Peng, Z. and Tour, J.M. (2011). Growth of graphene from food, insects, and waste. *ACS Nano*, *5*(9),: 7601–7607, doi: 10.1021/nn202625c.

[22] Algozeeb, W.A. Savas, P.E. Luong, D.X. Chen, W. Kittrell, C. Bhat, M. Shahsavari, R. and Tour, J.M. (2020). Flash graphene from plastic waste. *ACS Nano*, *14*(11),: 15595–15604, doi: 10.1021/acsnano.0c06328.

[23] Sun, L. Tian, C. Li, M. Meng, X. Wang, L. Wang, R. Yin, J. and Fu, H. (2013). From coconut shell to porous graphene-like nanosheets for high-power supercapacitors. *Journal of Materials Chemistry A*, *1*(21),: 6462–6470, doi: 10.1039/C3TA10897J.

[24] Jankovic, L. Gournis, D. Dimos, K. Karakassides, M.A. and Bakas, T. (2005). Catalytic production of carbon nanotubes over first row transition metal oxides supported on montmorillonite. *Journal of Physics: Conference Series*, *10*(1),: 178–181, doi: 10.1088/1742-6596/10/1/044.

[25] Sharma, S. Kalita, G. Hirano, R. Shinde, S.M. Papon, R. Ohtani, H. and Tanemura, M. (2014). Synthesis of graphene crystals from solid waste plastic by chemical vapor deposition. *Carbon*, *72*,: 66–73, doi: 10.1016/j.carbon.2014.01.051.

[26] Lian, Y.M. Utetiwabo, W. Zhou, Y. Huang, Z.H. Zhou, L. Muhammad, F. Chen, R.J. and Yang, W. (2019). From upcycled waste polyethylene plastic to graphene/mesoporous carbon for high-voltage supercapacitors. *Journal of Colloid and Interface Science*, *557*,: 55–64, doi: 10.1016/j.jcis.2019.09.003.

[27] Zanjani, J.S.M. Poudeh, L.H. Ozunlu, B.G. Yagci, Y.E. Menceloglu, Y. and Saner Okan, B. (2020). Development of waste tire-derived graphene reinforced polypropylene nanocomposites with controlled polymer grade, crystallization and mechanical characteristics via melt-mixing. *Polymer International*, *69*(9),: 771–779, doi: 10.1002/pi.6012.

[28] Huang, H. Peng, L. Fang, W. Cai, S. Chu, X. Liu, Y. Gao, W. Xu, Z. and Gao, C. (2020). A polyimide-pyrolyzed carbon waste approach for the scalable and controlled electrochemical preparation of size-tunable graphene. *Nanoscale*, *12*(22),: 11971–11978, doi: 10.1039/d0nr00725k.

[29] Mohamed, H.H. and Alsanea, A.A. (2020). TiO2/carbon dots decorated reduced graphene oxide composites from waste car bumper and TiO2 nanoparticles for photocatalytic applications. *Arabian Journal of Chemistry*, *13*(1),: 3082–3091, doi: 10.1016/j.arabjc.2018.08.016.

[30] Choi, D. Yeo, J.S. Joh, H.I. and Lee, S. (2018). Carbon Nanosheet from Polyethylene

Thin Film as a Transparent Conducting Film: ‘upcycling’ of Waste to Organic Photovoltaics Application. *ACS Sustainable Chemistry and Engineering*, *6*(9),: 12463–12470, doi: 10.1021/acssuschemeng.8b03066.

[31] Zhang, J. Yan, B. Wan, S. and Kong, Q. (2013). Converting polyethylene waste into large scale one-dimensional Fe 3O4@C composites by a facile one-pot process. *Industrial and Engineering Chemistry Research*, *52*(16),: 5708–5712, doi: 10.1021/ie4004392.

[32] Tripathi, P.K. Durbach, S. and Coville, N.J. (2017). Synthesis of Multi-Walled carbon nanotubes from plastic waste using a Stainless-Steel CVD reactor as catalyst. *Nanomaterials*, *7*(10), doi: 10.3390/nano7100284.

[33] Hedayati, A. Barnett, C. Swan, G. and Orbaek White, A. (2019). Chemical Recycling of Consumer-Grade Black Plastic into Electrically Conductive Carbon Nanotubes. *C*, *5*(2),: 32, doi: 10.3390/c5020032.

[34] Wu, C. Wang, Z. Wang, L. Williams, P.T. and Huang, J. (2012). Sustainable processing of waste plastics to produce high yield hydrogen-rich synthesis gas and high quality carbon nanotubes. *RSC Advances*, *2*(10),: 4045–4047, doi: 10.1039/c2ra20261a.

[35] Zhang, J. Zhang, L. Yang, H. Kong, Q. Liu, Y. and Yuan, A. (2014). Sustainable processing of waste polypropylene to produce high yield valuable Fe/carbon nanotube nanocomposites. *CrystEngComm*, *16*(37),: 8832–8840, doi: 10.1039/c4ce01064g.

[36] Zhang, Y. Wu, C. Nahil, M.A. and Williams, P. (2015). Pyrolysis-catalytic reforming/gasification of waste tires for production of carbon nanotubes and hydrogenEnergy and Fuels 29:3328–3334.

[37] Yao, D. Zhang, Y. Williams, P.T. Yang, H. and Chen, H. (2018). Co-production of hydrogen and carbon nanotubes from real-world waste plastics: Influence of catalyst composition and operational parameters. *Applied Catalysis B: Environmental*, *221*(September 2017),: 584–597, doi: 10.1016/j.apcatb.2017.09.035.

[38] Wang, J. Shen, B. Lan, M. Kang, D. and Wu, C. (2019). Carbon nanotubes (CNTs) production from catalytic pyrolysis of waste plastics: The influence of catalyst and reaction pressure. *Catalysis Today*, *351*(November 2018),: 50–57, doi:

10.1016/j.cattod.2019.01.058.

[39] Bazargan, A. and McKay, G. (2012). A review - Synthesis of carbon nanotubes from plastic wastes. *Chemical Engineering Journal*, *195–196*,: 377–391, doi: 10.1016/j.cej.2012.03.077.

[40] Kong, Q. and Zhang, J. (2007). Synthesis of straight and helical carbon nanotubes from catalytic pyrolysis of polyethylene. *Polymer Degradation and Stability*, *92*(11),: 2005–2010, doi: 10.1016/j.polymdegradstab.2007.08.002.

[41] Liu, J. Jiang, Z. Yu, H. and Tang, T. (2011). Catalytic pyrolysis of polypropylene to synthesize carbon nanotubes and hydrogen through a two-stage process. *Polymer Degradation and Stability*, *96*(10),: 1711–1719, doi: 10.1016/j.polymdegradstab.2011.08.008.

[42] Stanic, S. Koch, T. Schmid, K. Knaus, S. and Archodoulaki, V.M. (2021). Upcycling of polypropylene with various concentrations of peroxydicarbonate and dilauroyl peroxide and two processing steps. *Journal of Applied Polymer Science*, *138*(28),: 1–20, doi: 10.1002/app.50659.

[43] Zhuo, C. and Levendis, Y.A. (2014). Upcycling waste plastics into carbon nanomaterials: A reviewJ. Appl. Polym. Sci. 131:.

[44] Blank, L.M. Narancic, T. Mampel, J. Tiso, T. and O'Connor, K. (2020). Biotechnological upcycling of plastic waste and other non-conventional feedstocks in a circular economy. *Current Opinion in Biotechnology*, *62*,: 212–219, doi: 10.1016/j.copbio.2019.11.011.

[45] Zoe, Z. A Review on Upcycling: Current Body of Literature, Knowledge Gaps and a Way Forward Kyungeun Sung.

[46] Aji, M.P. Wati, A.L. Priyanto, A. Karunawan, J. Nuryadin, B.W. Wibowo, E. Marwoto, P. and Sulhadi. (2018). Polymer carbon dots from plastics waste upcycling. *Environmental Nanotechnology, Monitoring and Management*, *9*(January),: 136–140, doi: 10.1016/j.enmm.2018.01.003.

[47] Cui, L. Wang, X. Chen, N. Ji, B. and Qu, L. (2017). Trash to treasure: Converting plastic waste into a useful graphene foil. *Nanoscale*, *9*(26),: 9089–9094, doi: 10.1039/c7nr03580b.

[48] Jiang, Z. Song, R. Bi, W. Lu, J. and Tang, T. (2007). Polypropylene as a carbon source for the synthesis of multi-walled carbon nanotubes via catalytic combustion. *Carbon*, *45*(2),: 449–458, doi: 10.1016/j.carbon.2006.08.012.

[49] Choi, D. Jang, D. Joh, H.I. Reichmanis, E. and Lee, S. (2017). High Performance Graphitic Carbon from Waste Polyethylene: Thermal Oxidation as a Stabilization Pathway RevisitedChem. Mater. 29:9518–9527.

[50] R, S. Z, J. W, B. W, C. J, L. B, H. and T, T. (2007). The combined catalytic action of solid acids with nickel for the transformation of polypropylene into carbon nanotubes by pyrolysis. *Chemistry (Weinheim an der Bergstrasse, Germany)*, *13*(11),: 3234–3240, doi: 10.1002/CHEM.200601018.

[51] Bajad, G. Guguloth, V. Vijayakumar, R.P. and Bose, S. (2016). Conversion of plastic waste into CNTs using Ni/Mo/MgO catalyst - An optimization approach by mixture experiment. *Fullerenes Nanotubes and Carbon Nanostructures*, *24*(2),: 162–169, doi: 10.1080/1536383X.2015.1130704.

[52] Berktas, I. Hezarkhani, M. Haghighi Poudeh, L. and Saner Okan, B. (2020). Recent developments in the synthesis of graphene and graphene-like structures from waste sources by recycling and upcycling technologies: a reviewGraphene Technol. 5:59–73.

[53] Lapcik, L. Jindrova, P. Lapcikova, B. Tamblyn, R. Greenwood, R. and Rowson, N. (2008). Effect of the talc filler content on the mechanical properties of polypropylene composites. *Journal of Applied Polymer Science*, *110*(5),: 2742–2747, doi: 10.1002/app.28797.

[54] Maiti, S.N. and Sharma, K.K. (1992). Studies on polypropylene composites filled with talc particles. *Journal of materials science*, *27*(17),: 4605–4613.

[55] Shahidi, S.S. Mohammadi, B. Mohammadi, S. and Vessally, E. (2021). The effect of the hybrid multi-layered Graphene oxide/Talc as a hydrophobic agent in epoxy coating. *Plastics, Rubber and Composites*, doi: 10.1080/14658011.2021.1931772.

[56] Liu, K. Stadlbauer, W. Zitzenbacher, G. Paulik, C. and Burgstaller, C. (2016). Effects of surface modification of talc on mechanical properties of polypropylene/talc composites. *AIP Conference Proceedings*, *1713*(March),: 120008, doi: 10.1063/1.4942323.

[57] MORALES MORALES, J.A. (2017). Synthesis of hematite α-Fe2O3 nano powders by the controlled precipitation method. *Ciencia En Desarrollo*, *8*(1),: 99–107, doi: 10.19053/01217488.v8.n1.2017.4494.

[58] Hang, B.T. and Anh, T.T. (2021). Controlled synthesis of various Fe2O3 morphologies as energy storage materials. *Scientific Reports*, *11*(1),: 1–10, doi: 10.1038/s41598-021-84755-z.

[59] Hofmeister, A.M. and Bowey, J.E. (2006). Quantitative infrared spectra of hydrosilicates and related minerals. *Monthly Notices of the Royal Astronomical Society*, *367*(2),: 577–591, doi: 10.1111/j.1365-2966.2006.09894.x.

[60] Li, Y.S. Church, J.S. and Woodhead, A.L. (2012). Infrared and Raman spectroscopic studies on iron oxide magnetic nano-particles and their surface modifications. *Journal of Magnetism and Magnetic Materials*, *324*(8),: 1543–1550, doi: 10.1016/j.jmmm.2011.11.065.

[61] Zakirov, A.S. Navamathavan, R. Jang, Y.J. Jung, A.S. Choi, C.K. and Lee, K.M. (2007). A study on structural and electrical properties of low dielectric constant SiOC(–H) thin films deposited via PECVD. *Journal of the Korean Physical Society*, *50*(6),: 1809–1813, doi: 10.3938/jkps.50.1809.

[62] Ferrari, A.C. and Basko, D.M. (2013). Raman spectroscopy as a versatile tool for studying the properties of graphene. *Nature Nanotechnology*, *8*(4),: 235–246, doi: 10.1038/nnano.2013.46.

[63] Graf, D. Molitor, F. Ensslin, K. Stampfer, C. Jungen, A. Hierold, C. and Wirtz, L. (2007). Spatially Resolved Raman Spectroscopy of Single- and Few-Layer Graphene. *Nano Letters*, *7*(2),: 238–242, doi: 10.1021/NL061702A.

[64] Saner, B. Okyay, F. and Yürüm, Y. (2010). Utilization of multiple graphene layers in fuel cells. 1. An improved technique for the exfoliation of graphene-based nanosheets from graphite. *undefined*, *89*(8),: 1903–1910, doi: 10.1016/J.FUEL.2010.03.036.

[65] Ferrari, A. and Robertson, J. (2000). Interpretation of Raman spectra of disordered and amorphous carbon. *Physical Review B*, *61*(20),: 14095, doi: 10.1103/PhysRevB.61.14095.

[66] Nguyen, V.T. Le, H.D. Nguyen, V.C. Ngo, T.T.T. Le, D.Q. Nguyen, X.N. and Phan, N.M. (2013). Synthesis of multi-layer graphene films on copper tape by atmospheric pressure chemical vapor deposition method. *Advances in Natural Sciences: Nanoscience and Nanotechnology*, *4*(3),: 035012, doi: 10.1088/2043-6262/4/3/035012.

[67] Kogure, T. Kameda, J. Matsui, T. and Miyawaki, R. (2006). Stacking structure in disordered talc: Interpretation of its X-ray diffraction pattern by using pattern simulation and high-resolution transmission electron microscopy. *American Mineralogist*, *91*(8–9),: 1363–1370, doi: 10.2138/am.2006.2196.

[68] Ferrage, E. Martin, F. Petit, S.. Pejo-soucaille, S. Micoud, P. Fourty, G. Ferret, J.. Salvi, S. De Parseval, P. and Fortune, J.. P. (2003). Evaluation of talc morphology using FTIR and H/D substitution. *Clay Minerals*, *38*(2),: 141–150, doi: 10.1180/0009855033820084.

[69] Gao, Y. Hou, F. Hu, S. Wu, B. Wang, Y. Zhang, H. Jiang, B. and Fu, H. (2018). Graphene Quantum-Dot-Modified Hexagonal Tubular Carbon Nitride for Visible-Light Photocatalytic Hydrogen Evolution. *ChemCatChem*, *10*(6),: 1330–1335, doi: 10.1002/cctc.201701823.

[70] Stobinski, L. Lesiak, B. Malolepszy, A. Mazurkiewicz, M. Mierzwa, B. Zemek, J. Jiricek, P. and Bieloshapka, I. (2014). Graphene oxide and reduced graphene oxide studied by the XRD, TEM and electron spectroscopy methods. *Journal of Electron Spectroscopy and Related Phenomena*, *195*,: 145–154, doi: 10.1016/j.elspec.2014.07.003.

[71] Teknologi, J. Aziz, M. Teknologi, U. Jaafar, J. Teknologi, U. Study, D. Membrane, S.N. Methanol, D. Cell, F. and Jaafar, J. (2014). Preparation and Characterization of Graphene Membrane Electrode Assembly Jurnal Teknologi Full paper Preparation and Characterization of Graphene Membrane Electrode. *Jurnal Teknologi*, *9*(August),: 10–14.

[72] Callister, W.D. and Rethwisch, D.G. Fundamentals of materials science and engineering : an integrated approach91.

[73] Sharma, R. Chadha, N. and Saini, P. (2017). Determination of defect density, crystallite size and number of graphene layers in graphene analogues using X-ray

diffraction and Raman spectroscopy. *Indian Journal of Pure and Applied Physics*, *55*(9),: 625–629.

[74] Hallam, P.M. Gómez-Mingot, M. Kampouris, D.K. and Banks, C.E. (2012). Facile synthetic fabrication of iron oxide particles and novel hydrogen superoxide supercapacitors. *RSC Advances*, *2*(16),: 6672–6679, doi: 10.1039/c2ra01139e.

[75] Johra, F.T. Lee, J.W. and Jung, W.G. (2014). Facile and safe graphene preparation on solution based platform. *Journal of Industrial and Engineering Chemistry*, *20*(5),: 2883–2887, doi: 10.1016/j.jiec.2013.11.022.

[76] Díez, N.ˆliwak, A. Gryglewicz, S. Grzyb, B. and Gryglewicz, G. (2015). Enhanced reduction of graphene oxide by high-pressure hydrothermal treatment. *RSC Advances*, *5*(100),: 81831–81837, doi: 10.1039/c5ra14461b.

[77] Muzammil, I. Li, Y. and Lei, M. (2017). Cover Picture: Plasma Process. Polym. 10⁄2017. *Plasma Processes and Polymers*, *14*(10),: 1770019, doi: 10.1002/ppap.201770019.

[78] Using TEM and XRD to probe crystal orientation in organic thin films grown with OMBDdoi: 10.1088/1742-6596/371/1/012042.

[79] Catania, F. Marras, E. Giorcelli, M. Jagdale, P. Lavagna, L. Tagliaferro, A. and Bartoli, M. (2021). A review on recent advancements of graphene and graphene-related materials in biological applications. *Applied Sciences (Switzerland)*, *11*(2),: 1–21, doi: 10.3390/app11020614.

[80] Hummers, W.S. and Offeman, R.E. (1958). Preparation of Graphitic Oxide. *Journal of the American Chemical Society*, *80*(6),: 1339, doi: 10.1021/ja01539a017.

[81] Kumar, G.C.M. and Jalageri, M. (2020). Synthesis and characterization of graphene oxide by modified hummer method. *AIP Conference Proceedings*, *2247*(May), doi: 10.1063/5.0003864.

[82] Alam, S.N. Sharma, N. and Kumar, L. (2017). Synthesis of Graphene Oxide (GO) by Modified Hummers Method and Its Thermal Reduction to Obtain Reduced Graphene Oxide (rGO)*. *Graphene*, *06*(01),: 1–18, doi: 10.4236/graphene.2017.61001.

[83] Vieira, O. Ribeiro, R.S. Diaz de Tuesta, J.L. Gomes, H.T. and Silva, A.M.T. (2022).

A systematic literature review on the conversion of plastic wastes into valuable 2D graphene-based materials. *Chemical Engineering Journal*, *428*, doi: 10.1016/j.cej.2021.131399.

[84] Pandey, S. Karakoti, M. Dhali, S. Karki, N. SanthiBhushan, B. Tewari, C. Rana, S. Srivastava, A. Melkani, A.B. and Sahoo, N.G. (2019). Bulk synthesis of graphene nanosheets from plastic waste: An invincible method of solid waste management for better tomorrowWaste Manag. 88:48–55.

[85] Tatrari, G. Karakoti, M. Tewari, C. Pandey, S. Bohra, B.S. Dandapat, A. and Sahoo, N.G. (2021). Solid waste-derived carbon nanomaterials for supercapacitor applications: a recent overviewMater. Adv. 2:1454–1484.

[86] Wyss, K.M. Beckham, J.L. Chen, W. Luong, D.X. Hundi, P. Raghuraman, S. Shahsavari, R. and Tour, J.M. (2021). Converting plastic waste pyrolysis ash into flash graphene. *Carbon*, *174*,: 430–438, doi: 10.1016/j.carbon.2020.12.063.

[87] Calizo, I. Bao, W. Miao, F. Lau, C.N. and Balandin, A.A. (2007). The effect of substrates on the Raman spectrum of graphene: Graphene- on-sapphire and graphene-on-glass. *Applied Physics Letters*, *91*(20),: 201904, doi: 10.1063/1.2805024.

[88] Nanda, S.S. Kim, M.J. Yeom, K.S. An, S.S.A. Ju, H. and Yi, D.K. (2016). Raman spectrum of graphene with its versatile future perspectives. *TrAC Trends in Analytical Chemistry*, *80*,: 125–131, doi: 10.1016/J.TRAC.2016.02.024.

[89] Yoon, D. Moon, H. Cheong, H. Choi, J.S. Choi, J.A. and Park, B.H. (2009). Variations in the Raman spectrum as a function of the number of graphene layers. *Journal of the Korean Physical Society*, *55*(3),: 1299–1303, doi: 10.3938/jkps.55.1299.

[90] Tripathi, S.N. Rao, G.S.S. Mathur, A.B. and Jasra, R. (2017). Polyolefin/graphene nanocomposites: A review. *RSC Advances*, *7*(38),: 23615–23632, doi: 10.1039/c6ra28392f.

[91] Alle, N. and Lyngaae-Jørgensen, J. (1980). Polypropylene and polyethylene blends - I. Flow behaviour in capillaries. *Rheologica Acta*, *19*(1),: 94–103, doi: 10.1007/BF01523860.

[92] Zhao, X. Huang, D. Ewulonu, C.M. Wu, M. Wang, C. and Huang, Y. (2021). Polypropylene/graphene nanoplatelets nanocomposites with high conductivity via solid-state shear mixing. *E-Polymers*, *21*(1),: 520–532, doi: 10.1515/epoly-2021-0039.

[93] Ghasemi, F.A. Ghasemi, I. Menbari, S. Ayaz, M. and Ashori, A. (2016). Optimization of mechanical properties of polypropylene/talc/graphene composites using response surface methodology. *Polymer Testing*, *53*,: 283–292.

[94] Pukánszky, B. (1999). Fillers for polypropylene240–246, doi: 10.1007/978-94-011-4421-6_33.

[95] Ferrage, E. Martin, F. Boudet, A. Petit, S. Fourty, G. Jouffret, F. Micoud, P. De Parseval, P. Salvi, S. Bourgerette, C. Ferret, J. Saint-Gerard, Y. Buratto, S. and Fortune, J.P. (2002). Talc as nucleating agent of polypropylene: Morphology induced by lamellar particles addition and interface mineral-matrix modelization. *Journal of Materials Science*, *37*(8),: 1561–1573, doi: 10.1023/A:1014929121367.

[96] Gahleitner, M. Jääskeläinen, P. Ratajski, E. Paulik, C. Reussner, J. Wolfschwenger, J. and Neißl, W. (2005). Propylene-ethylene random copolymers: Comonomer effects on crystallinity and application properties. *Journal of Applied Polymer Science*, *95*(5),: 1073–1081, doi: 10.1002/app.21308.

[97] Yang, F. Wang, X. Ma, Z. Wang, B. Pan, L. and Li, Y. (2020). Copolymerization of propylene with higher α-olefins by a pyridylamidohafnium catalyst: An effective approach to polypropylene-based elastomer. *Polymers*, *12*(1), doi: 10.3390/polym12010089.

[98] Tang, L. Zhao, L. and Guan, L. 7 Graphene / Polymer Composite Materials : Processing , Properties and Applications.

[99] Geim, A.K. and Novoselov, K.S. (2007). The rise of graphene PROGRESS. *Nature Materials*, *6*(3),: 183–191, 17330084.

[100] Lee, C. Wei, X. Kysar, J.W. and Hone, J. (2008). Measurement of the elastic properties and intrinsic strength of monolayer graphene. *science*, *321*(5887),: 385–388.

[101] Balandin, A.A. Ghosh, S. Bao, W. Calizo, I. Teweldebrhan, D. Miao, F. and Lau,

C.N. (2008). Superior thermal conductivity of single-layer graphene. *Nano letters*, *8*(3),: 902–907.

[102] Zhu, Y. Murali, S. Cai, W. Li, X. Suk, J.W. Potts, J.R. and Ruoff, R.S. (2010). Graphene and graphene oxide: synthesis, properties, and applications. *Advanced materials*, *22*(35),: 3906–3924.

[103] Bolotin, K.I. Sikes, K.J. Jiang, Z. Klima, M. Fudenberg, G. Hone, J. Kim, P. and Stormer, H.L. (2008). Ultrahigh electron mobility in suspended graphene. *Solid State Communications*, *146*(9–10),: 351–355, doi: 10.1016/j.ssc.2008.02.024.

[104] Jun, Y.S. Um, J.G. Jiang, G. and Yu, A. (2018). A study on the effects of graphene nano-platelets (GnPs) sheet sizes from a few to hundred microns on the thermal, mechanical, and electrical properties of polypropylene (PP)/GnPs composites. *Express Polymer Letters*, *12*(10),: 885–897, doi: 10.3144/expresspolymlett.2018.76.

[105] Wang, J. Song, F. Ding, Y. and Shao, M. (2020). The incorporation of graphene to enhance mechanical properties of polypropylene self-reinforced polymer composites. *Materials and Design*, *195*,: 109073, doi: 10.1016/j.matdes.2020.109073.

[106] Liang, J.Z. Du, Q. Tsui, G.C.P. and Tang, C.Y. (2016). Tensile properties of graphene nano-platelets reinforced polypropylene composites. *Composites Part B: Engineering*, *95*,: 166–171, doi: 10.1016/j.compositesb.2016.04.011.

[107] Schrauwen, B.A.G. Janssen, R.P.M. Govaert, L.E. and Meijer, H.E.H. (2004). Intrinsic deformation behavior of semicrystalline polymers. *Macromolecules*, *37*(16),: 6069–6078, doi: 10.1021/ma035279t.

[108] Dericiler, K. Sadeghi, H.M. Yagci, Y.E. Sas, H.S. and Okan, B.S. (2021). Experimental and numerical investigation of flow and alignment behavior of waste tire-derived graphene nanoplatelets in PA66 matrix during melt-mixing and injection. *Polymers*, *13*(6), doi: 10.3390/polym13060949.

[109] López, J.P. Gironés, J. Alberto, J. El Mansouri, N.E. Llop, M. Mutjé, P. and Vilaseca, F. (2012). Stone-ground wood pulp-reinforced polypropylene composites: Water uptake and thermal properties. *BioResources*, *7*(4),: 5478–5487, doi: 10.15376/biores.7.4.5478-5487.

[110] Fosse, C. Bourdet, A. Ernault, E. Esposito, A. Delpouve, N. Delbreilh, L. Thiyagarajan, S. Knoop, R.J.I. and Dargent, E. (2019). Determination of the equilibrium enthalpy of melting of two-phase semi-crystalline polymers by fast scanning calorimetry. *Thermochimica Acta*, *677*(November 2018),: 67–78, doi: 10.1016/j.tca.2019.03.035.

[111] Arvidsson, R. (2017). Review of environmental life cycle assessment studies of graphene production. *Advanced Materials Letters*, *8*(3),: 187–195, doi: 10.5185/amlett.2017.1413.

[112] Pandey, S. Karakoti, M. Dhali, S. Karki, N. SanthiBhushan, B. Tewari, C. Rana, S. Srivastava, A. Melkani, A.B. and Sahoo, N.G. (2019). Bulk synthesis of graphene nanosheets from plastic waste: An invincible method of solid waste management for better tomorrow. *Waste Management*, *88*,: 48–55, doi: 10.1016/j.wasman.2019.03.023.

[113] Cossutta, M. McKechnie, J. and Pickering, S.J. (2017). A comparative LCA of different graphene production routes. *Green Chemistry*, *19*(24),: 5874–5884, doi: 10.1039/c7gc02444d.

[114] Arvidsson, R. Kushnir, D. Sandén, B.A. and Molander, S. (2014). Prospective life cycle assessment of graphene production by ultrasonication and chemical reduction. *Environmental Science and Technology*, *48*(8),: 4529–4536, doi: 10.1021/es405338k.

[115] Schrijvers, D. Loubet, P. and Sonnemann, G. (2020). Archetypes of goal and scope definitions for consistent allocation in LCA. *Sustainability (Switzerland)*, *12*(14), doi: 10.3390/su12145587.

[116] Gilbertson, L.M. Wender, B.A. Zimmerman, J.B. and Eckelman, M.J. (2015). Coordinating modeling and experimental research of engineered nanomaterials to improve life cycle assessment studies. *Environmental Science: Nano*, *2*(6),: 669–682, doi: 10.1039/c5en00097a.

[117] Civancik-Uslu, D. Ferrer, L. Puig, R. and Fullana-i-Palmer, P. (2018). Are functional fillers improving environmental behavior of plastics? A review on LCA studies. *Science of The Total Environment*, *626*,: 927–940, doi: 10.1016/j.scitotenv.2018.01.149.

[118] Baumann, H. and Tillman, A.M. (2004). The Hitch Hiker's Guide to LCA: An Orientation in Life Cycle Assessment Methodology and Application. *Professional Publishing House*.

[119] Santos, J. Pham, A. Stasinopoulos, P. and Giustozzi, F. (2021). Recycling waste plastics in roads: A life-cycle assessment study using primary data. *Science of the Total Environment, 751,*: 141842, doi: 10.1016/j.scitotenv.2020.141842.

[120] European Commission. (2018). Product Environmental Footprint Category Rules Guidance. *PEFCR Guidance document*, 238.

[121] Joint Research Centre -- Institute for Environment and Sustainability. (2010). ILCD Handbook - General guide on LCA - Provisons and action steps. .

[122] Cossutta, M. Vretenar, V. Centeno, T.A. Kotrusz, P. McKechnie, J. and Pickering, S.J. (2020). A comparative life cycle assessment of graphene and activated carbon in a supercapacitor application. *Journal of Cleaner Production, 242,*: 118468, doi: 10.1016/j.jclepro.2019.118468.